The Pennsylvania State University

The Graduate School

Department of Engineering Science and Mechanics

COLLOIDAL QUANTUM DOT-ENABLING AND ALTERNATING CURRENT DRIVEN GALLIUM NITRIDE BASED LIGHT EMITTING DIODE TECHNOLOGY

A Dissertation in

Engineering Science and Mechanics

by

Jie Liu

Submitted in Partial Fulfillment
of the Requirements
for the Degree of

Doctor of Philosophy

December 2013

The dissertation of Jie Liu was reviewed and approved* by the following:

Jian Xu
Associate Professor of Engineering Science
Dissertation Advisor
Chair of Committee

Osama O. Awadelkarim
Professor of Engineering Science

S. Ashok
Professor of Engineering Science

Stephen J. Fonash
Bayard D. Kunkle Professor of Engineering Science

Suzanne Mohney
Professor of Materials Science and Engineering

Judith A. Todd
P.B. Breneman Department Head Chair
Head of the Department of Engineering Science and Mechanics

*Signatures are on file in the Graduate School

ABSTRACT

The colloidal quantum dot-enabling light emitting diode (LED) technology has been developing rapidly in recent years due to the superior optical properties of colloidal quantum dots (QDs). Semiconductor QDs of various sizes and compositions can be used as the emissive media in the light emitting diodes, and can also be used as a novel type of phosphor in white light emitting diodes.

Nitride based LED technology have also attracted much attention since the early 1990s. Due to their high power, high efficiency, and long lifetime properties, gallium nitride (GaN) LEDs are becoming promising candidates for next-generation solid state lighting.

This dissertation attempts to advance the LED technology in three respects. Firstly, in order to improve the technology using colloidal QDs as the emissive media, the degradation mechanism of the colloidal QD LEDs was studied. The results reveal that the degradation of QD LEDs is associated with the reduction in the QD quantum efficiency. Two mechanisms were identified to account for the observed decrease of quantum yield: i.e., high temperature induced degradation during LED operation; and the diffusion of the carrier transport molecules into the QD emissive layer. To this end, the inorganic material of indium-gallium-zinc-oxide (IGZO) was introduced to replace tris(8-hydroxyquinoline) aluminum (Alq_3) as the electron transport medium, making it possible to obtain air-stable QD LEDs.

Secondly, to make the QD phosphors more efficient for color conversion in white LEDs, the nonradiative energy transfer between colloidal quantum dot-phosphors and

nanopillar nitride LEDs was studied. In this approach, QD phosphors were brought to close proximity of blue-emitting quantum wells (QWs) by nanopillar LED design. This is accompanied with a novel design of low-resistance p-type contact selectively deposited on the top of the nanopillars. Strong non-radiative energy transfer was observed from the indium gallium nitride (InGaN) QWs to the colloidal QD phosphors, leading to a significant enhancement in effective internal quantum efficiency. Furthermore, the nonradiative energy transfer between colloidal quantum dot-phosphors and indirect bandgap silicon carbide was also studied. Nonradiative energy transfer has been demonstrated as an effective path to achieve color tunable emission from indirect semiconductors diodes.

Finally, to drive the GaN LEDs under alternating current (AC) condition without external driver circuitry, a monolithic integration of LED arrays with on-chip Schottky diode Wheatstone bridge was demonstrated, for the first, to run the LEDs directly on the line voltage.

TABLE OF CONTENTS

LIST OF FIGURES

LIST OF TABLES

ACKNOWLEDGEMENTS

First of all, I would like to express my great appreciation to my advisor Dr. Jian Xu for making this research work possible. His valuable and constructive suggestions are very helpful during the development of this research. Moreover, I benefit a lot from him for giving me the strength, attitude and motivation to complete this research work.

I also wish to thank Dr. Osama O. Awadelkarim, Dr. S. Ashok, Dr. Stephen J. Fonash and Dr. Suzanne Mohney for serving on my committee and their willingness to give time to improve my research work.

I would like to offer my deep gratitude to my fellow colleagues: Dr. Fan Zhang, Dr. Lai Wei, Dr. Yu Zhang, Dr. Guanjun You, Dr. Xuefeng Zhang, Dr. Wenjia Hu, Dr. Myo Thein, Dr. Shawn Pickering, Zhenyu Jiang and Li Wang. This dissertation could not have been accomplished without their great and kind help.

I especially appreciate the help from my collaborators Dr. Suzanne Mohney and Won Hyuck Choi from Penn State University in United States; Dr. Joon Seop Kwak and Dr. Min Joo Park from Sunchon National University in Korea; Dr. John F Muth, Yan Wang, and Patrick Wellenius from North Carolina State University in United States; Dr. Feng Zhao from Washington State University in United States. Their excellent work are of great help to me.

Finally, I give my special thanks to my parents for their support and encouragement throughout my research.

Chapter 1

Introduction

1.1 Light emitting diode introduction

In the past several decades, the technologies in the fields of semiconductor materials and devices have advanced fast. They have made great impacts to our daily life by virtue of the invention of televisions, computers, cell phones, digital cameras, and many other microelectronic and optoelectronic devices and systems. Since electroluminescence (EL) was discovered in 1907 [1], light emitting diode (LED) technology, as a sub-field of semiconductor, has also been developed rapidly [2-4]. It is now playing an increasingly important role in many areas, spanning from solid state lighting to flat panel displays [5-7].

Lighting is very important in our daily lives. In 2010, more than 8 billion lamps were installed in United States, consumed 700 terawatts hour (TWh) energy annually, which counts to ~19% of total U.S. electricity use [8]. Billions of dollars are spent on lighting every year, and millions tons of carbon oxide were released into the atmosphere each year due to lighting. As a result, novel lighting technologies are always under investigation for less energy consumption, lower cost, and less carbon oxide release. .Nowadays, there are three widely used technologies in the general lighting area: incandescent lamps, fluorescent lamps, and LEDs.

The most popular lighting technology is based on incandescent lamps. The tungsten filament was sealed in a vacuum bulb or a bulb filled with inert gas. During operation, the filament is heated to a very high temperature to emit light employing the physical phenomenon known as incandescence. Incandescent lamps were invented more than one hundred years ago, and are still widely used to date, whereas at the same time, many other technologies, such as cameras, cassettes, and films, have been replaced by their digital competitors.

Another very popular lighting technology is the fluorescent lamp. During its operation, the cathode was heated up to emit electrons, when the electrons with high kinetic energy collide with the mercury gas atoms sealed in the tube, the energy will be transferred from the electrons to the atoms, exciting the electrons in the outer shell of mercury atoms to a higher, unstable energy level. When the excited outer-shell electrons relax back to the ground level, ultraviolet (UV) light is emitted. Next, the UV light is absorbed by the phosphors coated on the inner wall of the tube, producing white light radiation. Employing this technology, the luminous efficiency of the fluorescent lamps can reach ~3 times of the luminous efficiency of the incandescent lamp. In addition, the lifetime of fluorescent lamp can be around 5,000 to 10,000 hours, substantially longer than the 1,000 to 2,000 hours' rated lifetime of incandescent lamps [9].

LED technology, as a promising candidate for the next-generation solid state lighting, has attracted much attention recently. This technology employs semiconductor p-n or p-i-n junctions in the device active region. When a forward bias voltage is applied on an LED, the electrons and holes will be injected into the p-n junction and recombine radiatively. The energy is released in the form of photons, and thus light is emitted.

Employing this technology, the luminous efficiency can reach 2 to 3 times of the efficiency of the fluorescent lamp [9]. In addition, the lifetime of nitride LEDs can be ~50,000 to 100,000 hours, substantially longer than the ~10,000 hour-lifetime of fluorescent lamps [9].

In addition to higher efficiency and longer lifetime, an LED lamp has many other advantages. An LED is a semiconductor based device, no filament or filled gas is employed, hence its size can be made very small. A vacuum or hermetically sealed bulb is not required for this device. This property will enable many new applications of lighting devices, which cannot be matched by the conventional incandescent or fluorescent light bulbs that we use today. For example, the LEDs can be embedded into the wall, ceiling, and other building materials for specialized lighting [10]. In addition, the well- developed semiconductor processing techniques make it possible to integrate various sensors with the LEDs to achieve smart lighting [11, 12]. For example, the brightness and color of an LED lamp can be adjusted with a cell phone application in the way we want. Moreover, LEDs can be instant on, has no mercury, is environment friendly, and is dimmable by tuning the diode current.

Due to the above-mentioned superior properties, and significant advantages compared to the incandescent lamp and fluorescent lamp, the LED technology has been replacing the incandescent and fluorescent lamps in many applications. Since the output of LEDs can be made highly color saturated, and the industry is capable of designing and producing LEDs emitting different colors using different semiconductor compositions, colorful LEDs are replacing light bulbs with color filters in many fields that requesting inexpensive, high power, quasi-monochromatic light sources. For example, a significant

amount of traffic lights have been replaced by LED lamps in US. Although LED lamps still cost more than incandescent light sources at present, the higher luminous efficiency would make the overall energy saving significantly greater than incandescent lamps. In addition, the much longer lifetime of LEDs would also result in a much lower maintenance cost, which could further decrease the overall lamp running cost. Other than monochromatic light sources, another widespread application of LEDs is the backlight of liquid crystal displays (LCDs). Several years ago, compact fluorescent lamps were solely employed as the LCD backlights, now almost all the backlights are LEDs. The LEDs are also used in the headlights and brake lights of automobiles nowadays to replace the incandescent lamps. The next and most important application area to be penetrated by LEDs will be general lighting. Nevertheless, the bottleneck of LED penetration in this area is still the high cost of LED lamps, which is much higher than that of incandescent lamps and fluorescent lamps to date. Consequently, the industry is making every effort to lower the cost. It is envisioned that the LED lighting will become more and more popular in our daily lives upon the success of these efforts.

Besides lighting, the LED technology has also been grown rapidly in the emissive display area during these years. While the most popular technology of flat panel display is liquid crystal display (LCD) at this moment, organic light emitting diodes (OLEDs) appear as the emerging competitor by virtue of enhanced color purity, shorter response time, larger viewing angle, and simpler device configuration. In addition, OLEDs can be fabricated on curved and mechanically flexible substrates to build flexible display devices. Nowadays, OLED arrays have been employed widely in cell phone displays.

1.2 Light emitting diode fundamentals

The fundamentals of LED operation mechanism will be explained in detail in this section. As mentioned previously, the incandescent lamp employs a physical phenomenon known as incandescence. The filament needs to be heated to a very high temperature. The energy is converted to both visible and infrared light, the latter of which translates to a significant amount of heat radiation. For the fluorescent lamp, the mercury atoms collides with high energy electrons and emit UV light, the UV light is then absorbed by phosphors for white light generation. The mechanism underlying LED operation is electroluminescence. At the heart of an LED is a semiconductor p-n junction. When voltage forward bias voltage is applied on an LED device, the current is injected into the junction, and the light is produced when electrons and holes recombine radiatively in the quantum wells of the junction.

In the LEDs, light is emitted due to the radiative recombination of electrons and holes in the semiconductor material. Since the radiative recombination requires both electrons and holes, the probability of its occurrence is proportional to the product of electron and hole concentrations. As a result, the radiative recombination rate can be given by [13]

$$R = -\frac{dn}{dt} = -\frac{dp}{dt} = Bnp \qquad (1)$$

Where R is the radiative recombination rate of electrons and holes, n is the electron concentration, p is the hole concentration, and B is called bimolecular recombination coefficient. This equation is called bimolecular rate equation. A parameter called carrier lifetime τ, denotes the mean time it takes for a minority carrier to

recombine with a majority carrier, and can be derived from the bimolecular rate equation as follows.

$$\frac{dn}{dt} = -Bnp \quad (2)$$

$$n = n_0 e^{-Bpt} = n_0 e^{-\frac{t}{\tau_n}} \quad (3)$$

$$\tau_n = \frac{1}{Bp} = \frac{1}{BN_A} \quad (4)$$

The carrier lifetime for holes can be written as

$$\tau_p = \frac{1}{Bn} = \frac{1}{BN_D} \quad (5)$$

Where N_A is the acceptor concentration in p-type semiconductor, and N_D is the donor concentration in p-type semiconductor.

Those carrier lifetimes are obtained based on the radiative recombination. However, in the LEDs, the carriers would also undergo nonradiative recombination. The most common type of nonradiative recombination is due to the defects in the crystal. Those defects would trap electrons and holes, leading to the nonradiative recombination. The other type of nonradiative recombination is surface recombination. It is due to the stop of periodicity on the surface of bulk semiconductors, can be regarded as a special type of defect on the semiconductor surface acting as the carriers trap. Another type of nonradiative recombination is Auger recombination. In Auger recombination, an electron or hole is excited to a higher energy level in conduction or valence band with the recombination energy. Since this recombination requires three carriers to participate, its rate is much lower than the radiative recombination and other nonradiative recombination. It can be neglected unless the injected current is very large. As a result, the nonradiative recombination lifetime due to the defects can be written as [13]

$$\tau_n = \frac{1}{N_T \upsilon_n \sigma_n} \quad (6)$$

$$\tau_p = \frac{1}{N_T \upsilon_p \sigma_p} \quad (7)$$

Where N_T is the concentration of the defect traps, υ_n and υ_p are the electron and hole thermal velocities, σ_n and σ_p are the capture cross sections of the defect traps.

1.2.1 Light emitting diodes employing p-n junction

P-n junction can be conceived as a basic semiconductor structure, and the simplest LED is a p-n junction. The band diagrams of a p-n junction under equilibrium and forward bias conditions are shown in Fig. 1-1.

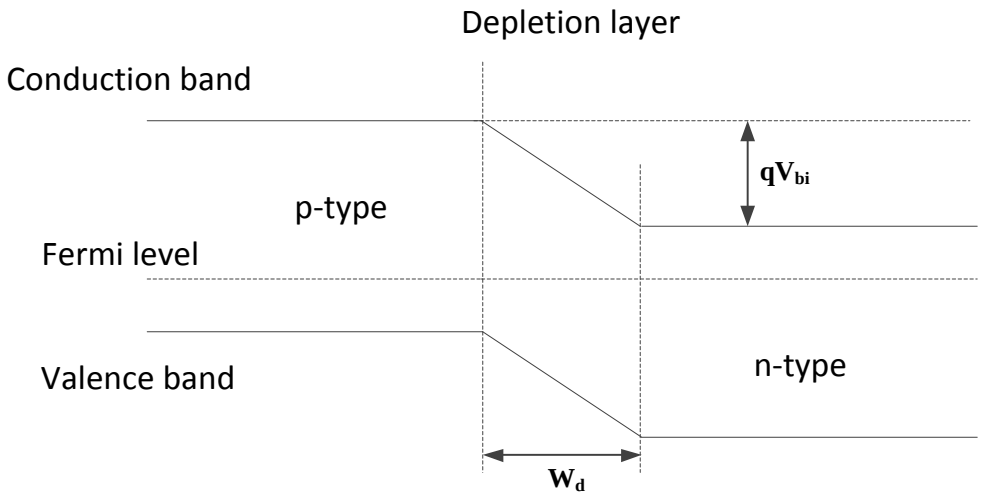

(a)

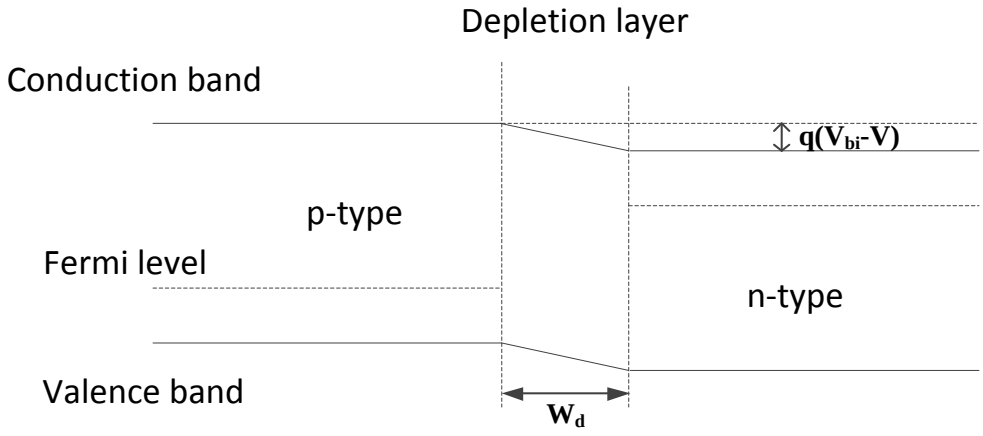

(b)

Figure 1-1. p-n junction energy band diagram under (a) equilibrium condition and (b) forward bias condition.

When the p-type and n-type semiconductors join each other to form an alloyed junction, the free electrons in the n-type semiconductor will diffuse to the p-side, and recombine with the majority holes in the p-type semiconductor. Meanwhile, the free holes in p-type semiconductor will diffuse to the n-type semiconductor, and recombine with the majority electron carriers in the n-type semiconductor. As a result, charge carriers in the vicinity of the junction will disappear, and static charge will be built up. This static charge layer is called depletion layer. The electric field built in this layer prevents the free electrons and holes in each side diffusing to the other side of the junction. Finally, the equilibrium condition would be reached, no net charge flow is allowed in the device as shown in Fig. 1-1(a).

When a forward biased voltage is applied across the p-n junction, which means that the p-type semiconductor is contacted as the anode and n-type semiconductor is connected as the cathode, holes in the p-type semiconductor and electrons in the n-type

semiconductor will be driven toward the depletion layer continuously, and recombine with each other both radiatively and nonradiatively. Part of the energy of the recombined electron-hole pairs is released in the form of photon emission; leading to the light output from the device.

1.2.2 Light emitting diodes employing double heterojunction

To achieve higher quantum efficiency, the double heterojunction structure is introduced into the LED design. In this structure, an undoped layer of semiconductor of narrow energy band gap is sandwiched between an n-type and a p-type cladding layers of wider energy band gap. The band diagrams of a double heterojunction under equilibrium and forward bias conditions are shown in Fig. 1-2.

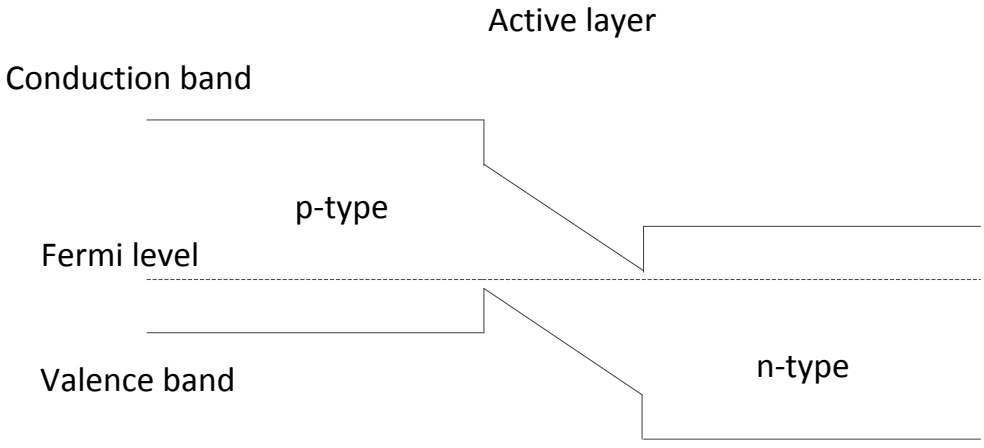

(a)

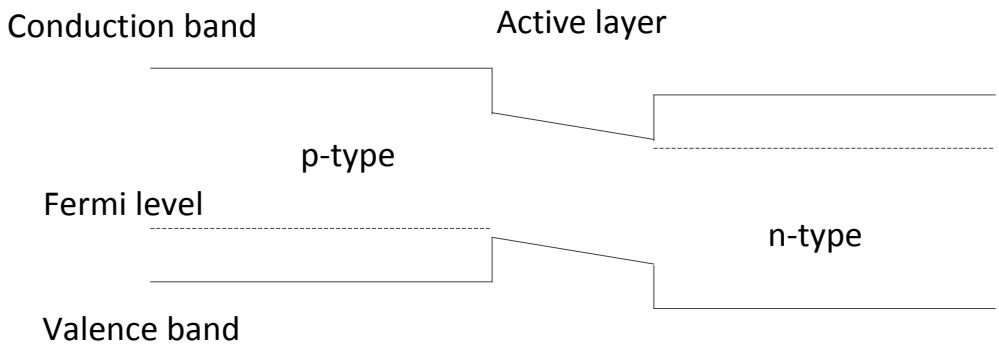

(b)

Figure 1-2. Double heterojunction under (a) equilibrium condition and (b) forward bias condition.

Under equilibrium condition, the narrow-band active layer acts as the depletion layer in the p-n junction, no carriers flow in the device. Under forward bias condition, the negative and positive carriers are driven to and confined in the sandwiched active region, and recombine with each other to emit light. The conduction and valance band offsets between the narrow and wide band semiconductors in the heterojunction pose barriers for the confinement of free carriers. The thickness of the active layer, usually less than 1 μm, is less than the diffusion length of both electrons and holes (10 μm or longer for III-V compound semiconductors). Consequently, this confinement effect in this structure would result in higher carrier concentration compared to homogeneous p-n junction structures. According to the radiative recombination carrier lifetime in Eqs (4) and (5), this higher carrier concentration would decrease the radiative recombination carrier lifetime, while the nonradiative recombination carrier lifetime is not changed according to Eqs (6) and (7). The internal quantum efficiency of an LED can be given by

$$\eta_{int} = \frac{\tau_r^{-1}}{\tau_r^{-1}+\tau_{nr}^{-1}} \qquad (8)$$

As a result, the quantum efficiency of an LED device will be increased by adopting the heterojunction structure.

1.2.3 Light emitting diodes employing multiple quantum well

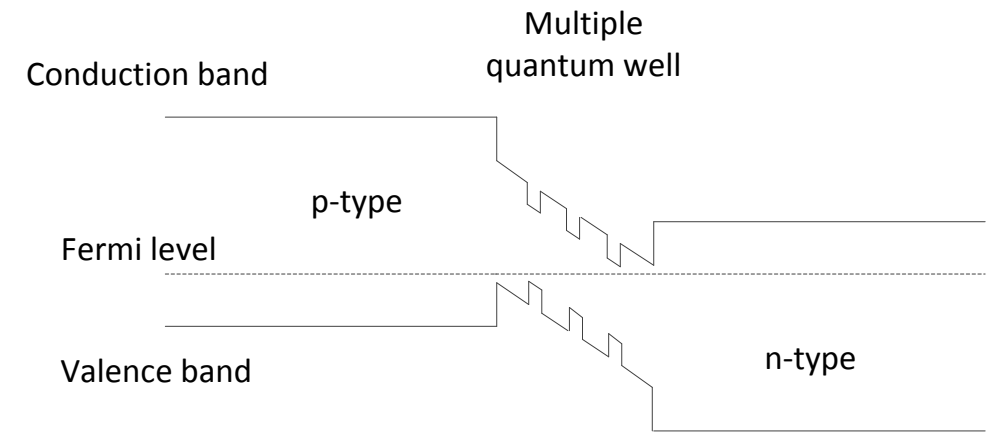

(a)

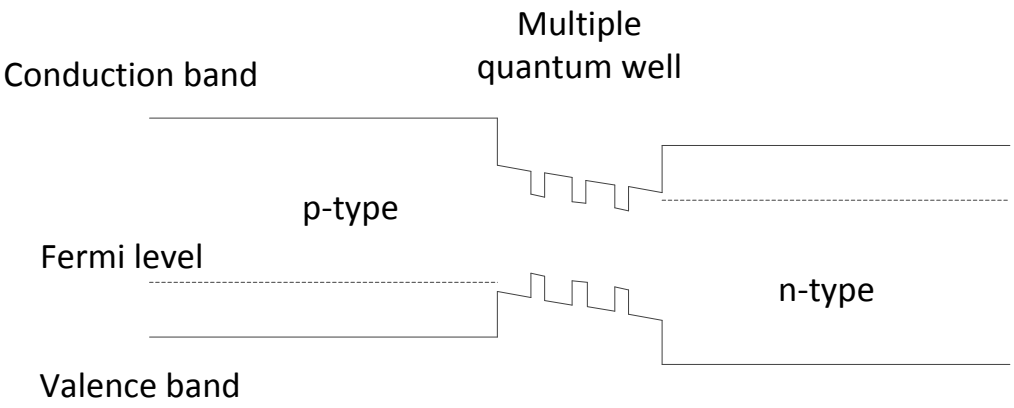

(b)

Figure 1-3. Multiple quantum well under (a) equilibrium condition and (b) forward bias condition.

The multiple quantum well (MQW) structure is also introduced into the LED design. The energy band diagrams of a MQW structure under equilibrium and forward

bias conditions are shown in Fig. 1-3. A quantum well (QW) usually has a thickness less than 50 nm, is much thinner than the narrow band active region of a heterojunction LED. The injected electrons and holes are confined in the QWs, and then recombine with each other. Due to the strong quantum confinement, the band gap of the QWs is larger than the bulk material. As a result, the emission wavelength can be changed by tuning the QWs structure. Nevertheless, the limited volume of QWs also leads to the reduction in the available number of electron-hole pairs for radiative recombination, and, as a result, a single quantum well could be saturated at low carrier injection densities, and the extra injected carriers will overflow the QW without recombination. This is why MQW structure is employed. In a MQW structure, the carriers overflowing an individual QW will be captured and confined by the adjacent QWs [13].

1.3 Novel LED materials and structures

There are several types of LEDs according to the material compositions used as the device active layers. One type is inorganic crystalline LEDs, based on III-V group semiconductor materials[14]. These inorganic semiconductor crystals can be used to build high-efficiency, high power light sources. Red to infrared emission can be obtained with III-Arsenide-Phosphide (III-As-P) LEDs [15], and ultraviolet to blue-green emission can be obtained from III-Nitride (III-N) LEDs [16]. Such crystalline III-V LEDs are widely used to fabricate indicators, LCD backlight, solid state lighting and traffic lights.

Another type of LED is thin film organic LEDs (OLEDs) [17, 18]. The EL from organic molecules was first observed in 1980's [18]. The active and charge transport materials used in OLEDs are organic molecules that are both electrically conductive and emissive at visible colors. There are several advantages for this type of LEDs in comparison with their inorganic crystalline counterparts. The cost of OLEDs is low due to solution processing capability, and OLEDs are thin, printable and can be fabricated on flexible substrates. As a result, OLEDs have been conceived as one of the most promising alternative techniques for next generation flat panel display. Nevertheless, OLEDs suffer from thermal and photochemical instabilities due to the low transition temperature of organic glasses and the redox properties of conductive molecules. To this end QD LEDs have been developed to combine the superior properties of both aforementioned LED technologies.

1.3.1 Colloidal quantum dot light emitting diodes

A quantum dot is a nanoscale semiconductor particle whose excitons, i.e., electron-hole pairs that bind through the Coulomb force, are strongly confined in three dimensions. When the dimensions of the semiconductor materials are of the order of the de Broglie wavelength, the quantum effects will become predominant for the electrical and optical processes therein. The strong quantum confinement hence imparts the quantum dots many unique electrical and optical properties.

For a long time, the study of QDs was restricted in the theoretical area due to the difficulties of fabrication. The development of molecular beam epitaxy technique realized the fabrication of QWs by growing very thin layers of semiconductor down to atomic precision. Although this technique was primarily used to fabricate QWs, it can also be used to make QDs by depositing a very small amount of semiconductor material on a substrate [19]. Due to the lattice mismatch between the semiconductor material and the substrate, the small amount of material can self-assemble into small islands or dots via built-in strain. However, this type of self-assembled QDs has a significant disadvantage: the size of the QDs cannot be precisely controlled via self-assembly formation; consequently, the size distribution of the QDs is broad, leading to a broad emission spectrum.

In 1994 another synthetic technique was developed by Murray *et al.* [20]. In this technique the nano-sized QDs grow out of solution, and QDs made by this method are usually called colloidal QDs. The size of the QDs synthesized by this technique is uniform and can be controlled precisely. Consequently, the bandwidth of emission and

excitonic absorption of the QDs can be as narrow as 30 nm. The photoluminescence (PL) quantum efficiency of those QDs can be as high as 80%. By tuning the size of the QDs, the emission color of CdSe/ZnS QDs can be tuned from red to blue, covering almost the entire visible spectrum [21].

Recently, chemically synthesized semiconductor colloidal QDs receive much attention because of their size-tunable wavelength emission, narrow emission bandwidth and high photoluminescence efficiencies [21-25]. Those QDs are composed of nanoscale semiconductor cores with radius smaller than the Bohr radius, and shells of wider band gap semiconductor for exciton confinement. Organic ligands are often employed to overcoat the QDs to passivate the surface states. The advances of the organometallic synthesis and the excellent optical properties of colloidal QDs have triggered the development of multiple quantum dot-enabling light emitting technologies.

One technology is using colloidal QDs as the active medium in a light emitting diode. Recent studies suggest that the low-cost, colloidal QDs can be used to replace the organic emitting materials in solution-processed LEDs by virtue of their superior optical properties, including high quantum yield, narrow emission bandwidth, and size-tunable wavelength over a broad spectral regime [23, 25]. The first colloidal QD LED was demonstrated by Alivisatos *et al*. in 1994 [23]. In their report, the colloidal QD LED employed a hybrid organic/inorganic structure, and the maximum luminance of the QD LED reached about 100 Cd/m^2. In that QD LED, the holes were injected into a p-paraphenylene vinylene (PPV) layer; the electrons were injected into a CdSe QDs layer. The free carriers formed excitons and recombined at the interface of PPV and QDs layers. This kind of hybrid organic/inorganic structure has since been widely used in the

following studies. Since then, colloidal QD LEDs have attracted much attention from worldwide researchers. The maximum luminance and efficiency of the devices have been increasing continuously. Seth Coe *et al*. demonstrated LEDs utilizing single monolayer of QDs in 2002 [22]. In this study, a monolayer of QDs is sandwiched between TPD and Alq_3, the luminance of 2000 Cd/m^2 and efficiency of 1.6 Cd/A can be obtained. In 2007, in collaboration of our Penn State optoelectronic laboratory, Sun *et al*. reported red, orange, yellow and green LEDs made from CdSe/ZnS core-shell QDs [25]. The maximum luminance of red QD LEDs was measured as high as 9064 Cd/m^2, and the electroluminescence efficiency reached 2.8 Cd/A. In that work, the hole transport material was changed to poly[N,N′-bis(4-butylphenyl)-N,N′-bis(phenyl)benzidine] (poly-TPD), and the electron transport layer changed to Tris(8-hydroxyquinolinato)aluminum (Alq_3) for enhanced carrier transport and injection properties. Nevertheless, while the fabricated QD-LEDs exhibited enhanced thermal and photochemical stabilities over their OLED counterparts, there has yet any in-depth understanding on the degradation mechanism of the new QD-LED configuration prior this work.

1.3.2 Colloidal quantum dot phosphors

The second quantum dot-enabling light emitting technology employs colloidal QDs as a new type of phosphor in white GaN LEDs. Due to the strong quantum confinement, semiconductor QDs, such as core/shell CdSe/(Zn,Cd)S QDs, are characteristic of sharp exciton absorption features, high luminescence efficiency, and size-tunable emission color spanning the entire visible spectrum. As a result, QDs of the

same chemical composition and different size can therefore provide multiple spectral components in the white LED output, with improved color qualities and aging performance.

At present, most white LEDs employ a blue InGaN LED and a green-yellow phosphor of cerium doped yttrium aluminum garnet (YAG) [26]. While this is the most inexpensive way of color down conversion, this kind of white LED cannot fully express natural white light in terms of both color temperature and color rendering index. The natural white light requires the mixture of the primary RGB colors, which is not met with the green-yellow phosphor approach by lacking the red component in the output spectra. As a result, researchers have attempted to identify a proper red phosphor. However, few red phosphors with high quantum efficiency and narrow bandwidth emission have been discovered so far. QDs, due to theirs high quantum efficiency, narrow bandwidth and tunable emission, can be a promising candidate for this purpose.

Hsueh-Shih Chen first employed red and green QDs on a InGaN LED to make a white LED in 2006 [27]. The LED emitted white light with a CIE-1931 coordinate of (0.33, 0.33) and color rendering index (CRI) value of 91. A detail explanation of CIE-1931 and CRI is given in Appendix. Later on, a white LED incorporating the combination of cyan, green, yellow and red quantum dots was demonstrated [28]. The output white light was reported to have CIE-1931 coordinate of (0.24, 0.33) and CRI value of 71. Sedat Nizamoglu *et al*. further increased those value in their work published in 2008 [29]. Their results showed a white LED with a CIE-1931 coordinate of (0.37, 0.30) and CRI value of 82.4. One of the most important applications of white LEDs is the backlights for LCDs. In 2010, Eunjoo Jang *et al*. demonstrated a 46 inch LCD TV

employing red and green colloidal quantum dots as phosphors in the backlight white LEDs [30]. The external quantum efficiency of the red and green QDs can reach 34% and 72%, respectively, and more than 100% of the color space in the National Television Systems Committee (NTSC) standard has been reproduced.

Moreover, perhaps the most significant potential of QD phosphors lies in the recent discovery that there exists a path for indirect injection of electron-hole pairs into QDs (for radiative recombination and thus band-edge emission from QDs) by non-contact, nonradiative energy transfer from a proximal InGaN quantum well. This nonradiative energy transfer was first demonstrated by Achermann *et al*. in 2004 [31]. In their work, they proposed a new scheme of pumping QDs by indirect injection of electron-hole pairs into QDs by non-contact, non-radiative energy transfer from an InGaN quantum well. It is fundamentally different from the multi-step 'down conversion' scheme and removes several of the intermediate steps involved in color conversion, thereby eliminating energy losses associated with these steps and increasing the efficiency.

However, according to the following studies [30-32], the nonradiative energy transfer only occurs when the QDs are in the immediate vicinity of the QW surfaces. This requirement is in conflict with the fact that a doped GaN contact layer needs to cap the InGaN QW to complete the p-i-n LED structure. In Achermann *et al.*'s work [31], spectroscopic measurements revealed that less than 13% of the radiative power of the QW was transferred to red emission from the QDs when the QW and QDs were separated by a 5nm-thick n-type capping layer for close proximity. Furthermore, the ultra-thin n-type capping layer, however, was not sufficiently conductive for current spreading,

which, in turn, reduced the LED efficiency. In another study [32], GaN-based LEDs were surface-patterned with deep-etched elliptical holes to accommodate colloidal QDs (acceptors) such that the nanocrystals were within close vicinity of the active layers (donors). Efficient nonradiative energy transfer was achieved via a short donor-acceptor distance, leading to a 43% increase in QD phosphor-emission over that provided by the conventional color down-conversion mechanism. However, the small volume of the trench holes drilled into the planar LED structure limit the amount of QD phosphors incorporated, and make the overall fraction of color conversion still significantly lower than the conventional green-yellow doped ceramic phosphor approach. It is expected that new QD-QW coupling architectures should be devised to address the existing drawbacks and to exploit the full potential of QD phosphors in solid state lighting. The second part of my dissertation work is dedicated to such a study.

1.3.3 Gallium nitride light emitting diodes

Gallium nitride (GaN) is a III-V group compound with 3.4 eV direct band-gap energy. It is widely used to fabricate high power, high efficient blue LEDs.

The development of GaN material can date back to early 1970s. At that time, bright red and green LEDs were available using GaAsP and GaP:N technologies respectively [15]. However, no proper material was discovered to make bright blue LEDs. Silicon carbide (SiC) was a candidate at that time, but due to its indirect band-gap, the efficiency of SiC LEDs was as low as 0.005% [33]. As a result, the researchers in

Radio Corporation of America (RCA) had tried to find a better material to make bright blue LEDs. The first single crystalline film of GaN was grown on sapphire substrate by Herbt Maruska *et al*. in 1970 [34]. Then the first GaN LED was demonstrated by Jacques Pankove *et al*. in 1972 [35].

After those early exciting discoveries in the GaN material, the research in this area ceased for several years due to two difficulties. Firstly, the single crystalline films of GaN initially grown over sapphire substrates exhibit poor crystal quality. Secondly, p-type doping of GaN can't be achieved due to the wide band nature of the nitride material and consequently, GaN p-n junctions can't be obtained at that time. The breakthrough was made in 1985, when the first single crystalline film of GaN with high crystal quality was epitaxially grown by Akasaki *et al.* employing metal organic chemical vapor deposition (MOCVD)[36]. Four years later, p-type GaN was realized with magnesium (Mg) as the acceptor dopant and electron beam annealing by the same research team [37]. This technical advance soon led to the demonstration of the first p-n junction GaN LED in 1989 [38]. Finally, the first InGaN/GaN double heterojunction LED was proposed and demonstrated with high efficiency by Shuji Nakamura of Nicha Corporation in 1993 [39]. Since then the nitride LEDs start to leave the research labs for technology transition. The nitride LED lamps have become commercially available since the beginning of the new century, and undergo rapid industrial development these years.

1.3.4 Alternating current gallium nitride light emitting diodes

A single junction GaN LED is operated under a low voltage (3V ~ 5V), direct current (DC) conditions and emits light only when the voltage is forward biased. This LED operation condition, however, conflicts with the alternating current (AC) line voltage requirements (120VAC/60Hz or 240VAC/50Hz) of US and European outlet sockets used in our daily lives. To address this problem, the most common method today is using an external driving circuit to convert the 110V ~ 240V AC voltage to a 3V ~ 5V DC voltage. However, the introduction of external electrical driver circuitry would bring additional power loss, increase the overall lamp cost, and limit the lifetime of the LED device.

Toward this end, intense investigation has been conducted to develop AC LEDs without electrical driving circuit. Hongxing Jiang *et al*. proposed an anti-parallel AC LED structure design with two LED arrays connected together as a parallel circuit in opposite direction [40], i.e., the anode of one LED array is connected to the cathode of the other LED array. Each array is composed of cascaded single junction LEDs. Ming-Te Lin *et al*. proposed another anti-parallel AC LED architecture [41],where multiple LED pairs are connected together as a series circuit. In each LED pair, two single junction LEDs are connected together as a parallel circuit in opposite direction. For both AC LED designs, the devices can be operated by an AC power supply, but only half of the LEDs in the circuitry would emit light upon each of the positive or negative half cycles of the AC voltage bias. Compared to the single junction LEDs driven by DC voltage, if the

same amount of light output power is required, the area of anti-parallel AC LEDs should be twice as large as the area of DC driven LEDs.

Hsi-Hsuan Yen *et al*. and Jaehee Cho *et al*. presented another different AC LED structure, which appears to be a more promising solution to the AC driving problem [42, 43]. In their patent applications, a Wheatstone bridge (WB) circuitry is integrated with an LED array for current rectification, and each of the four branches of the WB circuitry is composed of a series of single junction LEDs for high voltage bias. With the on-chip WB circuitry design, the LED array can emit light during both halves of the AC period. The effective emissive area of the LED chip rises to 70% with the new architecture design, but this value is still significantly lower than the DC LEDs. Moreover, since the cascaded LEDs on the four branches of the WB circuitry have to undergo reverse biased voltage during half of the alternating current period, it was found that those LEDs degrade rapidly due to the formation of Ga_2O_3 by combining the GaN, hole and hydroxide ions (OH-) under the reverse bias condition [44].

More recently, Hsi-Hsuan Yen *et al*. proposed to integrate Schottky diodes with LEDs to build on-chip WB circuitry for AC LED operation [45]. Two integration approaches are proposed, one method involves growing a rectifying layer of intrinsic semiconductor AlGaN on the LED wafer by epitaxy or deposition [46]. The other method is to form the rectifying region by ion implanting donor species into the top p-type GaN layer of the LED wafer [47]. These fabrication methods, however, request sophisticated post-growth modification of the LED epi-layer by deposition, ion implantation or diffusion, which would lead to the dramatic increase of the LED fabrication cost, and hence have never been employed to date. A more reliable and cost-effective approach is

yet to be developed to run LEDs on AC-line voltages prior to this doctoral dissertation work.

1.4 Measurement methods

In order to avoid repeated description of the measurement techniques employed present dissertation work, in what follows is a concise summary of the multiple measurement methods used in the dissertation study.

For QD LED characterization reported in chapter 2, the QD LEDs were driven, and the current-voltage relation of the devices was characterized by a Keithley 4200 semiconductor parameter analyzer. To obtain the device brightness, the emission from the devices was collected by a Newport 818SL silicon photodetector and then measured with a Newport 1830-C power meter. The detector was directed, at a fixed distance, to the ITO glass side of the LED. The signal output of the power meter was a portion of the QD LED forward emission, the ratio of the detected light intensity to the overall QD LED output power can be calculated from the detector to LED distance and the detector surface area. Finally the luminance (brightness) of the QD LED can be calculated by correlating the LED output power to the EL spectrum that was measured with an Ocean Optics UV-Vis-NIR spectrometer. The images of the LED output were taken with a Sony FWX700 FireWire color charged-coupling device camera with a C.3-mount lens. All the measurements were performed under ambient conditions.

For PL spectrum measurement, a 488nm-argon laser was used for excitation. An Ocean Optic UV-vis-NIR spectrophotometer was used to record the PL spectrum. PL decay measurement was performed with 80 femtosecond pulse excitation (λ~400nm) at the repetition rate of 1000 Hz. The PL emission of the samples was collected with a set of

lenses and detected with a fast-response photomultiplier tube (PMT). A GHz oscilloscope was used to record the traces.

PL decay measurements were performed with 80 femtosecond pulse excitation (λ~400nm) at the repetition rate of 1000 Hz. The PL emission of the samples was collected with a set of lenses and detected with a fast-response photomultiplier tube (PMT). A GHz oscilloscope was used to record the traces.

For nanopillar LEDs characterization in chapter 3, electrical pumping of the devices was implemented by forward-biasing the p-i-n junction of the nanopillars with a Keithley 4200 semiconductor parameter analyzer. The emission of the nanopillar LEDs was characterized with an integrating sphere-measurement to take into account the non-Lambertian radiation pattern of the nanopillar structure. The nanopillar sample was placed inside the integrating sphere (Thornlabs MA189), and the output emission of the sample was diffusely reflected by the barium sulfate-coated inner surface of the sphere and redistributed isotropically into all solid angles; the spectral and intensity detection of the light exiting from a small aperture at the sphere surface resulted in an accurate determination of the total number of photons from the nano-structured emitter. The output of the integrating sphere was coupled, via an optical fiber, to a spectrometer (Spectropro, ~0.1 nm spectral-resolution) equipped with a p-i-n photodetector. Both the dispersion of the spectrometer grating and the response of the photodetector were calibrated for the detection linearity. A barium sulfate-coated baffle was placed in front of the fiber coupler at the interior surface of the integration sphere to prevent the direct illumination of the optical fiber during the optical pumping. The second harmonic of the output (λ=400nm) of a Ti:sapphire femtosecond amplifier (800 nm, 1 kHz, 80fs,

Coherent Libra system) was introduced into the integrating sphere to excite the sample optically. An Ocean Optic UV-vis-NIR spectrophotometer was used to record the PL spectrum. For PL decay measurement, the nonlinear Kerr shutter technique was employed with a temporal resolution of ~1.5 ps [48, 49]. The PL from the InGaN QWs (λ~450nm) was collected and detected with a photomultiplier tube.

For high voltage (HV) LEDs and AC LEDs characterization in chapter 4, the current-voltage (I-V) relation of the devices was characterized by a Keithley 2612 semiconductor parameter analyzer to get higher output voltage. To obtain the output spectrum and external quantum efficiency of the devices, the LED was placed inside an integrating sphere, and the output emission of the device was diffusely reflected by the barium sulfate-coated inner surface of the sphere and redistributed isotropically into all solid angles; the spectral and intensity detection of the light exiting from a small aperture at the sphere surface resulted in an accurate determination of the total number of photons from the HV LED. The output of the integrating sphere was collected and characterized by the measurement system (Hopoo 2000).

1.5 Organization of the dissertation

This dissertation attempts to advance the LED technology in the following three respects.

Chapter 2 of the dissertation describes my work of investigating the degradation mechanism of colloidal QD LEDs in order to improve the performance of colloidal QD LEDs. The results reveal that the degradation of QD LEDs is associated with the reduction in the QD quantum efficiency. Two mechanisms were identified to account for the observed decrease of quantum yield: i.e., high temperature induced degradation during LED operation; and the diffusion of the carrier transport molecules into the QD emissive layer. To this end, the inorganic material of indium-gallium-zinc-oxide (IGZO) was introduced to replace tris(8-hydroxyquinoline) aluminum (Alq_3) as the electron transport medium, making it possible to obtain air-stable QD LEDs.

In chapter 3, to make the QD phosphors more efficient for color conversion in white LEDs, the nonradiative energy transfer between colloidal quantum dot-phosphors and nanopillar nitride LEDs was studied. In this approach, QD phosphors were brought to close proximity of blue-emitting quantum wells (QWs) by nanopillar LED design. This is accompanied with a novel design of low-resistance p-type contact selectively deposited on the top of the nanopillars. Strong non-radiative energy transfer was observed from the indium gallium nitride (InGaN) QWs to the colloidal QD phosphors, leading to a significant enhancement in effective internal quantum efficiency. Furthermore, the nonradiative energy transfer between colloidal quantum dot-phosphors and indirect bandgap silicon carbide was also studied. Nonradiative energy transfer has been

demonstrated as an effective path to achieve color tunable emission from indirect semiconductors diodes.

In chapter 4, to drive the GaN LEDs under alternating current (AC) condition without external driver circuitry, a monolithic integration of LED arrays with on-chip Schottky diode Wheatstone bridge was demonstrated, for the first time, to run the LEDs directly on the line voltage.

Chapter 5 of the dissertation discusses about the future work.

Reference

[1] H.J. Round, A note on carborundum, Electrical world, 49 (1907) 309.
[2] S.P. DenBaars, Gallium-nitride-based materials for blue to ultraviolet optoelectronics devices, P Ieee, 85 (1997) 1740-1749.
[3] T. Mukai, S. Nagahama, N. Iwasa, M. Senoh, T. Yamada, Nitride light-emitting diodes, Journal of Physics: Condensed Matter, 13 (2001) 7089.
[4] B. Geffroy, P. le Roy, C. Prat, Organic light-emitting diode (OLED) technology: materials, devices and display technologies, Polymer International, 55 (2006) 572-582.
[5] T. Komine, M. Nakagawa, Fundamental analysis for visible-light communication system using LED lights, Consumer Electronics, IEEE Transactions on, 50 (2004) 100-107.
[6] M.R. Krames, O.B. Shchekin, R. Mueller-Mach, G.O. Mueller, Z. Ling, G. Harbers, M.G. Craford, Status and Future of High-Power Light-Emitting Diodes for Solid-State Lighting, Display Technology, Journal of, 3 (2007) 160-175.
[7] P.E. Burrows, G. Gu, V. Bulovic, Z. Shen, S.R. Forrest, M.E. Thompson, Achieving full-color organic light-emitting devices for lightweight, flat-panel displays, Electron Devices, IEEE Transactions on, 44 (1997) 1188-1203.
[8] U.S. Department of Energy, 2010 U.S. Lighting Market Characterization, (2012).
[9] U.S. Department of Energy, Energy Savings Potential of Solid-State Lighting in General Illumination Applications, (2012).
[10] R.G. Villard, LED ceiling tile combination, LED fixture and ceiling tile, U.S. Patent No. 7645052 B2, (2008).
[11] E.F. Schubert, J.K. Kim, Solid-State Light Sources Getting Smart, Science, 308 (2005) 1274-1278.
[12] S. Bhardwaj, T. Ozcelebi, J. Lukkien, Smart lighting using LED luminaries, in: Pervasive Computing and Communications Workshops (PERCOM Workshops), 2010 8th IEEE International Conference on, 2010, pp. 654-659.
[13] E.F. Schubert, Light-Emitting Diodes, Cambridge University Press, New York, 2006.

[14] H.Q. Jia, L.W. Guo, W.X. Wang, H. Chen, Recent Progress in GaN-Based Light-Emitting Diodes, Adv Mater, 21 (2009) 4641-4646.
[15] M.G. Craford, D.L. Keune, W.O. Groves, A.H. Herzog, The luminescent properties of nitrogen doped GaAsP light emitting diodes, J Electron Mater, 2 (1973) 137-158.
[16] S. Nakamura, M. Senoh, N. Iwasa, S.-i. Nagahama, High-power InGaN single-quantum-well-structure blue and violet light-emitting diodes, Applied Physics Letters, 67 (1995) 1868-1870.
[17] J.H. Burroughes, D.D.C. Bradley, A.R. Brown, R.N. Marks, K. Mackay, R.H. Friend, P.L. Burns, A.B. Holmes, Light-Emitting-Diodes Based on Conjugated Polymers, Nature, 347 (1990) 539-541.
[18] C.W. Tang, S.A. Vanslyke, Organic Electroluminescent Diodes, Applied Physics Letters, 51 (1987) 913-915.
[19] P.M. Petroff, S.P. DenBaars, MBE and MOCVD growth and properties of self-assembling quantum dot arrays in III-V semiconductor structures, Superlattice Microst, 15 (1994) 15-15.
[20] C.B. Murray, D.J. Norris, M.G. Bawendi, Synthesis and characterization of nearly monodisperse CdE (E = sulfur, selenium, tellurium) semiconductor nanocrystallites, J Am Chem Soc, 115 (1993) 8706-8715.
[21] P. Reiss, J. Bleuse, A. Pron, Highly Luminescent CdSe/ZnSe Core/Shell Nanocrystals of Low Size Dispersion, Nano Lett, 2 (2002) 781-784.
[22] S. Coe, W.-K. Woo, M. Bawendi, V. Bulovic, Electroluminescence from single monolayers of nanocrystals in molecular organic devices, Nature, 420 (2002) 800-803.
[23] V.L. Colvin, M.C. Schlamp, A.P. Alivisatos, Light-emitting diodes made from cadmium selenide nanocrystals and a semiconducting polymer, Nature, 370 (1994) 354-357.
[24] Z. Tan, F. Zhang, T. Zhu, J. Xu, A.Y. Wang, J.D. Dixon, L. Li, Q. Zhang, S.E. Mohney, J. Ruzyllo, Bright and Color-Saturated Emission from Blue Light-Emitting Diodes Based on Solution-Processed Colloidal Nanocrystal Quantum Dots, Nano Lett, 7 (2007) 3803-3807.

[25] Q. Sun, Y.A. Wang, L.S. Li, D.Y. Wang, T. Zhu, J. Xu, C.H. Yang, Y.F. Li, Bright, multicoloured light-emitting diodes based on quantum dots, Nat Photonics, 1 (2007) 717-722.

[26] S. Fujita, A. Sakamoto, S. Tanabe, Luminescence Characteristics of YAG Glass-Ceramic Phosphor for White LED, Selected Topics in Quantum Electronics, IEEE Journal of, 14 (2008) 1387-1391.

[27] C. Hsueh-Shih, H. Cheng-Kuo, H. Hsin-Yen, InGaN-CdSe-ZnSe quantum dots white LEDs, Photonics Technology Letters, IEEE, 18 (2006) 193-195.

[28] S. Nizamoglu, et al., White light generation using CdSe/ZnS core–shell nanocrystals hybridized with InGaN/GaN light emitting diodes, Nanotechnology, 18 (2007) 065709.

[29] S. Nizamoglu, G. Zengin, H.V. Demir, Color-converting combinations of nanocrystal emitters for warm-white light generation with high color rendering index, Applied Physics Letters, 92 (2008) 031102.

[30] E. Jang, S. Jun, H. Jang, J. Lim, B. Kim, Y. Kim, White-Light-Emitting Diodes with Quantum Dot Color Converters for Display Backlights, Adv Mater, 22 (2010) 3076-3080.

[31] M. Achermann, M.A. Petruska, S. Kos, D.L. Smith, D.D. Koleske, V.I. Klimov, Energy-transfer pumping of semiconductor nanocrystals using an epitaxial quantum well, Nature, 429 (2004) 642-646.

[32] S. Chanyawadee, P.G. Lagoudakis, R.T. Harley, M.D.B. Charlton, D.V. Talapin, H.W. Huang, C.H. Lin, Increased Color-Conversion Efficiency in Hybrid Light-Emitting Diodes utilizing Non-Radiative Energy Transfer, Adv Mater, 22 (2010) 602-606.

[33] R.M. Potter, J.M. Blank, A. Addamiano, Silicon Carbide Light-Emitting Diodes, J Appl Phys, 40 (1969) 2253-2257.

[34] H.P. Maruska, J.J. Tietjen, THE PREPARATION AND PROPERTIES OF VAPOR-DEPOSITED SINGLE-CRYSTAL-LINE GaN, Applied Physics Letters, 15 (1969) 327-329.

[35] J.I. Pankove, E.A. Miller, D. Richman, J.E. Berkeyheiser, Electroluminescence in GaN, J Lumin, 4 (1971) 63-66.

[36] H. Amano, N. Sawaki, I. Akasaki, Y. Toyoda, Metalorganic vapor phase epitaxial growth of a high quality GaN film using an AlN buffer layer, Applied Physics Letters, 48 (1986) 353-355.

[37] H. Amano, M. Kito, K. Hiramatsu, I. Akasaki, P-Type Conduction in Mg-Doped GaN Treated with Low-Energy Electron Beam Irradiation (LEEBI), Jpn J Appl Phys, 28 (1989) L2112.

[38] H. Amano, I. Akasaki, Fabrication and Properties of GaN p-n Junction LED, Mater. Res. Soc. Extended Abstract, EA-21 (1990) 165-168.

[39] S. Nakamura, T. Mukai, M. Senoh, Candela-class high-brightness InGaN/AlGaN double-heterostructure blue-light-emitting diodes, Applied Physics Letters, 64 (1994) 1687-1689.

[40] H. Jiang, J. Lin, S. Jin, Light emitting diodes for high AC voltage operation and general lighting, U.S. Patent No. 6,957,899, (2005).

[41] M.-T. Lin, F.-C. Hwang, C.-T. Kuo, Structure of AC light-emitting diode dies, U.S. Patent No. 7,531,843, (2009).

[42] H.-H. Yen, H.-C. Kuo, W.-Y. Yeh, Characteristics of Single-Chip GaN-Based Alternating Current Light-Emitting Diode, Jpn J Appl Phys, 47 (2008) 8808.

[43] J. Cho, J. Jung, J.H. Chae, H. Kim, H. Kim, J.W. Lee, S. Yoon, C. Sone, T. Jang, Y. Park, E. Yoon, Alternating-current Light Emitting Diodes with a Diode Bridge Circuitry, Jpn J Appl Phys, 46 (2007) L1194.

[44] Y. Hsi-Hsuan, K. Hao-Chung, W.-Y. Yeh, Particular Failure Mechanism of GaN-Based Alternating Current Light-Emitting Diode Induced by GaOx Oxidation, Photonics Technology Letters, IEEE, 22 (2010) 1168-1170.

[45] W.-Y. Yeh, H.-H. Yen, Y.-J. Chan, The development of monolithic alternating current light-emitting diode, in, 2011, pp. 793910-793910-793912.

[46] J.-i. Chyi, G.-y. Lee, W.-s. Lin, Method for fabricating integrated alternating-current light-emitting-diode module, US Patent 20,130,034,919, (2013).

[47] H.-H. Yen, W.-Y. Yeh, Alternating current light-emitting device and fabrication method thereof, U.S. Patent No. 7,855,388, (2010).

[48] C. Zhang, F. Zhang, T. Zhu, A. Cheng, J. Xu, Q. Zhang, S.E. Mohney, R.H. Henderson, Y.A. Wang, Two-photon-pumped lasing from colloidal nanocrystal quantum dots, Opt. Lett., 33 (2008) 2437-2439.

[49] C. Zhang, J. Xu, T. Zhu, F. Zhang, Z. Tan, S.J. Schiff, H. Su, S. Gao, A.Y. Wang, Quantum efficiency of stimulated emission in colloidal semiconductor nanocrystal quantum dots, Phys Rev B, 80 (2009) 035333.

Chapter 2

Quantum dot light emitting diodes

2.1 Introduction

Recent studies suggest that the low-cost, colloidal semiconductor quantum dots (QDs) can be used to replace organic emitting materials in solution-processed light emitting diodes (LEDs) by virtue of their superior optical properties, including high quantum yield, narrow emission bandwidth, and size-tunable wavelength over a broad spectral regime [1-4].

Due to these unique properties of colloidal QDs, the QD LEDs have some advantages. The first one is the pure color of QD LED emission compared to organic LEDs (OLEDs) and other display technologies. QD LEDs can exceed the National Television Systems Committee (NTSC) color standard without any color filter. The second advantage is low power consumption due to the high quantum efficiency of the colloidal QDs. Similar to OLEDs, QD LEDs can be manufactured with low cost methods, and can be fabricated on both flexible and solid substrates. These advantages make the QD LEDs a good candidate for next-generation display technology.

2.1.1 Colloidal quantum dot fundamentals

A QD is a small semiconductor particle whose excitons are confined in three dimensions. When the dimension of a semiconductor device is of the order of the de Broglie wavelength, the quantum confinement effect would become significant. The dimension of a QD is usually less than 10 nanometers (10~50 atoms) in diameter. Due to this quantum confinement effect, it has many unique properties.

In order to understand the quantum confinement effect in QDs, we first refer to the one dimensional particle in a box model [5]. This is the simplest model in quantum mechanics, hence would allow insight into quantum confinement effect without the need for complicated mathematics.

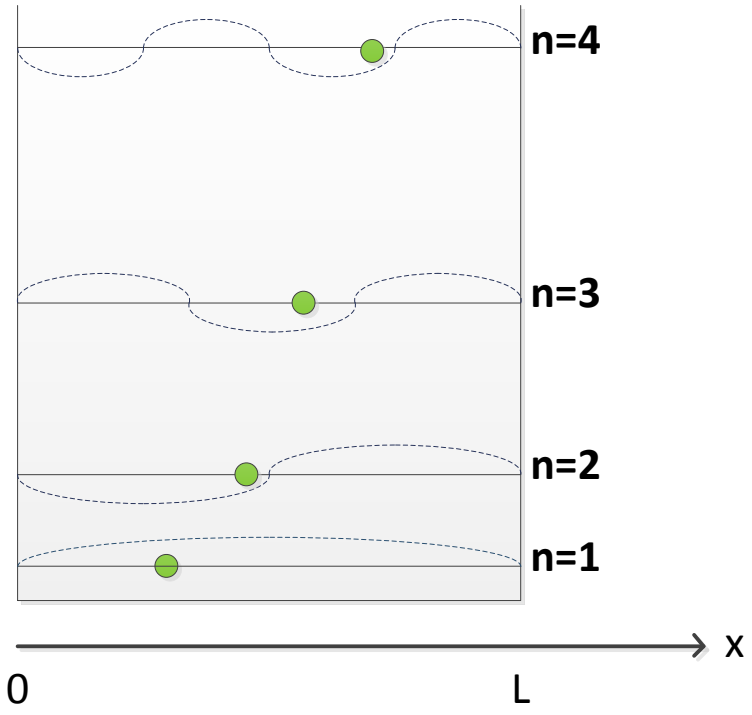

Figure 2-1 Particle in a box model.

In the one dimensional confined particle in a box model shown in Fig. 2-1, the particle may only move backwards and forwards along a straight line with impenetrable barriers at either end. Using this boundary condition to solve the Schrödinger equation, the wave function of the particle can be obtained:

$$\psi_n(x,t) = \begin{cases} Asin(k_n x)e^{-i\omega_n t}; & 0 < x < L \\ 0; & x \geq L \; or \; x \leq 0 \end{cases} \quad (1)$$

Where n is a positive integer, L is the size of the box. The wave number can be written as:

$$k_n = \frac{n\pi}{L} \quad (2)$$

Then the energy levels of the particle can be written as:

$$E_n = \frac{n^2\hbar^2\pi^2}{2mL^2} \quad (3)$$

These equations show that for this model, the particle's energy levels are discrete and can't have zero energy. The gaps between different energy levels are dependent on the dimension of the box. As a result, for the material with electrons and holes confined in one dimension, its band gap is no longer the same as the bulk material. The new band gap is the gap between the first energy level of the electrons in conduction band and the first energy level of holes in valence band, can be given by

$$E_g = E_{g_{bulk}} + \frac{\hbar^2\pi^2}{2L^2}\left(\frac{1}{m_e+m_h}\right) \quad (4)$$

Where $E_{g_{bulk}}$ is the band gap of the bulk material, m_e is the effective mass of the electron, and m_h is the effective mass of the hole. As shown in equation (4), if the

confining box length L decreases, the band gap will increase. This concept can also be applied to a QD whose carriers are quantum confined in three dimensions. Using Burs model [6], the band gap of a QD can be given by

$$E_{g_{QD}} = E_{g_{bulk}} + \frac{\hbar^2\pi^2}{2R^2}\left(\frac{1}{m_e+m_h}\right) - \frac{1.8e^2}{4\pi\varepsilon_0\varepsilon_r R} \quad (5)$$

Where R is the radius of the QD, and ε_r is the dielectric constant of the material. The second term on the right hand side of the equation is similar to the particle in a box model, is inversely proportional to R^2. The third term on the right hand side is due to the Coulombic attraction between the electron-hole pair, is inversely proportional to R. The second term is larger than the third term due to the stronger quantum confinement effect in the QD compared to Coulomb interaction. As a result, if the radius of the QD decreases, its band gap will increase.

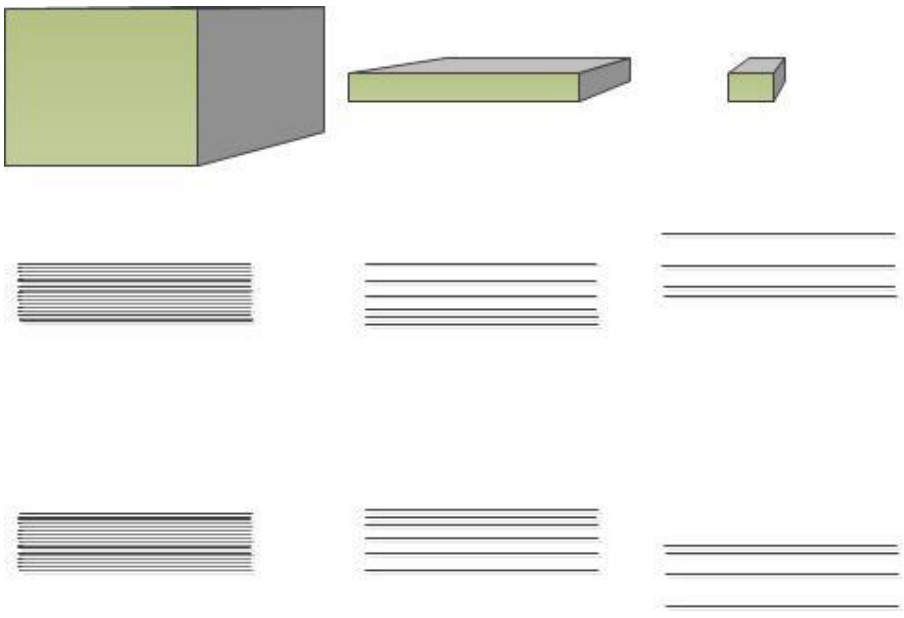

Figure 2-2 Energy levels in bulk semiconductor, quantum well and quantum dot.

Figure 2.2 shows the schematic diagram of energy levels in bulk semiconductor, quantum well (QW) and QD. It is shown that the energy levels of the QD are discrete, and its band gap is larger than the bulk semiconductor. In addition, its band gap is dependent on the dimension of the QD. The smaller the QD, the stronger the quantum confinement, the larger its band gap, and the bluer the emitted light.

To increase the quantum yield of the QD emission, several techniques are employed in QDs fabrication. The periodicity of atoms stops on the surface of a QD, creating dangling bonds for the atoms on the surface. These dangling bonds will trap electrons and holes. For example, in Cadmium (Cd) Selenide (Se) QDs, Cd dangling bonds will trap electrons and Se dangling bonds will trap holes. These electron and hole traps will increase the nonradiative recombination rate, consequently will decrease the QD emission quantum yield. To address this problem, organic ligands are employed to passivate the QDs surface traps.

However, the organic ligands can't passivate both the anionic and cationic surface traps simultaneously. Another technique using core-shell QD structure is employed to address this problem. In a core-shell QD structure, a thin layer of inorganic semiconductor is grown over the core QD. This semiconductor layer would not only protect the core from photo oxidation, but will also passivate both the anionic and cationic surface traps. With these two techniques, the quantum yield of CdSe/ZnS core-shell QDs with organic ligands can reach 80% to 90% [7].

2.1.2 Colloidal quantum dot light emitting diode fundamentals

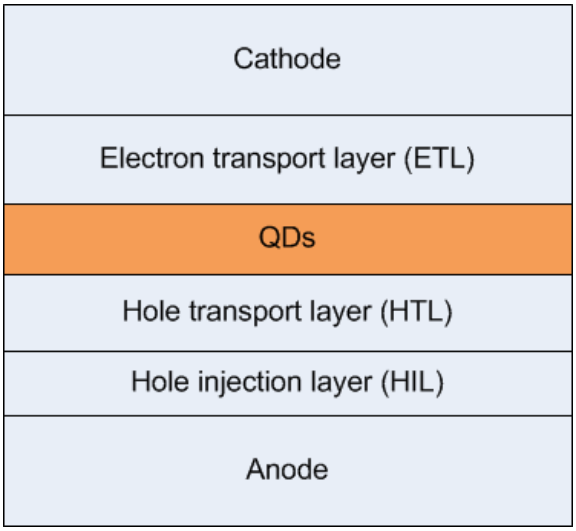

Figure 2-3 The structure of a typical QD LED.

Figure 2-3 shows the structure of a typical QD LED. This structure is similar to OLED structure, but the organic emission layer is replaced by the QDs emission layer. In the QD LED structure, the QDs emission layer is sandwiched between an electron transport layer (ETL) and a hole transport layer (HTL). A hole injection layer (HIL) is employed to assist holes injected from anode to the device easier.

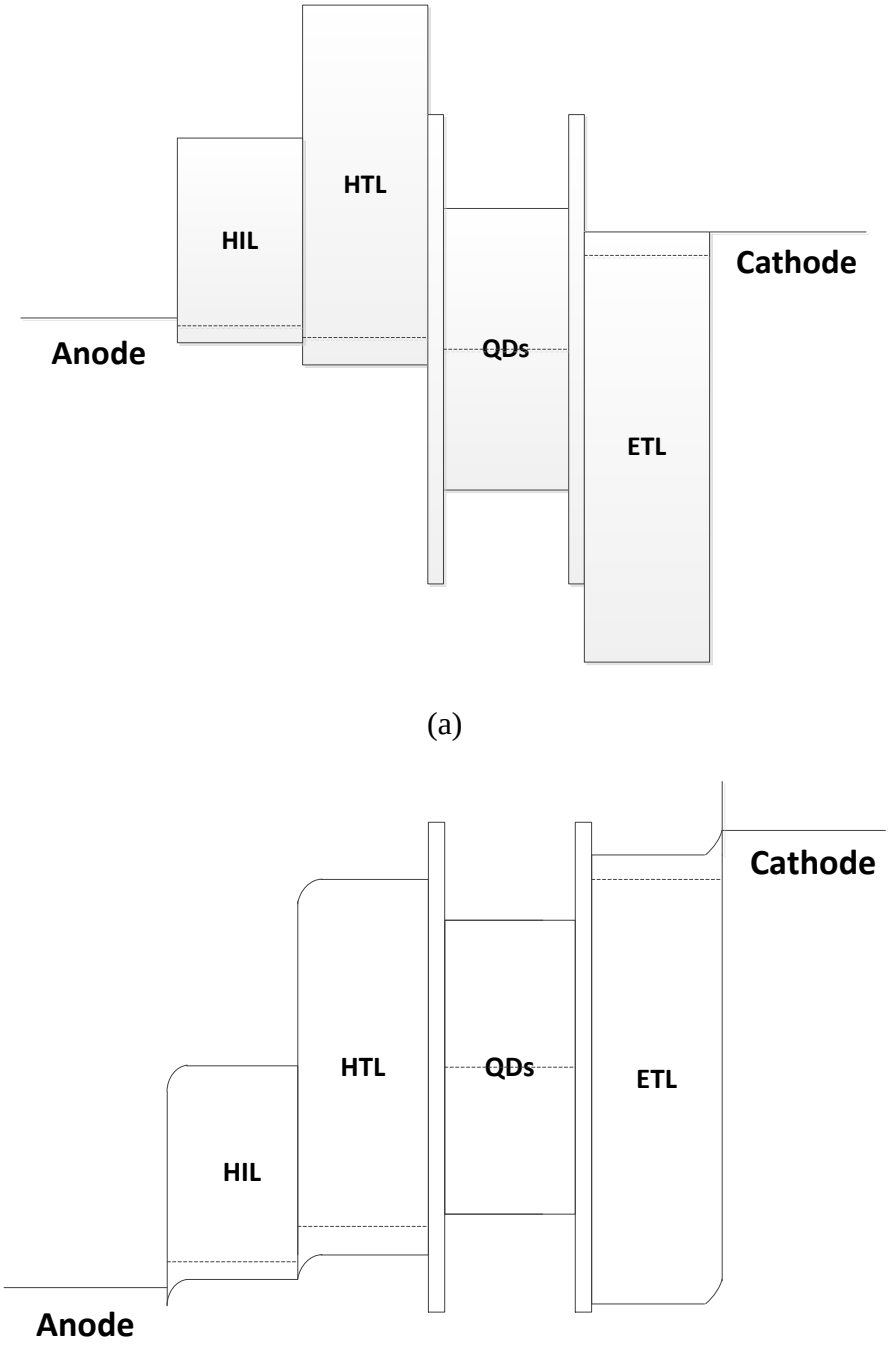

Figure 2-4 Band diagrams of (a) each layer of a typical quantum dot LED, and (b) the device under forward bias.

The band diagram of each layer in this structure is shown in Fig. 2-4 (a). When the device is forward biased, the band diagram is shown in Fig. 2-4 (b). The electrons are injected into the ETL, then transported to and captured in the QDs layer. The holes are injected into the HIL, then transported through HTL to and captured in the QDs layer. The electron-hole recombination occurs in the QDs layer and photons are emitted. The emitted wavelength is determined by the band gap of the QDs.

2.2 Degradation studies of colloidal quantum dot light emitting diodes

The degradation mechanism of CdSe/ZnS QD LEDs was investigated with photoluminescence (PL) spectrum and PL decay measurements. Our study reveals that the degradation is associated with the decreased quantum efficiency of the CdSe/ZnS QDs in the devices. Two mechanisms were identified to cause the observed decrease of quantum yield: high temperature induced degradation during LED operation; and the diffusion of the carrier transport molecules into the QD emissive layer.

2.2.1 Introduction

Recent studies suggest that the low-cost, colloidal semiconductor QDs can be used to replace organic emitting materials in solution-processed LEDs by virtue of their superior optical properties, including high quantum yield, narrow emission bandwidth, and size-tunable wavelength over a broad spectral regime [1-4]. Nevertheless, there have been few reports to date about studies on the degradation mechanisms of QD LEDs when compared to their organic counterparts [8-10].

In the present work, we took the first step towards understanding the degradation of CdSe/ZnS QD LEDs. Our results reveal that the degradation of QD LEDs is associated with the reduction in the QD quantum efficiency.

2.2.2 Device structure and fabrication

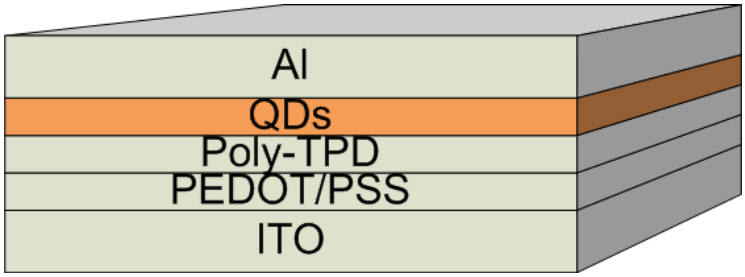

Figure 2-5. Schematic diagram of the structure of CdSe/ZnS QD LEDs.

Figure 2-5 shows the schematic diagram of the structure of the QD LEDs under study, consisting of indium tin oxide (ITO)/Poly(3,4-ethylenedioxythiophene) poly(styrenesulfonate) (PEDOT:PSS) (25 nm)/poly[*N*,*N*′-bis(4-butylphenyl)-*N*,*N*′-bis(phenyl)benzidine] (poly-TPD)(45 nm)/QDs (~3ML)/Al(150 nm). The ETL was not employed in this device since the widely used electron transport material (ETM) tris(8-hydroxyquinoline) aluminum (Alq_3) degrades significantly in air [11]. Device fabrication started with spin cast of PEDOT/PSS on UV-ozone treated ITO substrates, over which Poly-TPD was then solution cast from the chlorobenzene as the HTL. A QDs layer was then spin coated from the toluene solution as the emission layer (EML). The QDs employed in the study was colloidal CdSe/ZnS core/shell QDs (QSP-620, Ocean Nanotech LLC) that were surface-coated with amine ligands. Finally, the Al cathode, was fabricated by shadow-mask-evaporation at a pressure of $<3\times10^{-7}$ Torr.

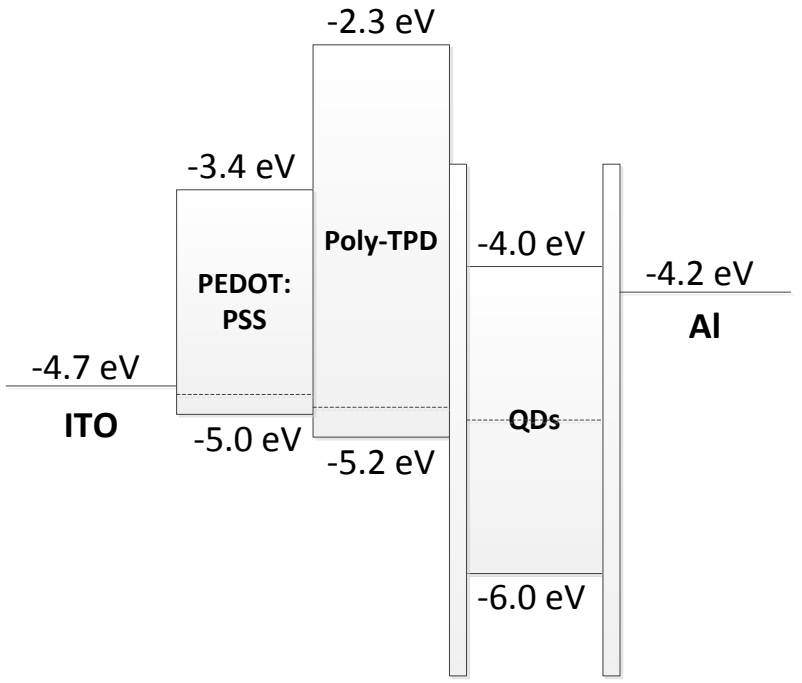

(a)

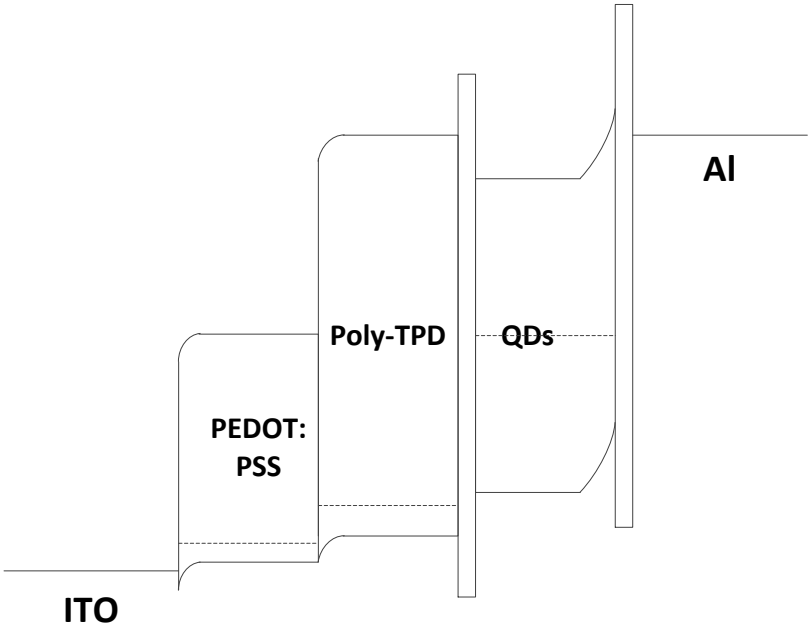

(b)

Figure 2-6. (a) Band diagram of each layer of the CdSe/ZnS QD LEDs used in this study. (b) Band diagram of the CdSe/ZnS QD LEDs under forward bias.

Figure 2-6 shows the band diagram of each layer of the CdSe/ZnS QD LEDs used in this study and the band diagram of the device under forward bias. Under forward bias condition, the electrons are tunneled into the QDs EML. The holes are injected into the HIL, then transported through HTL, and captured in the QDs EML. The electron-hole recombination occurs in the QDs EML and photons are emitted.

2.2.3 Results and discussion

2.2.3.1 Quantum dot light emitting diode degradation

To determine if the degradation of the fabricated QD LEDs exists, electroluminescence (EL) intensity was recorded as the function of time. In the measurement, two identical devices with the same structure were tested. One device was tested in dry N_2 in a glove box. The other device was tested in air. Both devices were driven by a constant current density of 100 mA/cm^2. All samples were characterized at room temperature without additional packaging.

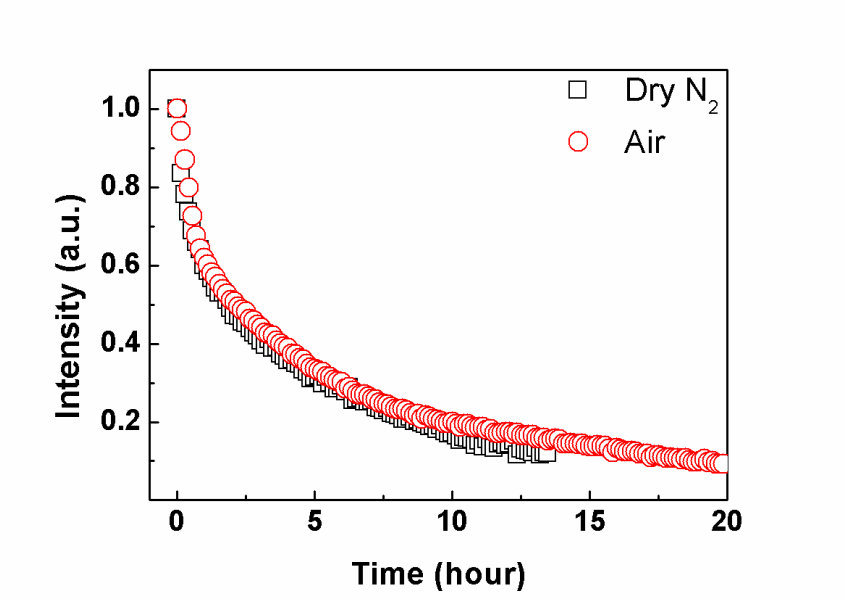

Figure 2-7. Time evolution of the electroluminescence intensity of the CdSe/ZnS QD LEDs at the driving current density of 100 mA/cm^2 in dry N_2 and in air, respectively.

Figure 2-7 shows the time dependence of the electroluminescence (EL) intensity of the QD LEDs. As expected, the degradation of EL is observed. In addition, we have found that the degradation rate of QD LEDs in dry N_2 is almost the same as that measured in air. This observation leads to an implication that the CdSe/ZnS QD LEDs can be operated in ambient environment without accelerated degradation. It is worth mentioning that the effects of ambient environment may be masked by other degradation mechanisms, which needs to be further studied in the future.

2.2.3.2 Reduced quantum efficiency of the quantum dots

To understand the underlying degradation mechanism, the PL spectrum and PL decay of the QDs in the devices were characterized. In this measurement, the QDs in two

devices with the same structure were tested. One device underwent the degradation measurement. The other device was a fresh sample without degradation measurement. The PL of the second device can be regarded as the PL of the first device before degradation measurement. Fig. 2-7(a) shows the PL spectra of the QDs in these two devices. It is clear that a decrease in PL intensity of the CdSe/ZnS QDs is observed after degradation measurement, revealing that the quantum efficiency of the QDs in the devices underwent degradation measurement was reduced.

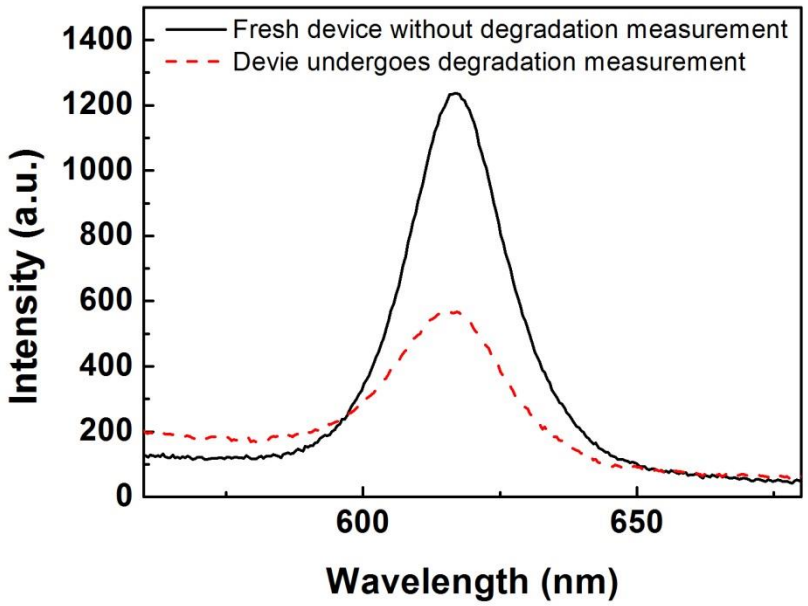

(a)

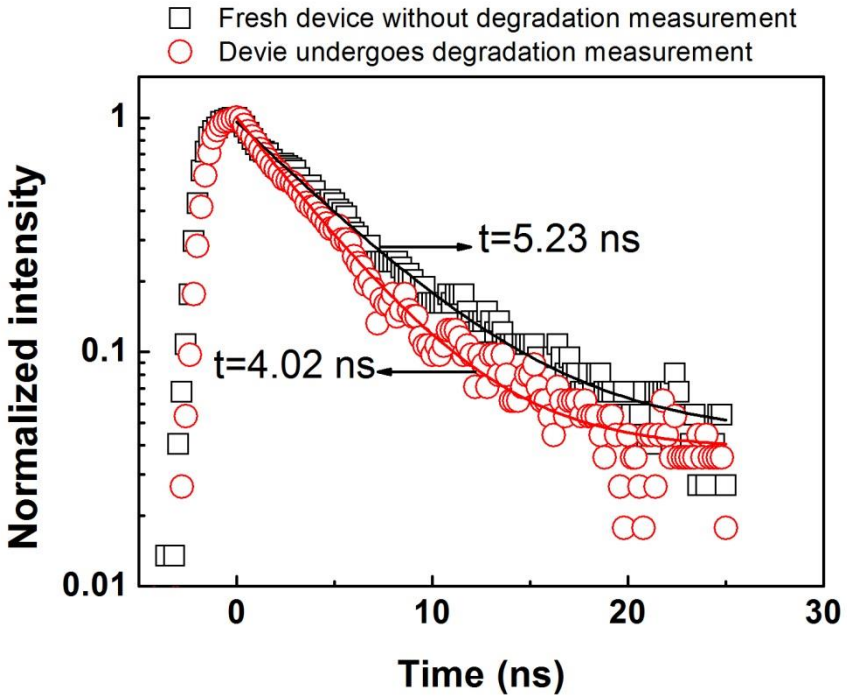

(b)

Figure 2-8. (a) Photoluminescence spectra and (b) PL decay of the QDs in two devices with the same structure: one device underwent the degradation measurement; the other device was a fresh sample without degradation measurement.

PL decay measurement was also performed. Fig. 2-8(b) shows the PL decay results of the same two samples. A faster decay was obtained for the sample undergone degradation, suggesting the presence of faster non-radiative pathways in the degraded QDs. Consequently, the quantum efficiency of the QDs was reduced, consistent with the result of PL spectrum study. This result reveals that the reduced quantum efficiency of the QDs in the devices accounts for the observed EL degradation.

2.2.3.3 Mechanisms cause the quantum efficiency reduction of the quantum dots

In order to discover what causes the decrease of quantum efficiency of the QDs, two mechanisms which could be responsible for this decrease were studied: high temperature during LED operation, and the diffusion of the hole transport material (HTM) into the QDs.

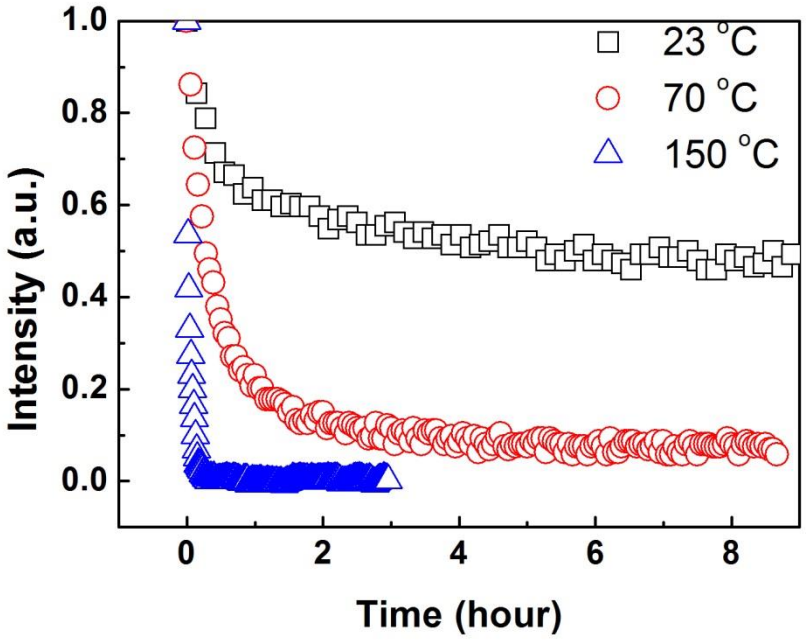

Figure 2-9. Time evolution of the photoluminescence intensity of three identical CdSe/ZnS QDs thin films at the temperatures of 23 ℃, 70 ℃, and 150 ℃ respectively.

Since the quantum efficiency of the LEDs is not 100%, a significant amount of energy is converted to heat. As a result, the temperature of the LEDs is usually higher than room temperature during operation. It can reach as high as 86 ℃ for OLEDs [12, 13]. The quantum efficiency of QDs could be reduced at this temperature. To verify this assumption, the time evolution of the PL intensity of CdSe/ZnS QDs thin films at

different temperatures was measured. Three identical CdSe/ZnS QD thin films were spin coated from toluene solution on clean glass substrates. Then they were placed on a hot plate set to different temperatures during the entire measurement to simulate the LEDs operating condition. The QDs thin films were excited by a 488 nm laser continuously. A 620 nm (peak wavelength of the QDs PL spectrum) band-pass filter was used to block the scattered excitation light.

The samples were characterized at room temperature (23 ℃), 70 ℃, and 150 ℃, respectively. The recorded time evolution traces of the normalized PL intensity are plotted in Fig. 2-9. It is shown that the PL intensity of the QDs decays faster at higher temperature, and the PL intensity decreases to 50%, 6%, and 0% of the initial value, for the sample measured at temperature of 23 ℃, 70 ℃, and 150 ℃ respectively. This result shows that high temperature would lead to the decrease of QDs quantum efficiency, consequently could cause the device degradation.

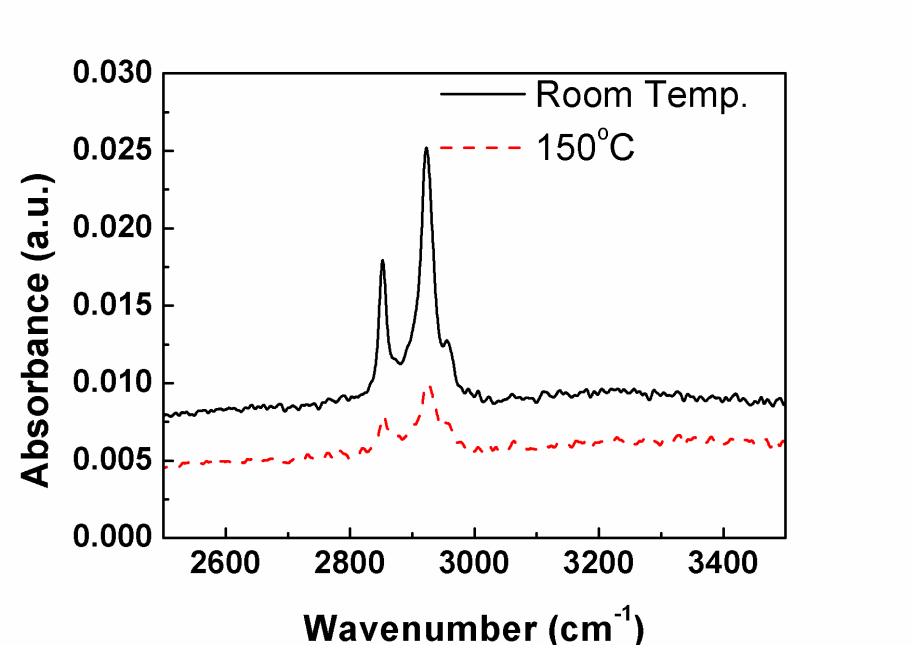

(a)

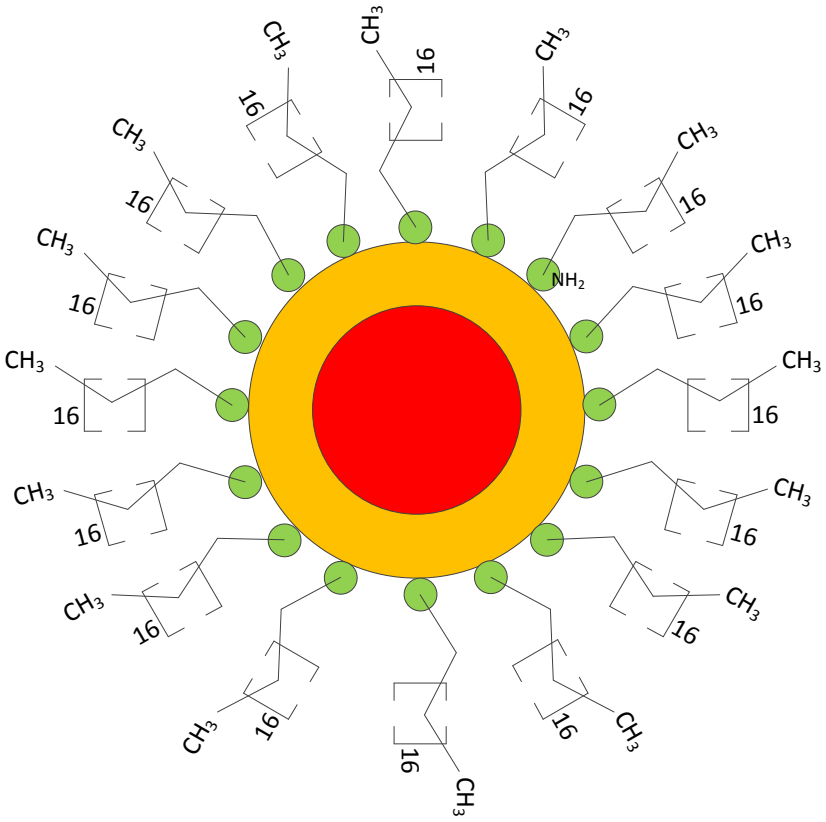

(b)

Figure 2-10. (a) Infrared absorption spectra of two CdSe/ZnS QDs thin films, one was placed at room temperature for 12 hours, while the other sample was annealed at 150 ℃ for 12 hours. (b) Schematic diagram of the structure of the core/shell CdSe/ZnS QDs with organic ligands of octadecylamine.

To further study what causes the QD quantum efficiency reduction at high temperature, Fourier transform infrared (FTIR) spectroscopy was employed to measure the infrared (IR) absorption spectra of the ligands of the QDs. Two identical CdSe/ZnS QDs thin films were spin coated from toluene solution on clean substrates. One sample was placed at room temperature for 12 hours, while the other sample was placed on a hotplate set at 150 ℃ for 12 hours. Both samples were prepared in dry nitrogen

environment. The IR absorption spectra of both samples were measured using an FTIR system, the result is shown in Fig. 2-10(a). The structure of the core/shell CdSe/ZnS QDs with organic ligands is shown in Fig. 2-10(b). The ligand of the CdSe/ZnS QDs employed in this study is octadecylamine (ODA) with the formula of $CH_3(CH_2)_{17}NH_2$. The CdSe/ZnS QDs are capped with the coordinating ligand of Amine group molecules. The ammonia chain of the amine ligand coordinates to the Zn ions at the surface of CdSe/ZnS quantum dots. The peak positions of the C-H stretching modes can be observed at ~2850 and ~2920 cm^{-1}. It is shown that the peak intensity drops a lot for the annealed sample compared to the room temperature sample, indicating that a significant amount of the ligand molecules are delocalized via broken bonds/oxidation/evaporation during annealing. It is mentioned previously that the ligands of the QDs have the function of surface passivation, and can increase the quantum efficiency of the QDs. As a result, the delocalization of ligands could result in the decrease of quantum efficiency, and consequently their destruction could be the cause of the degradation during LED operation.

Another possible mechanism causes the degradation is the diffusion of the HTM into the QDs. To verify this assumption, the PL spectra of poly-TPD mixed CdSe/ZnS QDs thin films were measured. For sample preparation, three mixtures of QDs and poly-TPD with weight ratios of CdSe/ZnS QDs to poly-TPD are 1:0, 99:1, and 1:1, respectively are dissolved in the same volume of chlorobenzene solvent. Thus three solutions with the same QDs concentration but different poly-TPD concentrations were obtained. Then three thin films were spin coated at the same speed from these three solutions. The 488nm pump laser will not excite poly-TPD molecules due to the large

band-gap of this material. Sample preparation and measurement were both performed at room temperature.

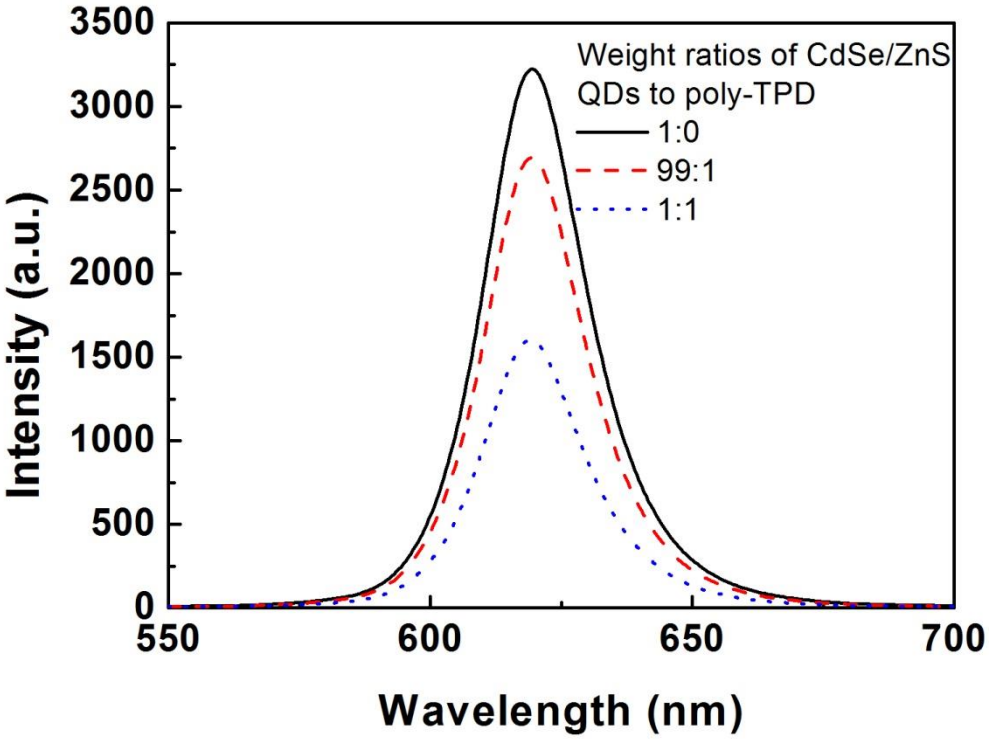

Figure 2-11. Photoluminescence spectra of three CdSe/ZnS QDs thin films mixed with different amounts of poly-TPD. The weight ratios of CdSe/ZnS QDs to poly-TPD are 1:0, 99:1, and 1:1, respectively.

For the thin films with 99:1 and 1:1 weight ratios of QDs to poly-TPD, the PL decreases by 16% and 50% respectively compared to that of the CdSe/ZnS QD film without poly-TPD. This result shows that PL decreases with increasing the amount of mixed poly-TPD, implies that the diffusion of the HTM into the QDs could lead to the reduction of QDs quantum efficiency. The measured decrease of PL intensity in the HTM mixed QD films is less significant than the decrease due at high temperature. It postulated

that this proposed diffusion of the HTM into the QDs mechanism does not dominate in the initial stage of the LED aging process, but may still become significant in the long run with HTM accumulating in the emission layer of QD LEDs.

2.2.4 Conclusion

In conclusion, the degradation mechanisms of QD LEDs were investigated in this work. PL spectrum and PL decay measurements were performed to study the mechanism of the devices degradation. The observed decrease in PL intensity and increase in decay rate of PL intensity reveal that the degradation of QD LEDs is associated with a reduction of the QD quantum efficiency. Two mechanisms were identified to cause the observed decrease of quantum yield: high temperature induced degradation during LED operation; and the diffusion of the carrier transport molecules into the QD emissive layer.

2.3 Colloidal quantum dot light emitting diodes using indium gallium zinc oxide as electron transport medium

2.3.1 Introduction

Recently quantum dots light emitting diodes have attracted much attention due to some unique and superior properties of QDs, such as high quantum efficiency, size tunable emission wavelength over broad band spectral ranges, and narrow emission bandwidth [1-4]. QDs can also be made from low cost, solution based synthesis technology, QD thin films can be spin coated rom QD solutions, and QDs are compatible with flexible substrates [7, 14]. These properties make QD LEDs can be easily fabricated. In addition, due to the inorganic nature of QDs, they are resistant to oxidation, this makes it possible to obtain air-stable QD LEDs.

A typical QD LED device structure is constituted of multiple layers of QDs sandwiched between hole transport layer (HTL) and electron transport layer (ETL). Nowadays, most QD LEDs employ organic material as electron transport material, such as tris(8-hydroxyquinoline) aluminum (Alq_3) [2, 4, 15]. The organic electron transport material has the advantage of low cost and easy processability. However, it is oxygen sensitive, easily degraded, not transparent and has low carrier mobility. Recently, researchers are trying to employ inorganic material as the electron transport material, such as Zinc Tin Oxide (ZTO) and Zinc Oxide (ZnO) [16, 17]. The inorganic electron transport material is air stable, transparent and has higher carrier mobility. In 2008, J. M. Caruge *et al*. demonstrated a QD LED employing sputtered, amorphous inorganic semiconductor $ZnO:SnO_2$ (ZTO) as robust electron transport material [18]. The peak

brightness of this QD LED can reach 1950 Cd/m^2 and the peak luminescence efficiency is 0.064 Cd/A. More recently Lei Qian *et al*. reported QD LEDs using ZnO nanoparticles as electron transport material [19]. Their device has maximum brightness and luminescence efficiency of 4200 Cd/m^2 and 0.32 Cd/A for blue, 68000 Cd/m^2 and 7.5 Cd/A for green, 31000 Cd/m^2 and 3.9 Cd/A for orange-red emission. The performance of this device is pretty good. However, the ZnO nanoparticle is not air-stable; it is sensitive to moisture in the air.

Recent studies in Indium-Gallium-Zinc-Oxide (IGZO) shows it could be a good candidate for the electron transport material due to its high electron mobility [20-23]. In this study, the ETL of IGZO was integrated into the device employing the technique of pulsed laser deposition (PLD) at room temperature. In order to optimize the output power and efficiency of the QD LEDs, IGZO films of various thickness and conductivity have been tested in the device structure. As a result, we demonstrate a device of pure red emission with the maximum brightness of 3600 Cd/m^2 and maximum luminescence efficiency of 0.31 Cd/A. For comparison, a control device with Alq_3 as electron transport material was also fabricated and characterized, exhibiting the maximum brightness of 636 Cd/m^2 and maximum luminescence efficiency of 0.19 Cd/A.

2.3.2 Device structure and fabrication

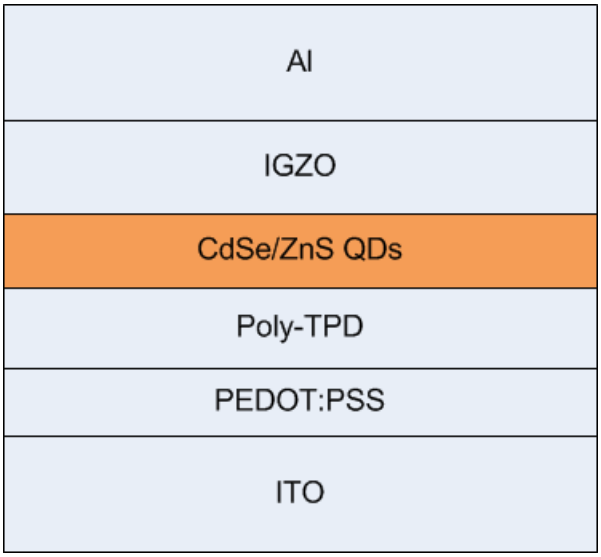

Figure 2-12. Schematic of the structure of QD LEDs.

Figure 2-12 shows the schematic structure of the QD LEDs under study, consisting of indium tin oxide (ITO)/Poly(3,4-ethylenedioxythiophene) poly(styrenesulfonate) (PEDOT:PSS) (25 nm)/poly[N,N′-bis(4-butylphenyl)-N,N′-bis(phenyl)benzidine] (poly-TPD) (45 nm)/QDs (~3ML)/IGZO/Al (150 nm). Device fabrication started with spin cast of PEDOT/PSS on UV-ozone treated ITO substrates, over which Poly-TPD was then solution cast from the chlorobenzene as the HTL. A QD layer was then spin coated from the toluene solution as the EML. The QD employed in the study was colloidal CdSe/ZnS core/shell QDs (QSP-620, Ocean Nanotech LLC) that were surface-coated with amine ligands. Later IGZO thin film was prepared by our collaborator Dr. John F Muth's group in North Carolina State University in United States. The IGZO thin film was deposited at room temperature using pulsed laser deposition technique [24]. This technique uses $InGaO_3(ZnO)_5$ ablation targets, by ablating material

from the target in an oxygen ambient in an oxygen ambient, uniform IGZO films can be deposited. The properties of the IGZO thin films can be tuned by tuning the oxygen pressure and film thickness (deposition time). Finally, the Al cathode, was fabricated by shadow-mask-evaporation at a pressure of $<3\times10^{-7}$ Torr.

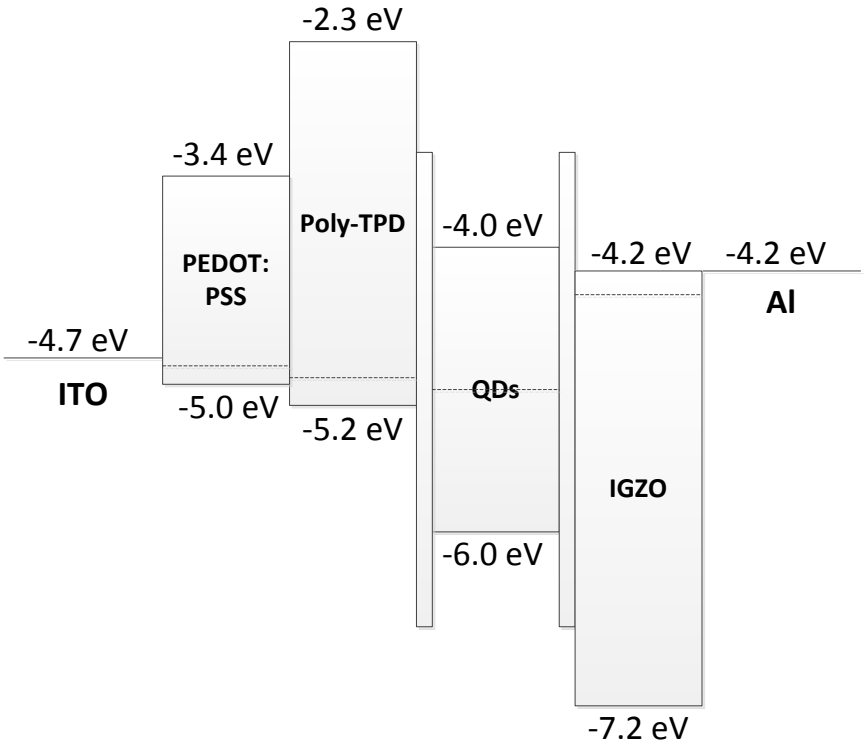

(a)

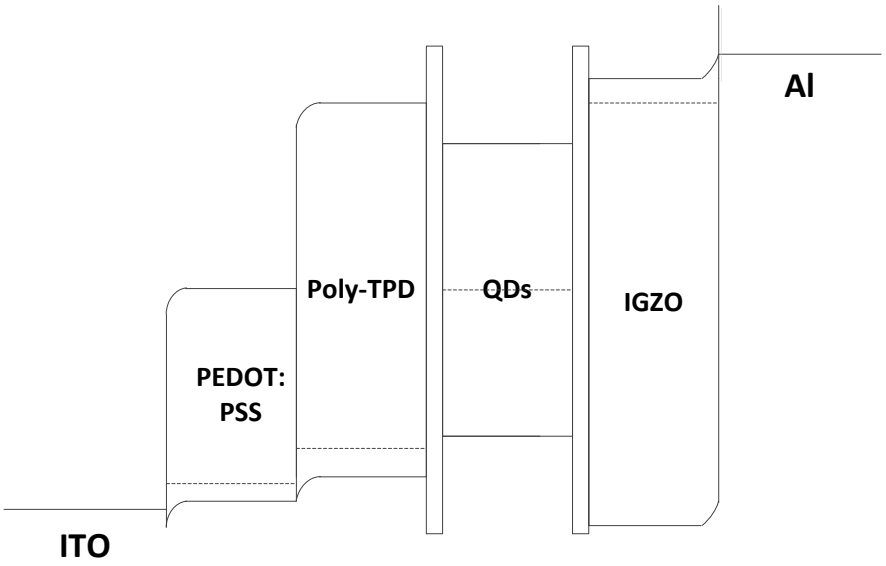

(b)

Figure 2-13. (a) Band diagram of each layer of the QD LEDs used in this study. (b) Band diagram of the QD LEDs under forward bias.

Figure 2-13 shows the band diagram of each layer of the QD LEDs used in this study and the band diagram of the device under forward bias. Under forward bias, the electrons will be transported through ETL, and captured in the QDs EML. The holes will be injected into the HIL, then transported through HTL, and captured in the QDs EML. The electron-hole recombination occurs there and photons are emitted.

2.3.3 Results and discussion

For device characterization, all measurements were taken at room temperature in air without additional packaging.

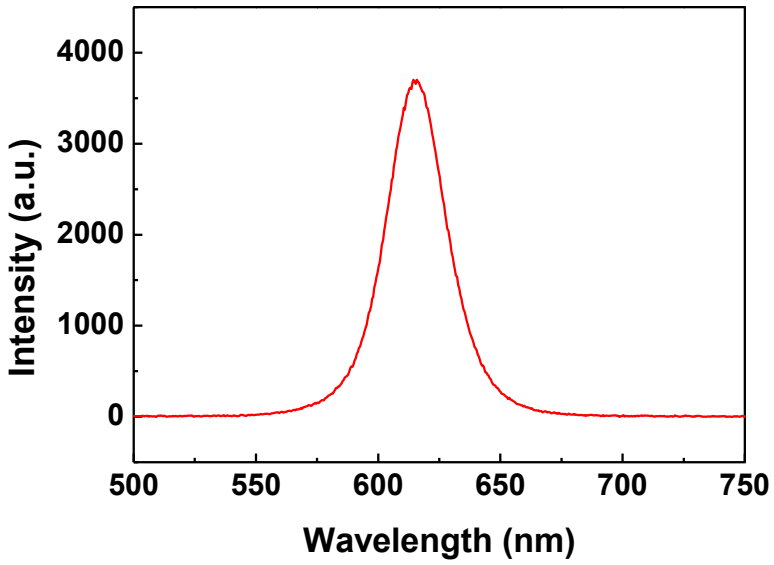

Figure 2-14. Electroluminescence spectrum of the QD LEDs.

Figure 2-14 shows the EL spectrum of the QD LEDs. The peak wavelength locates at 615 nm, and the full width at half maximum (FWHM) bandwidth is 28.5 nm. No noticeable other wavelength emissions were measured. This result shows the electron hole radiative recombination only occurs in QDs EML.

In order to optimize the output power and efficiency of the QD LEDs, IGZO films of various thickness and conductivity have been tested in the device structures. First of all, the thickness of the IGZO thin film was fixed at 15 nm, while the conductivity of thin film was changed. By tuning the pressure of the oxygen during IGZO thin film deposition, its conductivity can be tuned. The higher pressure of the oxygen, the lower conductivity of the IGZO thin film has.

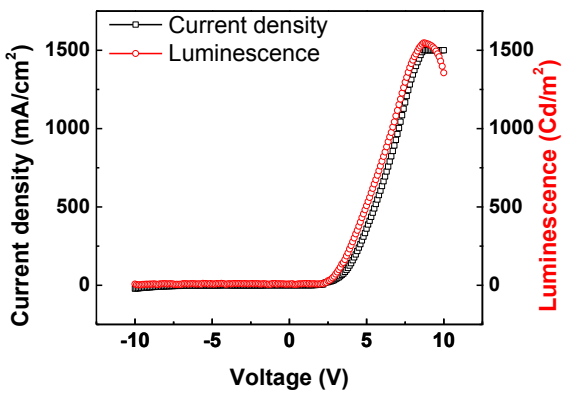
Current density
Luminescence
Current density (mA/cm^2)
Luminescence (Cd/m^2)
Voltage (V)

(a)

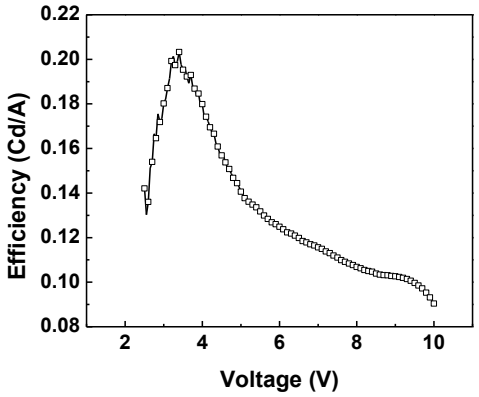
Efficiency (Cd/A)
Voltage (V)

(b)

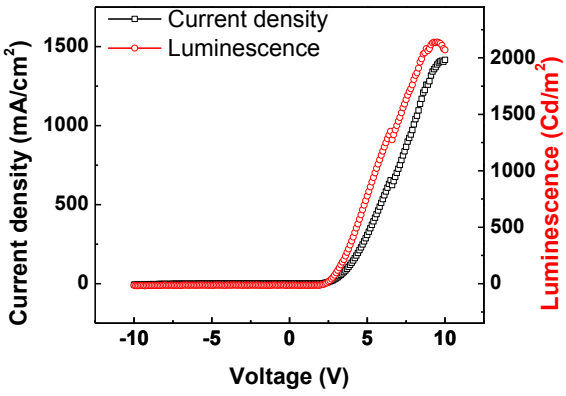
Current density
Luminescence
Current density (mA/cm^2)
Luminescence (Cd/m^2)
Voltage (V)

(c)

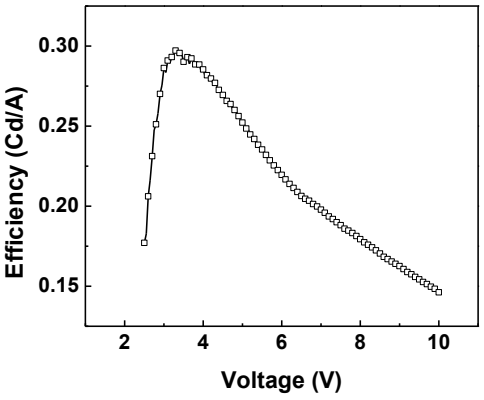
Efficiency (Cd/A)
Voltage (V)

(d)

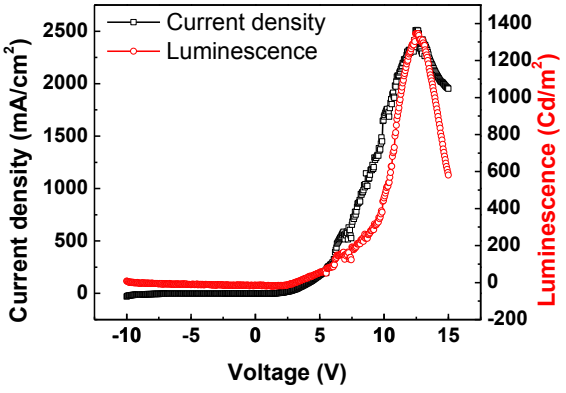
Current density
Luminescence
Current density (mA/cm^2)
Luminescence (Cd/m^2)
Voltage (V)

(e)

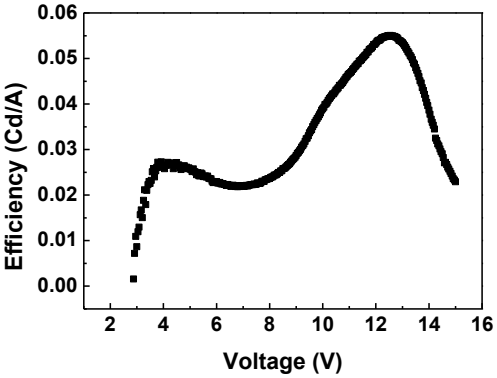
Efficiency (Cd/A)
Voltage (V)

(f)

Figure 2-15. Current-luminance-voltage (I-L-V) and efficiency of the QD LEDs with 15 nm IGZO thin films deposited at (a) (b) 40 mTorr, (c) (d) 60 mTorr, and (e) (f) 200 mTorr.

Figure 2-15 shows the current-luminance-voltage (I-L-V) and efficiency of the QD LEDs with 15 nm IGZO thin films deposited at different oxygen pressures. For the IGZO thin film deposited at 40 mTorr, the maximum brightness and luminescence efficiency are 1547 Cd/m^2 and 0.20 Cd/A. For the IGZO thin film deposited at 60 mTorr, these two parameters are 2140 Cd/m^2 and 0.30 Cd/A. For the IGZO thin film deposited at 200 mTorr, these two parameters are 1348 Cd/m^2 and 0.06 Cd/A. As a result, the performance of the devices changes with the conductivity of IGZO thin films. To optimize the device performance, the recombination center of the carriers should be inside the QD emission layer, thus the conductivity of the ETL and HTL should match with each other to meet this requirement. Consequently, the conductivity of ETL should not be too large or too small, which confirms the results in Fig. 2-15. The device with IGZO deposited at 60 mTorr has the best performance.

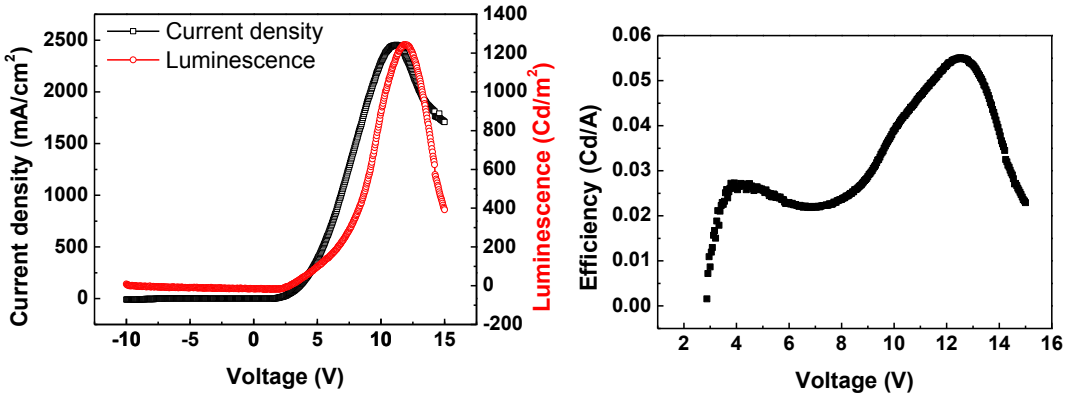

(a) (b)

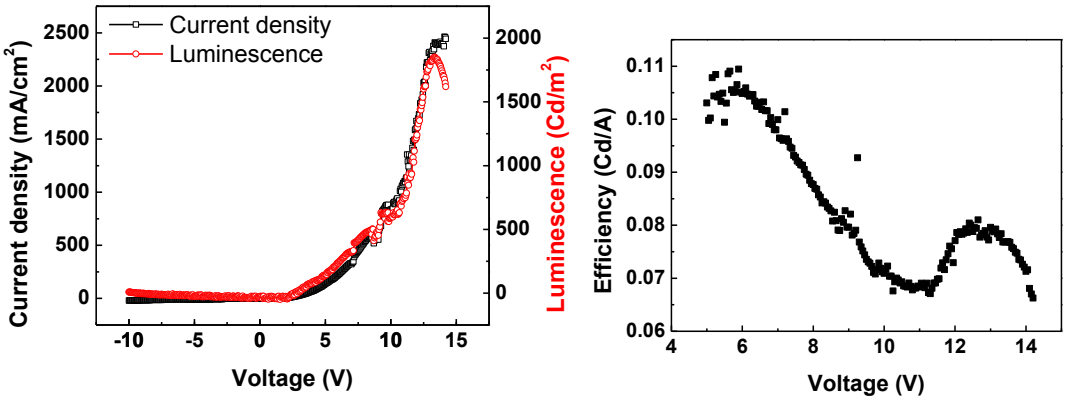

(c) (d)

Figure 2-16. Current-luminance-voltage (I-L-V) and efficiency of the QD LEDs with (a) (b) 15 nm and (c) (d) 60 nm IGZO thin films deposited at 80 mTorr.

Next, the deposition oxygen pressure of IGZO thin film was fixed, while the thickness of the thin film was changed. Fig. 2-16 shows the I-L-V and efficiency of the QD LEDs with different IGZO thin film thickness. For the device with 15 nm IGZO thin film deposited at 80 mTorr, the maximum brightness and luminescence efficiency are 1247 Cd/m^2 and 0.06 Cd/A. For the device with 60 nm IGZO thin film deposited at 80 mTorr, these two parameters are 1851 Cd/m^2 and 0.11 Cd/A. The device with thicker IGZO film has better performance. However, due to the same reason that the conductivity of the ETL and HTL should match with each other to make the recombination center of the carriers in the QD emission layer, the IGZO film should not be too thick.

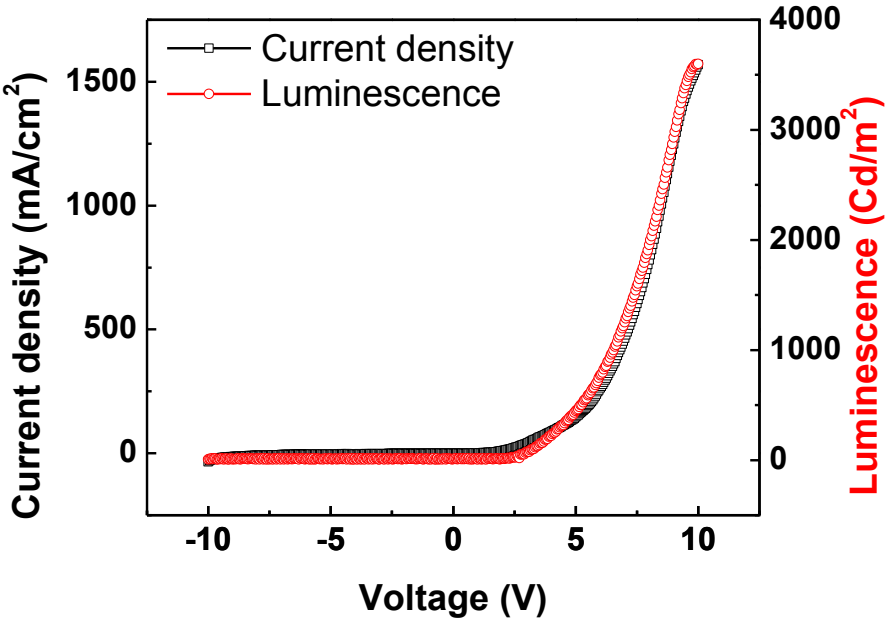

(a)

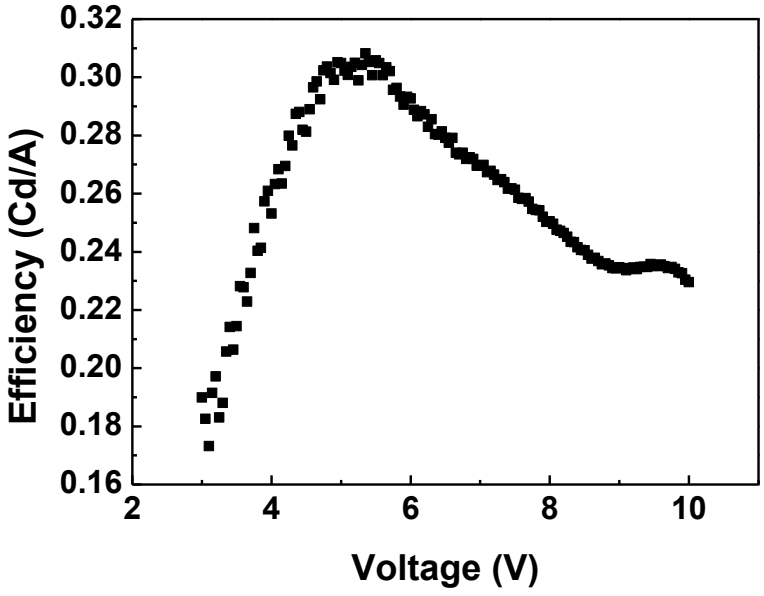

(b)

Figure 2-17. (a) Current-luminance-voltage (I-L-V) and (b) efficiency of the QD LEDs with 60 nm IGZO thin film deposited at 60 mTorr.

After devices with IGZO films of various thickness and conductivity were tested, a device with best performance was demonstrated, as shown in Fig. 2-17. The maximum brightness is 3600 Cd/m^2, the maximum luminescence efficiency is 0.31 Cd/A, and the turn on voltage is 2.6 V.

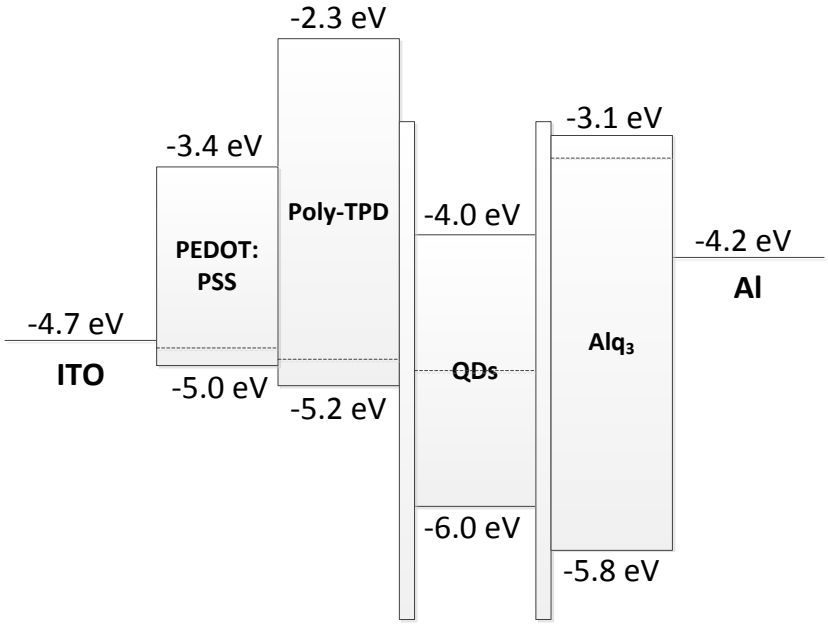

(a)

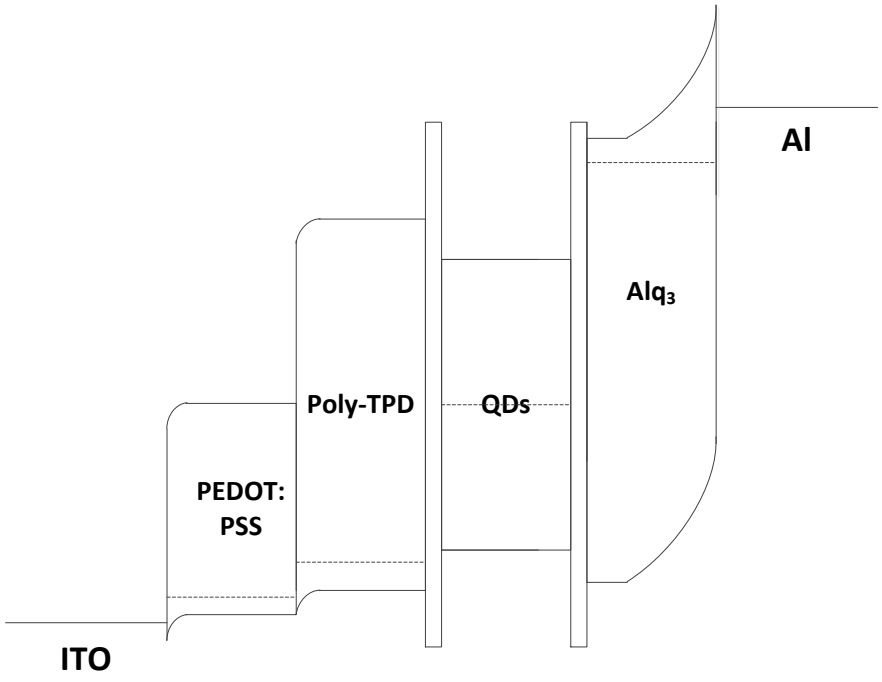

(b)

Figure 2-18. Band diagram (a) of each layer (b) under forward bias of the control QD LEDs with 15 nm Alq_3 thin films as ETL.

For comparison, a control device was also fabricated and characterized. The structure of the control device is the same except it uses 15 nm Alq_3 thin film as ETL. The band diagrams of each layer and the device under forward bias were shown in Fig. 2-18. There is a large misalignment between the work function of the Al cathode and the lowest unoccupied molecular orbital (LUMO) level of Alq_3.This band misalignment would make it difficult for electrons injected into the Alq_3 ETL.

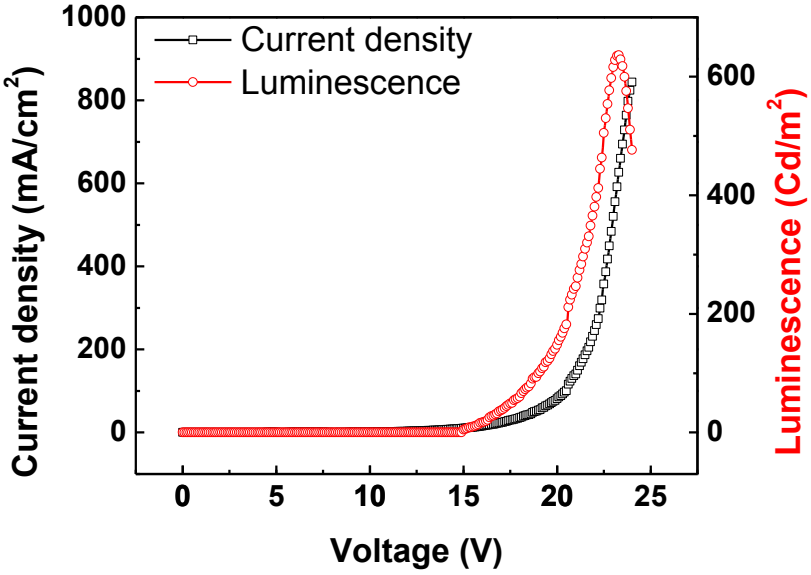

(a)

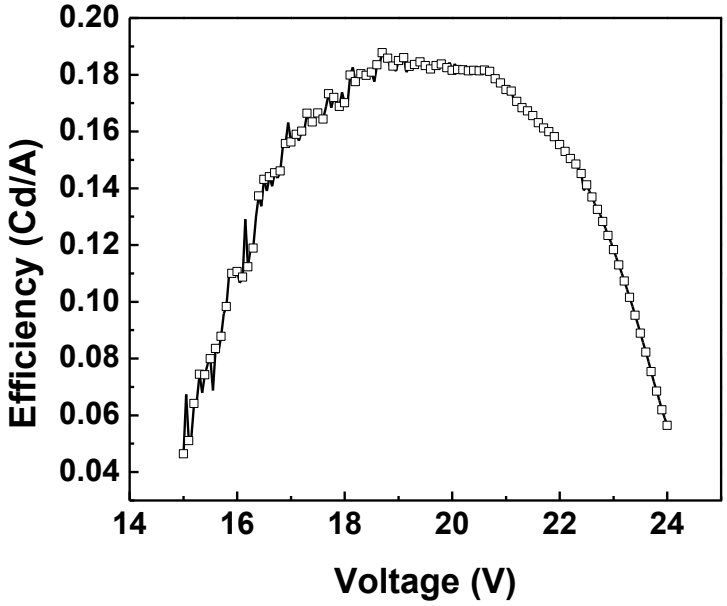

(b)

Figure 2-19. (a) Current-luminance-voltage (I-L-V) and (b) efficiency of the control QD LEDs with 15 nm Alq_3 thin films as ETL.

The characterization results are shown in Fig. 2-19. The turn on voltage 15.5V is much larger than the 2.6V value for the device with IGZO, confirming the assumption based on the band diagram. The maximum brightness is 636 Cd/m^2, the maximum luminescence efficiency is 0.19 Cd/A. The decrease in maximum brightness and luminescence efficiency could be attributed to the reason that the thickness of the Alq_3 ETL is not optimized to meet the requirement that the conductivity of the ETL and HTL should match with each other to make the recombination center of the carriers in the QD emission layer.

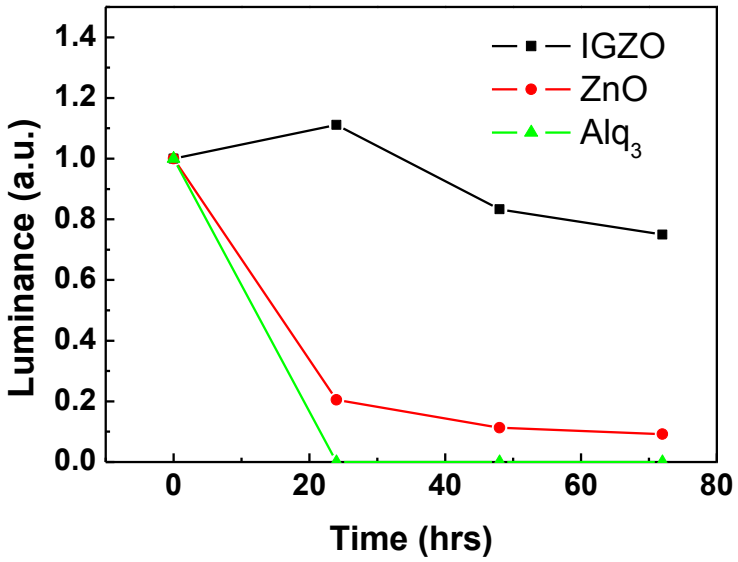

Figure 2-20. Normalized luminance of the QD LEDs using IGZO, ZnO nanoparticles, Alq_3 as ETL, devices were measured every 24 hours at driving voltage of 8V for devices with IGZO and ZnO nanoparticles, 22V for device with Alq_3.

In order to determine if the device is air-stable, the shelf life-time test was performed. Three devices with IGZO, ZnO nanoparticles, Alq_3 as ETL were placed in air atmosphere, and were characterized every 24 hours. Fig. 2-20 shows the normalized

luminance of each device. They were measured at driving voltage of 8V for devices with IGZO and ZnO nanoparticles, 22V for device with Alq_3. The QD LEDs using Alq_3 as ETL didn't emit any light after 24 hours, which can be expected since Alq_3 is sensitive to the oxygen and moisture in the air. The luminance of QD LEDs using ZnO nanoparticles as ETL also degraded fast. This could be caused by the reason that ZnO nanoparticles are sensitive to the moisture in the air. The luminance of QD LEDs using IGZO as ETL degraded relatively slowly. As a result, with IGZO as the ETL, it is possible to obtain an air-stable QD LED.

2.3.4 Conclusion

In summary, the IGZO ETL was integrated in QD LEDs employing PLD technology at room temperature. An optimized device was demonstrated by tuning the oxygen pressure of the IGZO deposition and the thin film thickness. The maximum brightness and luminescence efficiency of the optimized device can reach 3600 Cd/m^2 and 0.39 Cd/A. The turn on voltage can be as low as 2.6 V. A control device using 15 nm Alq_3 thin film as ETL was also fabricated and characterized. The maximum brightness and luminescence efficiency of the control device are 636 Cd/m^2 and 0.19 Cd/A. The turn on voltage is 15.5V. In the shelf life-time measurement, the performance of the QD LEDs using IGZO as ETL is also much better than the QD LEDs using ZnO nanoparticles or Alq_3 as ETL, which makes it possible to obtain an air-stable QD LED.

Reference

[1] V.L. Colvin, M.C. Schlamp, A.P. Alivisatos, Light-emitting diodes made from cadmium selenide nanocrystals and a semiconducting polymer, Nature, 370 (1994) 354-357.

[2] S. Coe, W.-K. Woo, M. Bawendi, V. Bulovic, Electroluminescence from single monolayers of nanocrystals in molecular organic devices, Nature, 420 (2002) 800-803.

[3] Z. Tan, F. Zhang, T. Zhu, J. Xu, A.Y. Wang, J.D. Dixon, L. Li, Q. Zhang, S.E. Mohney, J. Ruzyllo, Bright and Color-Saturated Emission from Blue Light-Emitting Diodes Based on Solution-Processed Colloidal Nanocrystal Quantum Dots, Nano Lett, 7 (2007) 3803-3807.

[4] Q. Sun, Y.A. Wang, L.S. Li, D.Y. Wang, T. Zhu, J. Xu, C.H. Yang, Y.F. Li, Bright, multicoloured light-emitting diodes based on quantum dots, Nat Photonics, 1 (2007) 717-722.

[5] http://en.wikipedia.org/wiki/Particle_in_a_box.

[6] L.E. Brus, Electron–electron and electron- hole interactions in small semiconductor crystallites: The size dependence of the lowest excited electronic state, The Journal of Chemical Physics, 80 (1984) 4403-4409.

[7] Y. Shirasaki, G.J. Supran, M.G. Bawendi, V. Bulovic, Emergence of colloidal quantum-dot light-emitting technologies, Nat Photon, 7 (2013) 13-23.

[8] Z.D. Popovic, H. Aziz, Reliability and degradation of small molecule-based organic light-emitting devices (OLEDs), Ieee J Sel Top Quant, 8 (2002) 362-371.

[9] H. Aziz, Z.D. Popovic, Degradation phenomena in small-molecule organic light-emitting devices, Chem Mater, 16 (2004) 4522-4532.

[10] F. So, D. Kondakov, Degradation Mechanisms in Small-Molecule and Polymer Organic Light-Emitting Diodes, Adv Mater, 9999 (2010) NA.

[11] A.B. Djurišić, T.W. Lau, L.S.M. Lam, W.K. Chan, Influence of atmospheric exposure of tris (8-hydroxyquinoline) aluminum (Alq3): a photoluminescence and absorption study, Appl Phys A, 78 (2004) 375-380.

[12] X. Zhou, J. He, L.S. Liao, M. Lu, X.M. Ding, X.Y. Hou, X.M. Zhang, X.Q. He, S.T. Lee, Real-Time Observation of Temperature Rise and Thermal Breakdown Processes in Organic LEDs Using an IR Imaging and Analysis System, Adv Mater, 12 (2000) 265-269.

[13] S. Chung, J.-H. Lee, J. Jeong, J.-J. Kim, Y. Hong, Substrate thermal conductivity effect on heat dissipation and lifetime improvement of organic light-emitting diodes, Applied Physics Letters, 94 (2009) -.

[14] Z. Tan, X. Jian, Z. Chunfeng, T. Zhu, Z. Fan, B. Hedrick, S. Pickering, J. Wu, H. Su, S. Gao, A.Y. Wang, B. Kimball, J. Ruzyllo, N.S. Dellas, S.E. Mohney, Colloidal nanocrystal-based light-emitting diodes fabricated on plastic toward flexible quantum dot optoelectronics, J Appl Phys, 105 (2009) 034312-034312-034315.

[15] J.-M. Caruge, J.E. Halpert, V. Bulović, M.G. Bawendi, NiO as an Inorganic Hole-Transporting Layer in Quantum-Dot Light-Emitting Devices, Nano Lett, 6 (2006) 2991-2994.

[16] V. Wood, M.J. Panzer, J.E. Halpert, J.M. Caruge, M.G. Bawendi, V. Bulović, Selection of Metal Oxide Charge Transport Layers for Colloidal Quantum Dot LEDs, Acs Nano, 3 (2009) 3581-3586.

[17] V. Wood, M.J. Panzer, J.-M. Caruge, J.E. Halpert, M.G. Bawendi, V. Bulović, Air-Stable Operation of Transparent, Colloidal Quantum Dot Based LEDs with a Unipolar Device Architecture, Nano Lett, 10 (2009) 24-29.

[18] J.M. Caruge, J.E. Halpert, V. Wood, V. Bulovic, M.G. Bawendi, Colloidal quantum-dot light-emitting diodes with metal-oxide charge transport layers, Nat Photon, 2 (2008) 247-250.

[19] L. Qian, Y. Zheng, J. Xue, P.H. Holloway, Stable and efficient quantum-dot light-emitting diodes based on solution-processed multilayer structures, Nat Photon, 5 (2011) 543-548.

[20] L. Wang, D.W. Matson, E. Polikarpov, J.S. Swensen, C.C. Bonham, L. Cosimbescu, J.J. Berry, D.S. Ginley, D.J. Gaspar, A.B. Padmaperuma, Highly efficient blue organic light emitting device using indium-free transparent anode Ga:ZnO with scalability for large area coating, J Appl Phys, 107 (2010) -.

[21] M. Kimura, T. Kamiya, T. Nakanishi, K. Nomura, H. Hosono, Intrinsic carrier mobility in amorphous In--Ga--Zn--O thin-film transistors determined by combined field-effect technique, Applied Physics Letters, 96 (2010) 262105-262103.

[22] M.-C. Chen, T.-C. Chang, C.-T. Tsai, S.-Y. Huang, S.-C. Chen, C.-W. Hu, S.M. Sze, M.-J. Tsai, Influence of electrode material on the resistive memory switching property of indium gallium zinc oxide thin films, Applied Physics Letters, 96 (2010) 262110-262113.

[23] L. Haojun, P. Wellenius, L. Lunardi, J.F. Muth, Transparent IGZO-Based Logic Gates, Electron Device Letters, IEEE, 33 (2012) 673-675.

[24] A. Suresh, P. Gollakota, P. Wellenius, A. Dhawan, J.F. Muth, Transparent, high mobility InGaZnO thin films deposited by PLD, Thin Solid Films, 516 (2008) 1326-1329.

Chapter 3

Nonradiative energy transfer between colloidal quantum dot-phosphors and inorganic diodes

3.1 Introduction

3.1.1 Förster resonance energy transfer

Förster resonance energy transfer (FRET) is a type of energy transfer between two chromophores. The diagram of the FRET mechanism is shown in Fig. 3-1. A donor chromophore in its electronic excited state can transfer energy to an acceptor chromophore through a nonradiative pathway due to the dipole-dipole coupling.

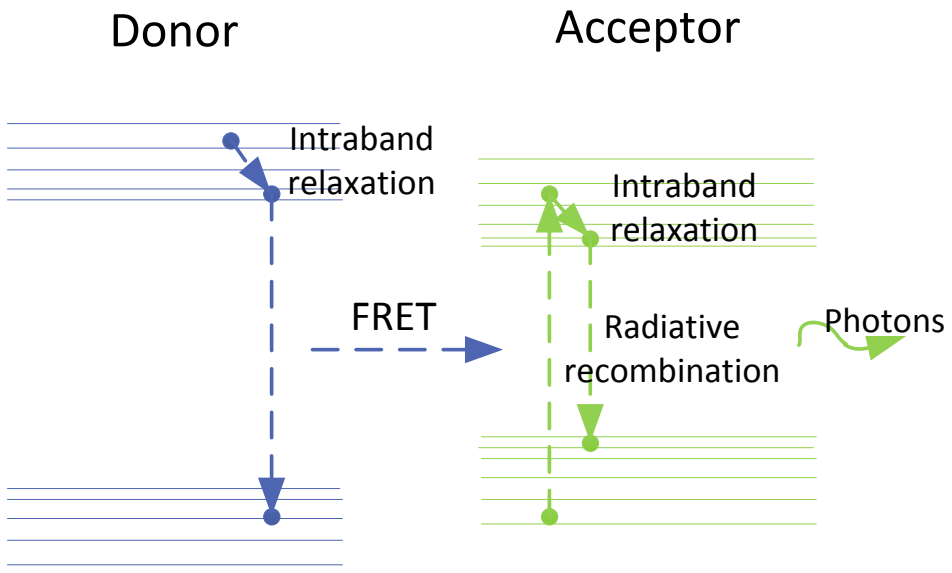

Figure 3-1 Förster resonance energy transfer mechanism.

This nonradiative energy transfer efficiency is inversely proportional sixth power of the distance between these two chromophores, which is highly sensitive to this distance. As a result, the FRET can only be observed when two chromophores are very close to each other.

3.1.2 Nonradiative energy transfer between colloidal quantum dot-phosphors and quantum wells

A Förster type resonance energy transfer between colloidal quantum dot-phosphors and quantum wells (QWs) was recently observed and reported [1]. As mentioned previously, colloidal compound quantum dots (QDs) have recently been introduced to white light emitting diode (LED) technology as a new family of phosphor materials with many superior properties [2-5]. Due to strong quantum confinement, semiconductor QDs, such as core/shell CdSe/(Zn,Cd)S QDs, are characterized by sharp exciton absorption features, high luminescence efficiency, and size-tunable emission color spanning the entire visible spectrum [6]. Much work has been done in utilizing QDs as the emissive material in LEDs [6-8]. Perhaps the most significant potential of QD-phosphors lies in the recent discovery that there exists a path for indirect injection of electron-hole pairs into QDs (for radiative recombination and thus band-edge emission from QDs) by non-contact, nonradiative energy transfer from a proximal indium gallium nitride (InGaN) QW [1]. This non-contact nonradiative energy transfer is due to the similar mechanism as FRET, as shown in Fig. 3-2.

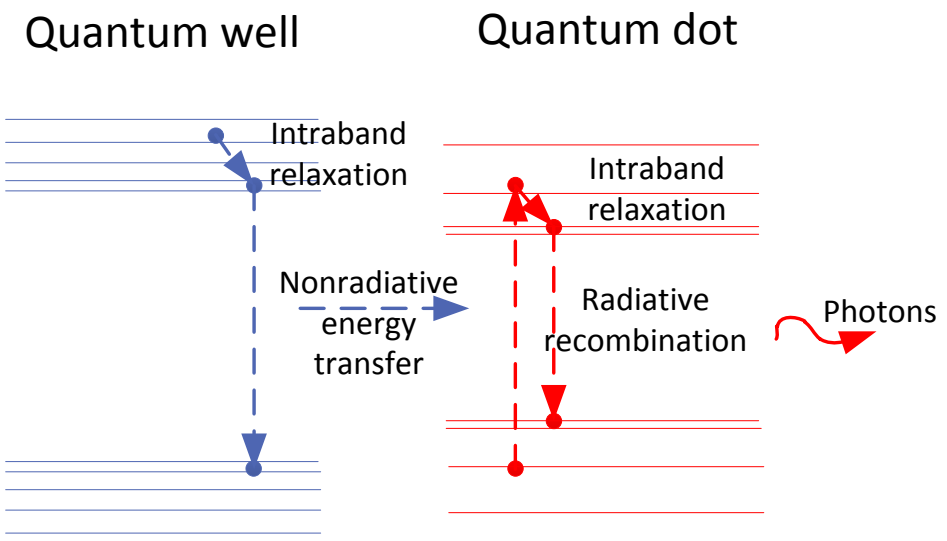

Figure 3-2 Mechanism of nonradiative energy transfer between quantum well and quantum dot.

If the QDs are in the immediate vicinity of a QW, there will be a new relaxation path for the carriers in the QW transferred into the QDs. This indirect, non-radiative energy transfer path is due to the dipole-dipole interactions associated with QW-QD coupling. After the energy transferred to the QDs, those high energy carriers will experience a fast intraband relaxation, and finally recombine primarily radiatively, emitting photons with energy determined by the QD size. Using this pathway to transfer energy to QDs has the potential of higher color conversion efficiency, because it removes several intermediate steps involved in the conventional multi step down conversion scheme for conventional phosphors such as absorption and re-emission, thereby eliminating energy losses associated with these steps.

3.2 Nonradiative energy transfer between colloidal quantum dot-phosphors and nanopillar nitride LEDs

In this section the study of the nonradiative energy transfer between colloidal quantum dot phosphors and nitride nanopillar light emitting diodes is presented. An epitaxial p-i-n indium gallium nitride (InGaN) / gallium nitride (GaN) multiple quantum well heterostructure was patterned and dry-etched to form dense arrays of nanopillars using a novel etch mask consisting of self-assembled In_3Sn clusters. Colloidal QD phosphors have been deposited into the gaps between the nanopillars, leading to sidewall coupling between the QDs and InGaN QW emitters. In this approach, close QW-QD contact and a low-resistance design of the LED contact layer were achieved simultaneously. Strong non-radiative energy transfer was observed from the InGaN QW to the colloidal QD phosphors, which led to a significant enhancement in effective internal quantum efficiency. Photoluminescence (PL) decay was used to characterize the energy transfer process between the QW and QDs. The measured rate of non-radiative QD-QW energy-transfer agrees well with the value calculated from the quantum efficiency data for the QDs in the nanopillar LEDs.

3.2.1 Introduction

Colloidal compound quantum dots (QDs) have recently been introduced to white LED technology as a new family of phosphor materials with many superior properties [2-5]. Due to strong quantum confinement, semiconductor QDs, such as core/shell CdSe/(Zn,Cd)S QDs, are characterized by sharp exciton absorption features, high

luminescence efficiency, and size-tunable emission color spanning the entire visible spectrum [6]. QDs of the same chemical composition and different size can therefore be employed to provide multiple spectral components in the white LEDs output, with improved color qualities and aging performance [9]. Perhaps the most significant potential of QD phosphors lies in the recent discovery that there exists a path for indirect injection of electron-hole pairs into QDs (for radiative recombination and thus band-edge emission from QDs) by non-contact, nonradiative energy transfer from a proximal InGaN quantum well (QW) [1]. This indirect, nonradiative energy transfer path is considered to be the consequence of dipole-dipole interactions associated with QW-QD coupling and the extremely fast intraband relaxation in colloidal QDs (subpicosecond time scales). It is fundamentally different from the multi-step 'down conversion' scheme and removes several of the intermediate steps involved in color conversion, thereby eliminating energy losses associated with these steps and increasing the efficiency [10-12].

While the QD approach holds great potential for solid state lighting, the fabrication of efficient QD phosphor-based LEDs cannot be accomplished with conventional nitride LED configurations. In designing QD-QW coupled white LEDs, it is essential to keep the QDs in the immediate vicinity of the QW surface as the non-radiative energy transfer rate, $\gamma = \tau_{ET}^{-1}$, scales as d^{-4}, where d is the QD-QW distance [3]. This requirement is in conflict with the fact that a doped GaN contact layer needs to cap the InGaN QW to complete the p-i-n LED structure. Recently, Achermann *et al.* observed color conversion in an electrically pumped LED using nonradiative energy transfer between an indium gallium nitride (InGaN) / gallium nitride (GaN) QW and a monolayer of CdSe/ZnS QDs [10]. Spectroscopic measurements revealed that 13% of the radiative

power of the QW was transferred to red emission from the QDs when the QW and QDs were separated by a 5nm-thick n-type capping layer for close proximity. The ultra-thin n-type capping layer, however, was not sufficiently conductive for current spreading, which, in turn, reduced the LED efficiency. In another study [13], GaN-based LEDs were surface-patterned with deep-etched elliptical holes to accommodate colloidal QDs (acceptors) such that the nanocrystals were within close vicinity of the active layers (donors). Efficient nonradiative energy transfer was achieved via a short donor-acceptor distance, leading to a 43% increase in QD phosphor-emission over that provided by the conventional color down-conversion mechanism.

We present an alternative QD-QW coupling approach to address the conflict between the need for close proximity of QWs and QDs and the use of a sufficiently thick contact layer with a low resistance for LED operation. The p-i-n InGaN/GaN multiple quantum well (MQW) heterostructure was patterned and dry-etched to form dense arrays of nanopillars using a novel etch mask consisting of self-assembled In_3Sn clusters. Colloidal QD phosphors have been deposited into the gaps between the InGaN/GaN nanopillar LEDs, leading to sidewall coupling between the QDs and InGaN MQW emitters. The immediate QW-QD contact and low-resistance design of the LED contact layer can therefore be achieved simultaneously. Strong non-radiative energy transfer was observed from the InGaN MQW to the colloidal QD phosphors, which led to a significant enhancement in effective internal quantum efficiency for the QDs incorporated in nanopillar LEDs in comparison with those deposited over planar LED structures. PL decay was used to characterize the energy transfer process between the QWs and QDs. The measured rate of non-radiative QD-QW energy-transfer agrees well with the value

calculated from the quantum efficiency data for the QDs deposited in the nanopillar LEDs.

3.2.2 Device structure and fabrication

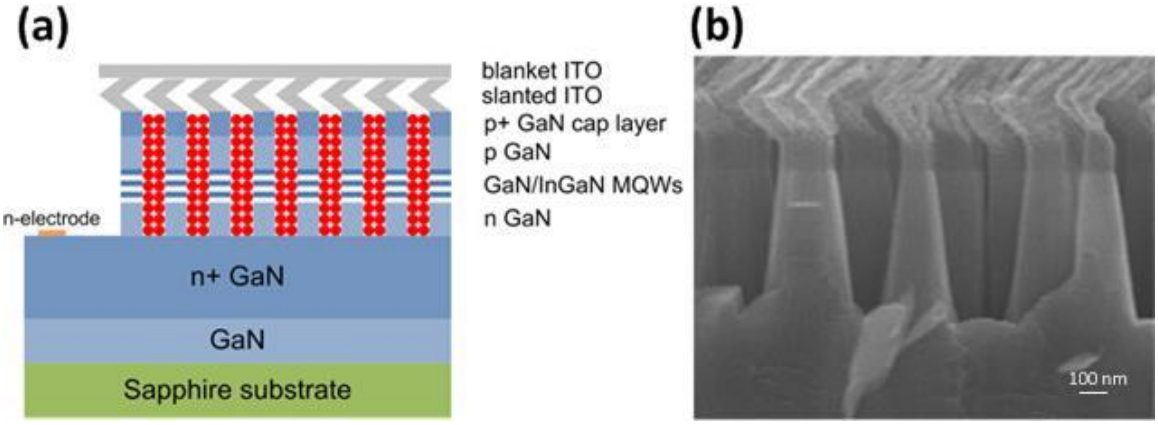

Figure 3-3. (a) Schematic of the nanopillar LEDs for the MQW-QD coupling configuration. (b) Cross-sectional SEM image of a nanopillar LED device.

Figure 3-3 shows schematically a nanopillar LED structure infiltrated with QD phosphors. Each nanopillar is configured with an InGaN/GaN MQW-embedded p-i-n heterojunction, comprising a sapphire substrate, an n^+ ($N_d \approx 5\times10^{18}cm^{-3}$) GaN buffer layer (~2 μm), an n-type ($N_d \approx 1\times10^{18}cm^{-3}$) GaN layer (~0.1 μm), three pairs of 10nm-thick $In_{0.1}Ga_{0.9}N$ quantum wells sandwiched between 50nm-thick GaN barriers, a p-type ($N_a \approx 1\times10^{18}cm^{-3}$) GaN layer (~0.2 μm), as well as a p-type ($N_a \approx 1\times10^{19}cm^{-3}$) GaN capping layer (~0.2 μm). Silicon and magnesium are the n- and p-type dopants in the LED heterojunction, respectively. The nanopillars are ~200nm in diameter, sharing the common base of the n-type GaN buffer layer, and are fabricated with a Ti/Al n-type bottom contact and a slanted indium-tin-oxide (ITO) nanowire structure serving as the p-

type top contact [14]. Finally, the sidewall surface of the nanopillars is conformably coated with QD phosphors.

The InGaN/GaN nanopillar structure is fabricated by our collaborator Dr. Joon Seop Kwak's group in Sunchon National University in Korea [15]. It is fabricated by inductively-coupled-plasma (ICP) etching using a novel etch mask of self-assembled In_3Sn nanodots, which is described as follows: A SiO_2 layer was first deposited on the top surface of the LED wafer by plasma-enhanced chemical vapor deposition (PECVD), and an indium tin oxide (ITO) layer was subsequently deposited onto the SiO_2 layer with electron beam evaporation. The as-deposited ITO film can be assumed as an oxygen-poor ITO layer, which has a mixture of metallic phase and ITO phase, since the ITO films were deposited by using electron beam evaporator [16]. Next, the sample was dipped into 3% hydrochloric (HCl) acid solution to dissolve the ITO phase, which left self-assembled metallic clusters on the SiO_2 layer. The SiO_2 layer was then patterned with a fluorine-based dry etching process using In_3Sn clusters as the etch mask. Finally, the InGaN/GaN nanopillar heterostructure was formed by dry-etching the LED wafer via the patterned SiO_2 hard mask. By controlling the size of the In_3Sn clusters and the ICP etching conditions, nanopillars of diameters ~200nm and ~50% filling factor were fabricated successfully. An etching depth of ~0.6 μm was designed to reach the n-type layer of the LED heterojunction and to laterally expose the emissive quantum wells along the sidewall of the nanopillars.

After the nanopillar structure was created, the oxide hard mask was stripped with buffered oxide etch (BOE), and Ti/Al (5nm/200nm) contact was patterned and deposited on n-type GaN as n-type electrode. For the formation of the p-type electrode, two types

of devices were fabricated. One type employed p-type GaN surfaces as the electrode, the other type deposited ITO on top of p-type GaN as the electrode. To make the ITO electrode, a slanted ITO nanowire structure was deposited on top of the nanopillars by the oblique-angle deposition method using electron beam evaporation. During the deposition, the sample stage was tilted at a large angle such that the vaporized source atoms reach the top surface of the nanopillars at a grazing angle. The high-aspect-ratio nanopillars block the vapor from reaching the lower pillar sections and the gap in between via the "shadowing effect", preventing electrical shorting of the device. In so doing, zigzagged ITO nanowires were produced on top of the nanopillars using two consecutive deposition angles (85 and -85 °), as illustrated with a cross-sectional scanning electron microscopy (SEM) image (Fig. 3-3(b)). This step was followed by a normal-angle ITO deposition (0 °) to connect the nanowires with a continuous blanket ITO film and annealing in nitrogen to enhance the conductivity and transparency of the ITO. The slanted ITO and blanket ITO is patterned with a lift-off process to make sure its area is smaller than the nanopillar area. Therefore, QDs solution can enter the gaps between the nanopillars more easily.

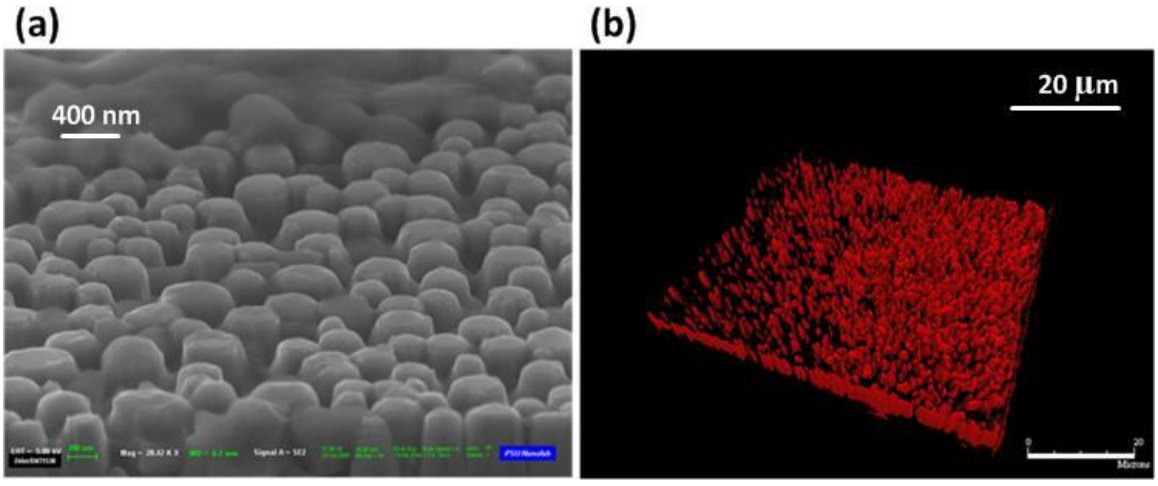

Figure 3-4. (a) SEM image and (b) Z-scan confocal fluorescent microscope image of the QD-coated nanopillars.

Finally, a layer of colloidal CdSe/CdS core/shell QDs (QSP-620, Ocean Nanotech LLC) with PL emission centered at 620nm was deposited over the surface of the nanopillars by soaking the nanopillar device in the QD solution for ~12 hours. Figure 3-4(a) and (b) show, respectively, the SEM image and z-scan 3D confocal fluorescent microscope image of the QD-coated nanopillars (before slanted ITO deposited), confirming the conformal deposition of QDs over the sidewalls of the nanopillar structure.

3.2.3 Results and discussion

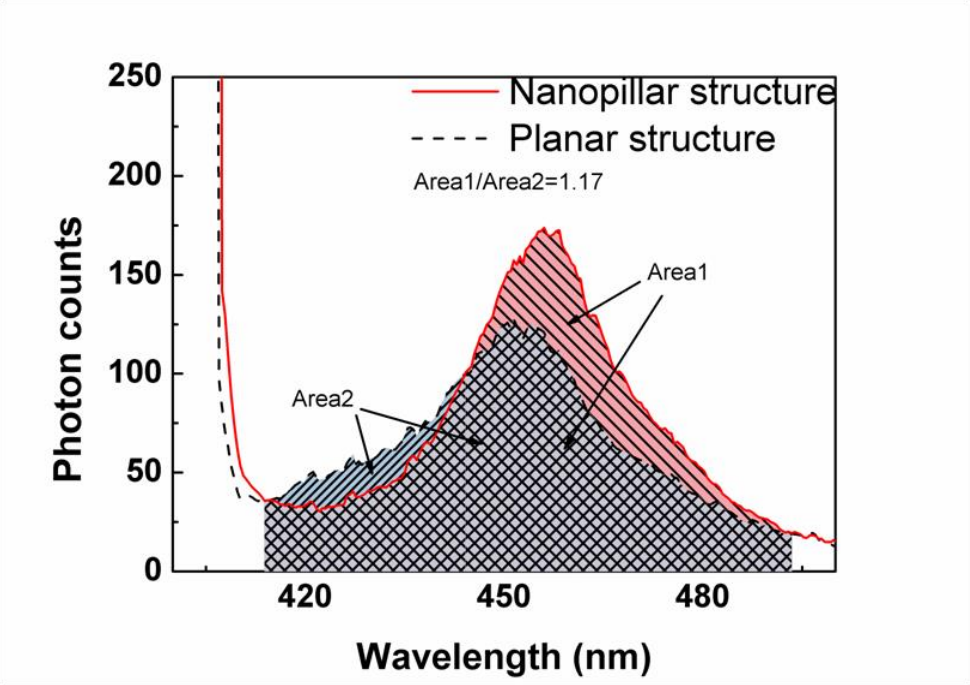

Figure 3-5. Photoluminescence spectra of the nitride LED heterostructure before and after the nanopillar processing.

Figure 3-5 compares the PL spectra of the GaN heterojunction before and after the nanopillar processing. The PL intensity of the InGaN QWs was spectrally integrated from 410nm to 490nm, showing a ratio of 1.17:1 between the PL emission of the nanopillar and planar structure. The observed PL enhancement for the InGaN/GaN nanopillars can be interpreted considering two mechanisms. First, the radiative recombination efficiency of (In, Ga)N is not susceptible to the surface states created during the dry etching-formation of nanopillars due to the ionic nature of the material [17]. Secondly, light extraction efficiency is substantially improved in the nanopillars by means of the reduction in total internal reflection. Hence the nanopillar LED structure with augmented brightness provides us with a proper template to investigate the nonradiative recombination between colloidal QDs and InGaN QWs for high color conversion efficiency.

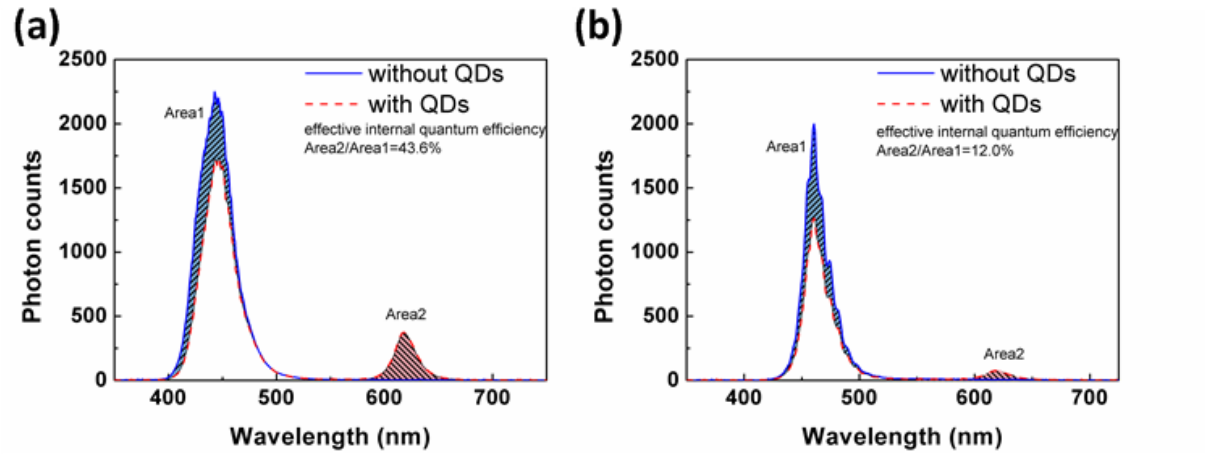

Figure 3-6. (a) Electroluminescence spectra of the nanopillar LED sample with and without QD coupling; (b) Electroluminescence spectra of a planar control sample with and without QD coupling. Both samples are from the same LED heterostructure.

The output spectra of a nanopillar LED prior to and after QD deposition was plotted in Fig. 3-6(a). The LED was forward biased with a current density of 62.5mA/cm^2. The shaded areas represent, respectively, the portion of nitride (blue) emission absorbed by the QD coating and the red emission from the same layer of QDs. The color-conversion quantum efficiency (η_c), defined as the ratio of the photon count from the QD emission ($N_{QD}^{QW\leftrightarrow QD}$) upon QW-QD coupling to that from the net QW emission without QD coupling (N^{QW}), $\eta_c = N_{QD}^{QW\leftrightarrow QD} / N^{QW}$, was calculated to be ~12.4%. In addition, an effective internal quantum efficiency of QD emission, $\eta_{eqi} = N_{QD}^{QW\leftrightarrow QD} / \left(N^{QW} - N_{QW}^{QW\leftrightarrow QD} \right)$, was defined in the present study, wherein $N_{QW}^{QW\leftrightarrow QD}$ represents the photon count of blue emission from the coupled QW-QD system. An effective internal quantum efficiency of η_{eqi}=43.6% was calculated from the output spectra of the nanopillar LED (Fig. 3-6a).

For the sake of comparison, a control sample was prepared by depositing QDs on the top surface of a planar LED structure containing an identical p-i-n heterojunction as well as a planar top ITO contact. The deposition condition was carefully tailored to ensure that approximately the same number of QDs were deposited on both the planar and nanopillar LEDs, which was verified by optical density (OD) characterization. In the control sample, QDs are physically separated from the InGaN quantum wells by a 240nm-thick p-type GaN capping layer as well as a 200nm-thick ITO coating. The color conversion in the control sample can be implemented only via the processes of absorption and re-emission that are typical for the PL phenomenon. The emission spectra of the planar control sample prior to and after the QD deposition are shown in Fig. 3-6(b). The

internal quantum efficiency of the QDs in the planar control sample was calculated to be $\eta_{eqi} \approx 12.0\%$, which is consistent with the intrinsic PL quantum yield (η_i) of the QD films that was measured with the integrating sphere technique.

Compared with QDs in the control sample, the effective internal quantum efficiency of the QDs incorporated in a nanopillar LED exhibits a remarkable augmentation from 12.0% to 43.6%, increased to 3.63 times of the value of the control sample. Since the intrinsic quantum yield of the QDs (η_i) does not exhibit any dependence on the substrate topography, the dramatically enhanced effective internal quantum efficiency of the QDs in nanopillar LEDs can be interpreted only by the presence of substantial nonradiative energy transfer between the QDs and QWs at the sidewall of the nanopillars.

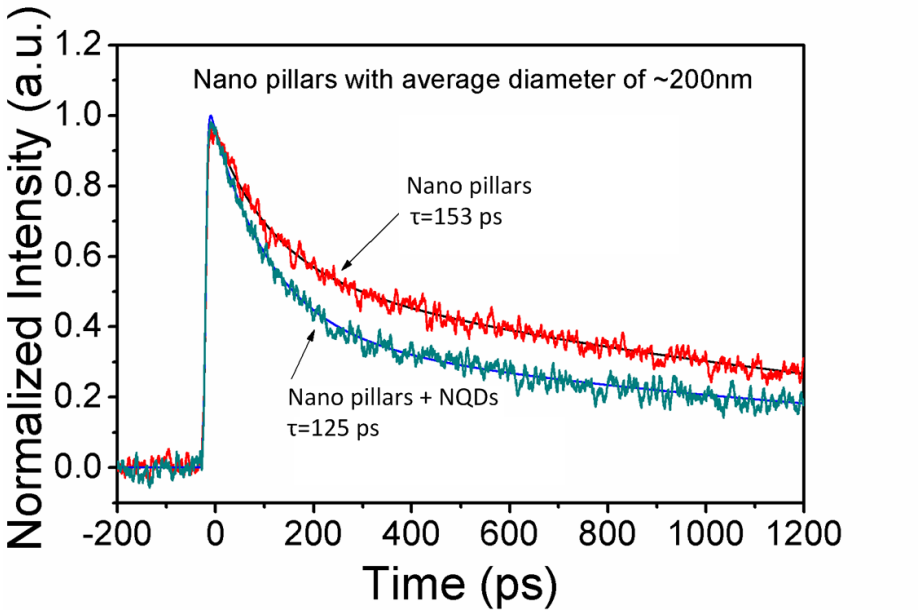

Figure 3-7. Photoluminescence decay characterization of a nanopillar LED sample with and without QD overcoating. The nanopillars exhibit an average diameter of ~200nm.

Finally, a PL decay study was conducted to confirm the existence of the nonradiative energy transfer. As illustrated in Fig. 3-7, a decay lifetime of ~150 ps was measured in the nanopillars without QDs, whereas the lifetime drops to 125 ps upon the QD deposition over the surfaces of the nanopillars, indicating the carriers in the InGaN QWs decay faster with the presence of QDs. Since the deposition of QDs does not change the intrinsic carrier dynamics of the InGaN QWs, this faster decay suggests that an additional relaxation channel is introduced for the carriers in the InGaN QWs, which can only be the nonradiative energy transfer from QWs to QDs. The rate of nonradiative energy transfer, $r_{transfer}^{QW\to QD}$, can therefore be determined directly as $r_{transfer}^{QW\to QD}=\frac{1}{125}-\frac{1}{153}=1.46\text{ns}^{-1}$. This value becomes comparable to the rate of radiative recombination, suggesting the important role of non-radiative energy transfer in the color conversion process of QD-coupled nanopillar LEDs.

The rate of nonradiative energy transfer can also be obtained and confirmed from the electroluminescence results in Fig. 3-6. The luminescence of the QDs in the nanopillar structure can be expressed as

$$N_{QD}^{QW\leftrightarrow QD}=\eta_i\left(N^{QW}-N_{QW}^{QW\leftrightarrow QD}\right)+j\eta_i\frac{r_{transfer}^{QW\to QD}}{r_r^{QW}+r_{nr}^{QW}+r_{transfer}^{QW\to QD}} \quad (1)$$

$$N^{QW}-N_{QW}^{QW\leftrightarrow QD}=j\left(1-T\right)\frac{r_r^{QW}}{r_r^{QW}+r_{nr}^{QW}+r_{transfer}^{QW\to QD}} \quad (2)$$

where $N^{QW}-N_{QW}^{QW\leftrightarrow QD}$ measures the portion of the QW (blue) emission absorbed by the QDs, j is the current injection into the InGaN QWs, $(1–T)$ is the absorbance of the QDs incorporated in the LEDs, r_r^{QW} is the rate of radiative recombination in the InGaN QWs,

$r_{transfer}^{QW\to QD}$ the rate of nonradiative energy transfer between CdSe/ZnS QDs and InGaN QWs, and r_{nr}^{QW} the rate of nonradiative relaxation in the InGaN QWs. In Eq. (1), the first term represents the QD emission due to the absorption-re-emission processes, whereas the second term represents the QD emission due to nonradiative energy transfer. The effective internal quantum efficiency of the QDs is therefore

$$\eta_{eqi} = \eta_i \left(1 + \frac{r_{transfer}^{QW\to QD}}{r_r^{QW}(1-T)} \right) \qquad (3)$$

In the present work, $r_{transfer}^{QW\to QD}$ can be calculated from Eq. 3 using the measured parameters, η_{eqi}~43.6.0%, η_i~12.0%, (1-T) ~25.2%, as well as the reported value for r_r^{QW} ~2.0 ns^{-1}, which gives $r_{transfer}^{QW\to QD} \sim 1.32$ ns^{-1}. This result agrees well with the energy transfer rate (1.46 ns^{-1}) obtained from the aforementioned PL decay study, which adds further evidence to the presence of nonradiative energy transfer between InGaN QWs and CdSe/ZnS QDs.

3.2.4 Conclusion

In summary, with the nanopillar nitride LED structure, close QW-QD contact and a low-resistance design of the LED contact layer were achieved simultaneously. Strong non-radiative energy transfer was observed from the InGaN QW to the colloidal QD phosphors, which led to a significant enhancement in effective internal quantum efficiency. In addition, PL decay measurement was employed to characterize the energy

transfer process between the QW and QDs. The measured rate of non-radiative QD-QW energy-transfer agrees well with the value calculated from the quantum efficiency data for the QDs in the nanopillar LEDs.

3.3 Nonradiative energy transfer between colloidal quantum dot-phosphors and silicon carbide diodes

In this section, nonradiative energy transfer between colloidal quantum dot-phosphors and the active region of an indirect band-gap semiconductor diode was investigated. A silicon carbide (SiC) p-n junction was fabricated and surface-patterned with arrays of holes, facilitating the sidewall coupling between the QDs and the SiC p-n junction. Nonradiative energy transfer was observed from the SiC diode to the colloidal QD-phosphors, which was characterized with a color conversion efficiency of 3.1%. Photoluminescence decay measurements were conducted to verify and characterize the energy transfer process between the diode and QDs. The carrier recombination lifetime of SiC was found to decrease upon the presence of QD-phosphors, which provides further evidence for the presence of the nonradiative energy transfer path between the QDs and the SiC diode.

3.3.1 Introduction

The technology of white LEDs is playing a key role in solid state lighting; most of the white LEDs currently in use employ blue emitters in combination with yellow phosphors to produce white light from the emission of complementary colors. However, such white output is inferior in "color rendering" ability to natural daylight, which is characterized by a low color rendering index (CRI). Colloidal compound QDs have recently been introduced to white LED technology as a new family of phosphors due to their superior optical properties [7, 18-20], including high quantum yield, narrow

emission bandwidth, and size tunable emission wavelength over a broad spectral regime. Therefore, QDs of the same chemical composition, but varying sizes, can be employed as phosphors to provide multiple spectral components in white LED output [21, 22].

The potential uses of QD phosphors has increased due to the recent discovery of a path for indirect injection of electron-hole pairs into QDs by non-contact, nonradiative energy transfer from the bulk junction of direct band-gap semiconductors that are in close proximity to the nanoparticles [1]. When QDs are in the immediate vicinity of the carrier recombination region of the p-n junction of direct band-gap semiconductors, there exists a unique relaxation path for the free carriers in the bulk semiconductor transferring their energy into the QDs. This indirect, nonradiative energy path arises from the dipole-dipole interaction associated with the quantum coupling between QDs and direct band-gap semiconductors [1]. In solid state lighting, this newly uncovered pathway has been proposed to facilitate energy transfer from blue-emitting InGaN quantum wells into green and red CdSe/ZnS core-shell QD phosphors. The nonradiative energy transfer can potentially enhance the efficiency of the color conversion process because it removes several intermediate steps involved in the conventional multi-step down conversion scheme, such as absorption and re-emission, thereby eliminating energy losses associated with these steps.

While this novel application of QD phosphors has been widely investigated [10, 23, 24], all the studies reported to date are focused on the energy coupling between QDs and direct band-gap semiconductors, such as InGaN and GaN. We report in this communication our studies of nonradiative energy transfer between QD-phosphors and the p-n junction of an indirect band-gap semiconductor. A SiC p-n junction was

fabricated and surface-patterned with arrays of holes, facilitating sidewall-coupling between the QDs and the SiC p-n junction. Nonradiative energy transfer was observed from the SiC diode to colloidal QD-phosphors that accumulated in the holes. Enhanced red emission of QDs was measured from characterization of the electroluminescence spectra of the diode, with a color conversion quantum efficiency calculated to be 3.1%. PL decay was also performed, and the PL decay lifetime of the SiC junction was found to decrease from 24.1 ns to 21.7 ns following the QD deposition, further confirming the existence of the nonradiative energy transfer path between the QDs and the SiC diode.

3.3.2 Device structure and fabrication

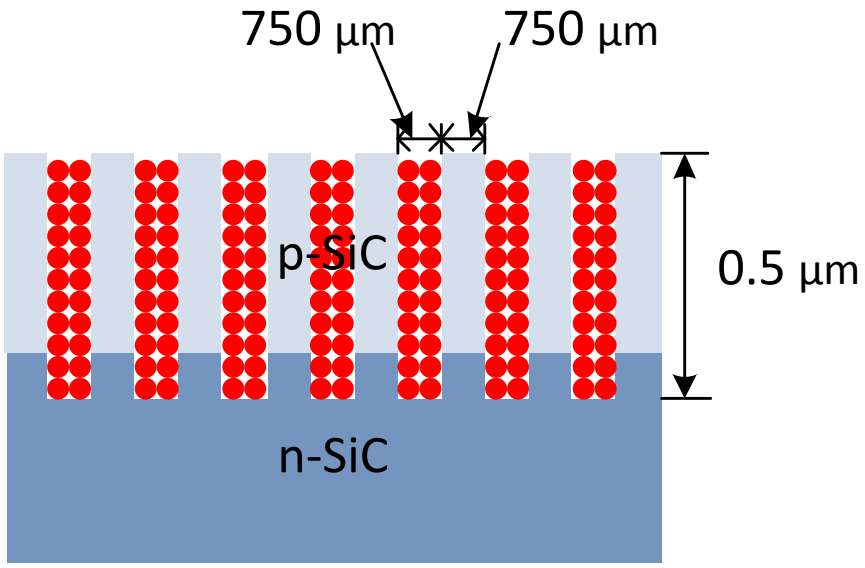

(a)

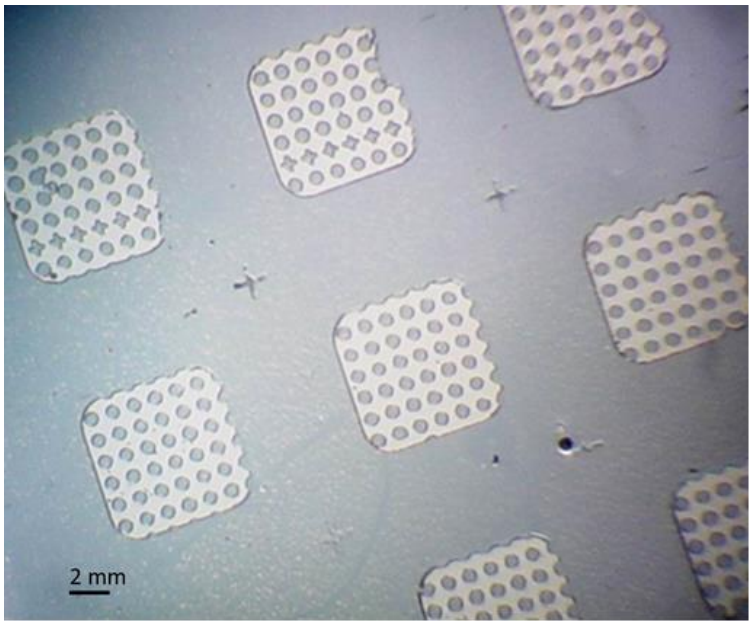

(b)

Figure 3-8. (a) Schematic of the SiC diode (b) Top view of the SiC diode.

Figure 3-8(a) shows schematically the SiC diode with arrays of holes that are infiltrated with QDs. The SiC diode with arrays of holes is fabricated by our collaborator Dr. Feng Zhao's group in Washington State University in United States. Each hole is configured to trench through the p-n homojunction, with a 2 μm/1×10^{16} cm^{-3} n-type epitaxial 4H-SiC layer doped by nitrogen grown on an 8 °off-axis n-type 4H-SiC wafer. The p-type regions, with an area of 1×1 mm^2, were formed by aluminum ion implantation with the energy/dose of 100 keV/1.5×10^{15} cm^{-2}, followed by an implant anneal process at 1600 ℃ for 30 minutes. To avoid Si outgassing from the sample during annealing, a graphite layer was used to protect the surface during the implant anneal. A 1000Å Ni layer was deposited on the backside of the sample by e-beam evaporation to form the n-type cathode contact. Photolithography was then used to pattern the anode contact arrays

with 750μm hole openings in the p-type front side of the sample, as illustrated in the photomicrograph (Fig. 3-8b). Finally, a Ti/Al/Ti/Ni (200Å/400Å /200Å/1000Å) metal stack was deposited by e-beam evaporation and followed by lift-off to form the p-type anode contacts. Both anode and cathode contacts were annealed by rapid thermal annealing (RTA) at 1000 ℃ for 2 minutes to form ohmic contacts. The holes on the anode contacts have a nominal depth of 0.5μm, which were etched through the p-type SiC layer and into the n-type SiC layer by reactive ion etching (RIE) using SF_6 process gas. The QD phosphor employed in the study was colloidal CdSe/ZnS core/shell QDs (QSP-620, Ocean Nanotech LLC) that were surface-coated with amine ligands. The nanoparticles exhibited a PL peak at λ=620 nm, and were accumulated into the holes of the SiC diode by soaking the devices in a toluene solution of QDs for 12 hours.

3.3.3 Results and discussion

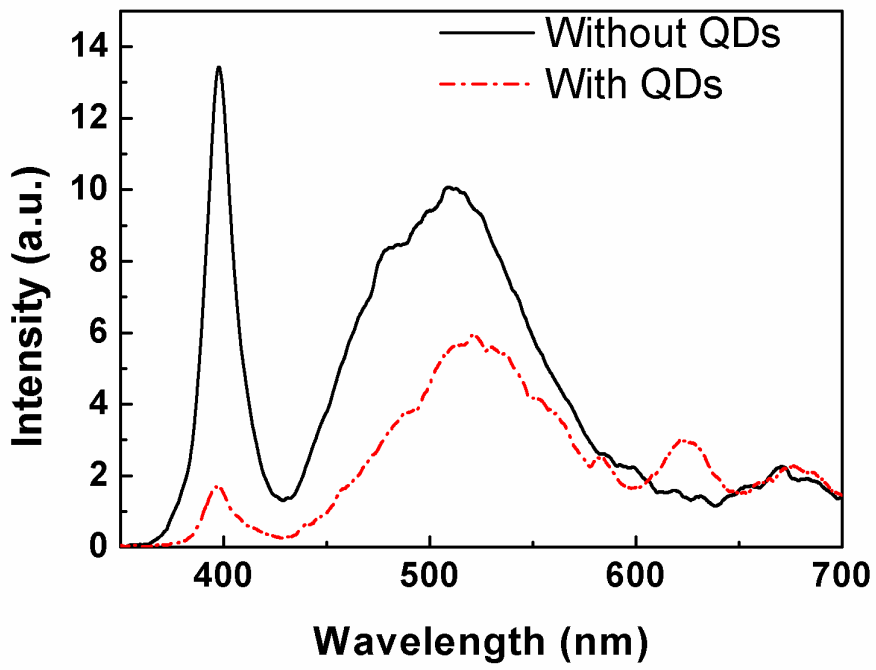

Figure 3-9. Electroluminescence spectra of the SiC diode with and without coupled QDs.

In this experiment, the diode was forward-biased with a 90mA pulse-current at the repetition rate of 1000 Hz and 50% duty cycle. The output electroluminescence (EL) spectra of a SiC diode prior to and after QD infiltration are plotted in Fig. 3-9. Since SiC is an indirect band-gap semiconductor, the EL emission of the diode is weak and comprised of two primary spectral features: a near ultra violet (UV) band and a green band. The near UV emission is intrinsically narrow and arises from carrier relaxation via the indirect band-gap of SiC, while the broader green band is due to defect states of the material [25]. After the QD infiltration, the red emission can be observed resulting from the coupling between QDs and SiC. The color conversion (quantum) efficiency (η_c),

defined as the ratio of the photon counts from SiC-QD coupled device ($N_{QD}^{SiC\leftrightarrow QD}$) to that from the net SiC emission(N^{SiC}), $\eta_c = N_{QD}^{SiC\leftrightarrow QD} / N^{SiC}$, was calculated to be 3.1% from Fig. 3-9, by calculating the ratio of the area of red QD emission to that of the blue-green emission of the pristine SiC diode prior to QD deposition.

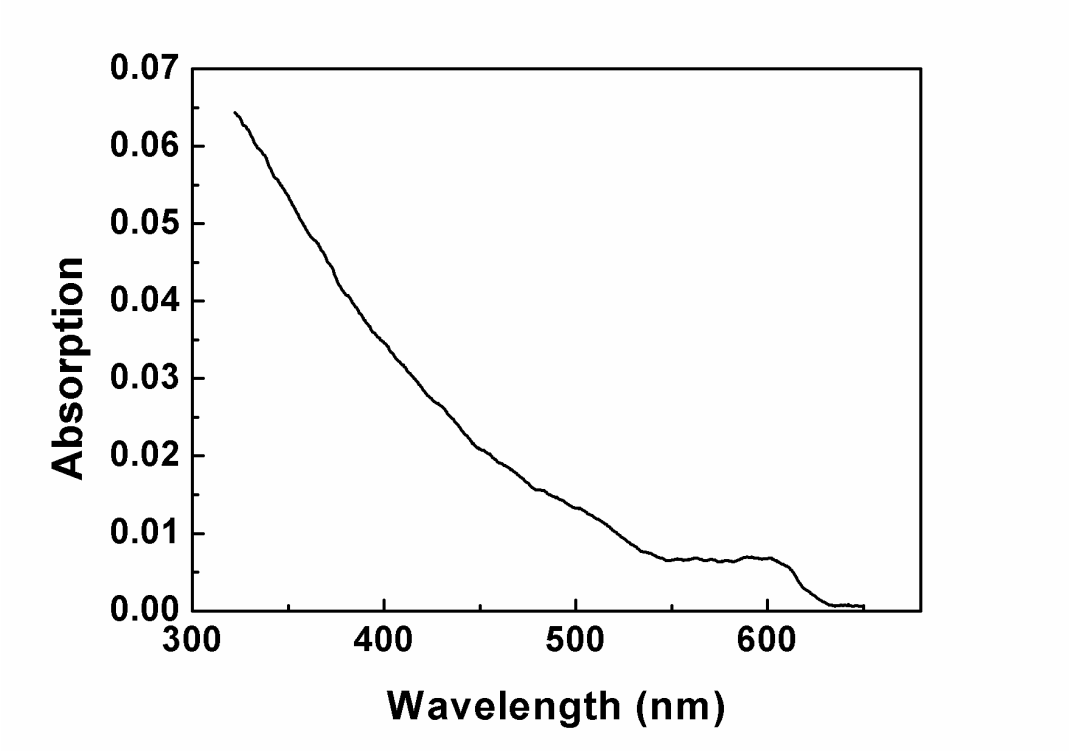

(a)

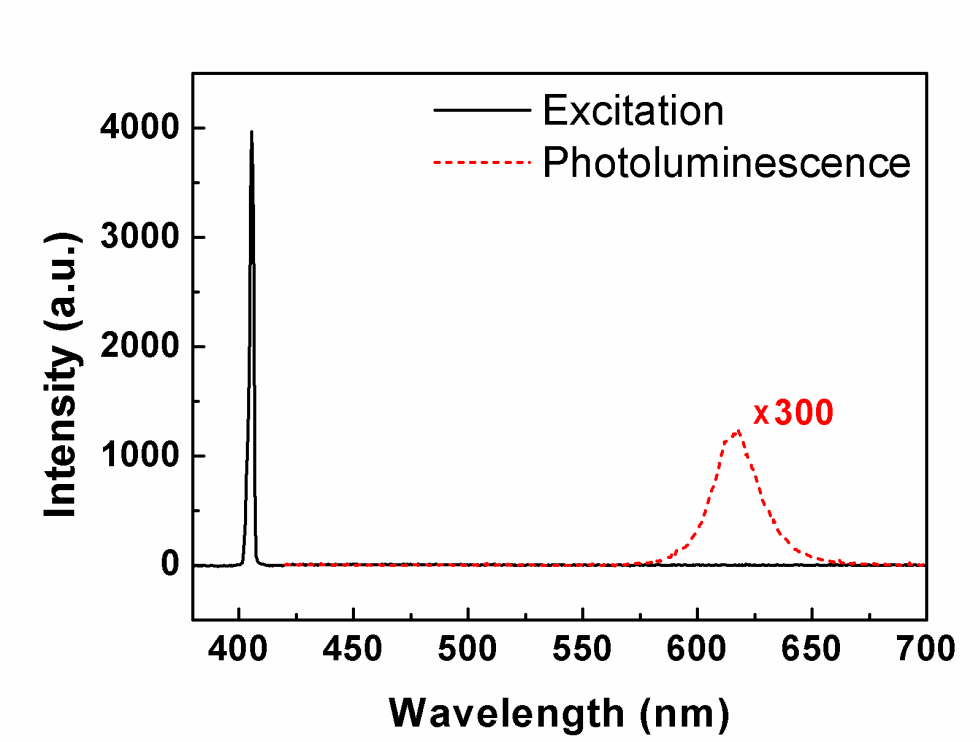

(b)

Figure 3-10. (a) Absorption spectrum of the QD thin film (b) Excitation and photoluminescence spectra of the QD thin film.

In order to accurately assess the fraction of the color conversion efficiency due to the nonradiative energy transfer process, it is necessary to exclude the contribution to the observed QD emission via the traditional absorption/re-emission path. A control sample of QD film was obtained on a UV-ozone cleaned glass substrate via the same soaking processes that used in the aforementioned QD deposition on SiC sample. The absorption spectrum of the QD film was recorded using a Perkin-Elmer Lambda 19 UV/visible/near infrared spectrometer, as shown in Fig. 3-10(a). The mean absorbance of the SiC emission by the QD film can be calculated by integrating spectra of the QD absorption and the EL emission of SiC diode, yielding a value of 0.017. Next, the integration sphere

technique was used to determine the quantum yield of the QD film, using a pump source of 405nm diode laser. The spectra of the excitation and PL of the thin film were presented in Fig. 3-10(b), and the measured quantum yield is ~ 36.9%. Given the fact that the quantum yield of QDs varies little with the excitation wavelength, the conversion efficiency of the traditional absorption/re-emission path can be consequently calculated as the product of the mean absorbance (0.017) and the QD quantum yield (36.9%) of the QD film, resulting in an efficiency of ~0.63%. As such, the quantum efficiency of the QD emission via the nonradiative energy transfer path can be determined as 3.1%-0.63% = 2.47%. The above analysis reveals that the pronounced attenuation in the EL intensity following the QD incorporation into the SiC diode is not induced by the traditional absorption/re-emission of the QD film, but instead by the non-radiative energy transfer between QDs and SiC diode.

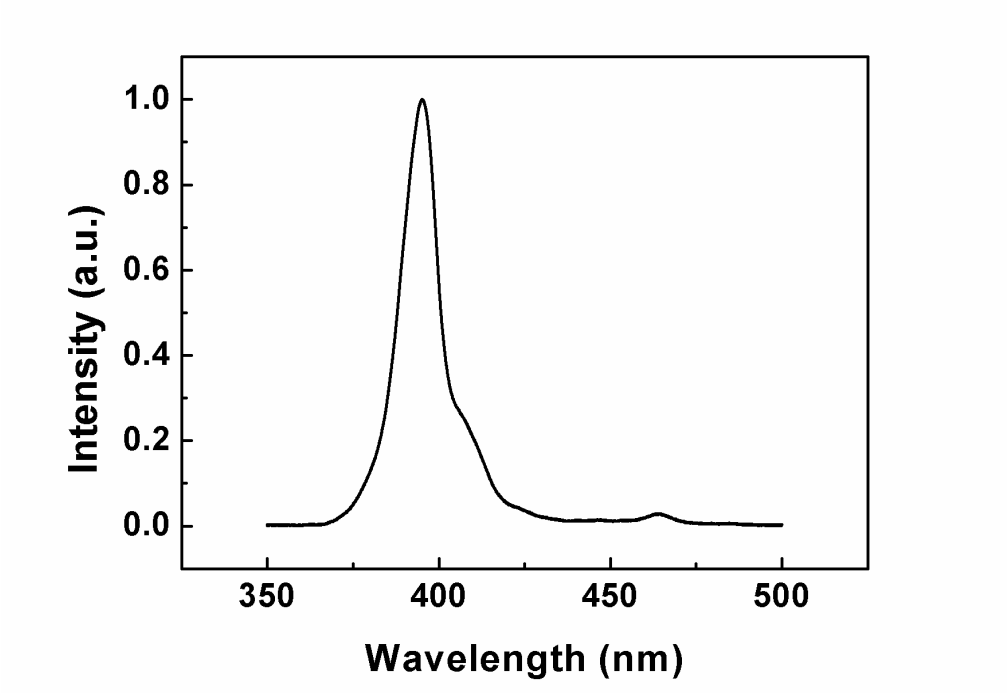

(a)

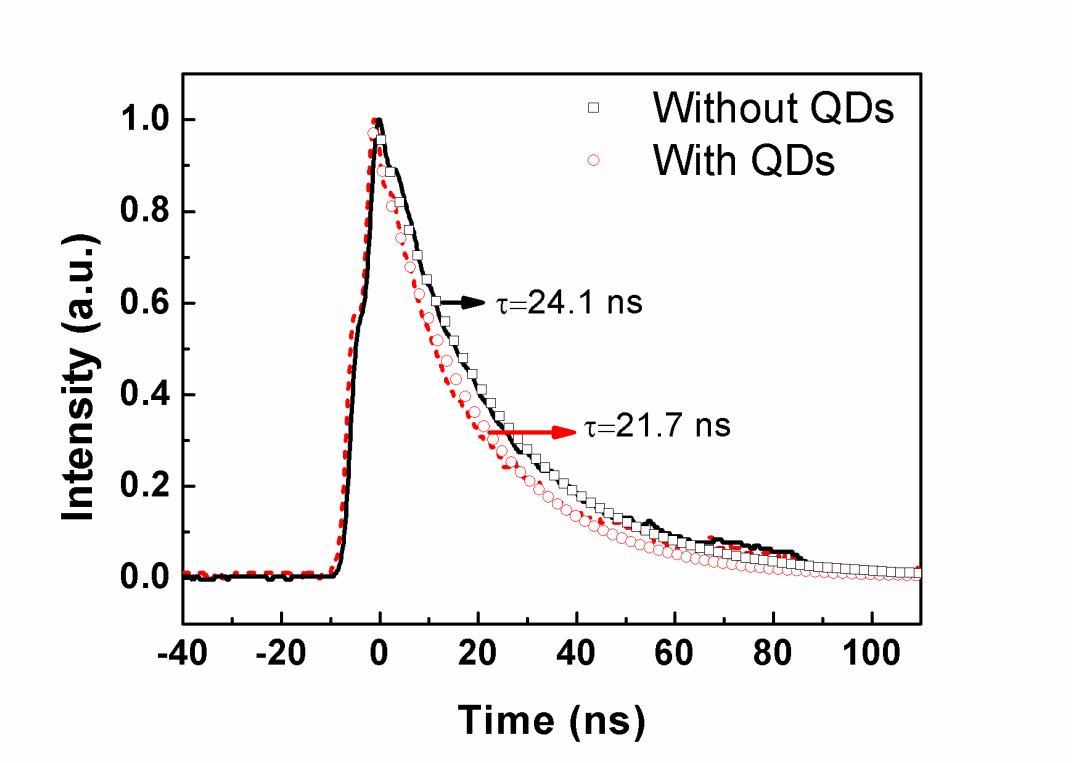

(b)

Figure 3-11. (a) Photoluminescence spectrum of the SiC diode without QDs. (b) Photoluminescence decay of the SiC (392 nm) with and without QDs coating.

Finally, PL decay measurements were conducted to determine the rate of nonradiative energy transfer between QDs and the SiC p-n junction. The PL spectrum of the SiC material exhibits a peak at ~392 nm, which matches well with the indirect band-gap energy (~3.2 eV) of SiC (Fig. 3-11a). By resolving the temporal decay of the indirect band-gap emission of the SiC diode with and without QD phosphor coating, the carrier relaxation process in the p-n junction was revealed, as plotted in Fig. 3-11(b). A recombination lifetime of ~24.1 ns was measured in the diode without the QD phosphors, whereas the lifetime dropped to 21.7 ns after QD phosphor deposition, indicating that the carriers in the SiC diode relax faster in the presence of QDs. Since the deposition of QDs

does not change the intrinsic carrier dynamics of the SiC diode, this faster decay suggests that an additional relaxation channel is introduced, which can only be the nonradiative energy transfer from SiC to QDs. The energy transfer rate can be readily determined as $1/21.7\text{-}1/24.1=4.59\,\mu s^{-1}$. Although this rate is approximately two or three orders of magnitude lower than the radiative recombination rate of some direct band-gap semiconductors, such as InGaN or gallium arsenide (GaAs) [26], nonradiative energy transfer has been demonstrated as an effective path to achieve color tunable emission from indirect band gap semiconductors.

3.3.4 Conclusion

In conclusion, nonradiative energy transfer was observed from the SiC diode to colloidal QD-phosphors that accumulated in the holes. Enhanced red emission of QDs was measured from characterization of the electroluminescence spectra of the diode, with a color conversion quantum efficiency calculated to be 3.1%. The PL decay lifetime of the SiC junction was found to decrease from 24.1 ns to 21.7 ns following the QD deposition, further confirming the existence of the nonradiative energy transfer path between the QDs and the SiC diode.

Reference

[1] M. Achermann, M.A. Petruska, S. Kos, D.L. Smith, D.D. Koleske, V.I. Klimov, Energy-transfer pumping of semiconductor nanocrystals using an epitaxial quantum well, Nature, 429 (2004) 642-646.

[2] S.V. Kershaw, M. Harrison, A.L. Rogach, A. Kornowski, Development of IR-emitting colloidal II-VI quantum-dot materials, Selected Topics in Quantum Electronics, IEEE Journal of, 6 (2000) 534-543.

[3] S. Coe-Sullivan, W.-K. Woo, J.S. Steckel, M. Bawendi, V. Bulović, Tuning the performance of hybrid organic/inorganic quantum dot light-emitting devices, Org Electron, 4 (2003) 123-130.

[4] J.S. Steckel, P. Snee, S. Coe-Sullivan, J.P. Zimmer, J.E. Halpert, P. Anikeeva, L.-A. Kim, V. Bulovic, M.G. Bawendi, Color-Saturated Green-Emitting QD-LEDs, Angewandte Chemie International Edition, 45 (2006) 5796-5799.

[5] J.S. Steckel, J.P. Zimmer, S. Coe-Sullivan, N.E. Stott, V. Bulović, M.G. Bawendi, Blue Luminescence from (CdS)ZnS Core–Shell Nanocrystals, Angewandte Chemie International Edition, 43 (2004) 2154-2158.

[6] Q. Sun, Y.A. Wang, L.S. Li, D. Wang, T. Zhu, J. Xu, C. Yang, Y. Li, Bright, multicoloured light-emitting diodes based on quantum dots, Nat Photon, 1 (2007) 717-722.

[7] Z. Tan, F. Zhang, T. Zhu, J. Xu, A.Y. Wang, J.D. Dixon, L. Li, Q. Zhang, S.E. Mohney, J. Ruzyllo, Bright and Color-Saturated Emission from Blue Light-Emitting Diodes Based on Solution-Processed Colloidal Nanocrystal Quantum Dots, Nano Lett, 7 (2007) 3803-3807.

[8] Y. Shirasaki, G.J. Supran, M.G. Bawendi, V. Bulovic, Emergence of colloidal quantum-dot light-emitting technologies, Nat Photon, 7 (2013) 13-23.

[9] H.-S. Chen, H. Cheng-Kuo, H.-Y. Hong, InGaN-CdSe-ZnSe quantum dots white LEDs, Photonics Technology Letters, IEEE, 18 (2006) 193-195.

[10] M. Achermann, M.A. Petruska, D.D. Koleske, M.H. Crawford, V.I. Klimov, Nanocrystal-Based Light-Emitting Diodes Utilizing High-Efficiency Nonradiative Energy Transfer for Color Conversion, Nano Lett, 6 (2006) 1396-1400.
[11] S. Nizamoglu, E. Sari, B. Jong-Hyeob, I.-H. Lee, H.V. Demir, Green/Yellow Solid-State Lighting via Radiative and Nonradiative Energy Transfer Involving Colloidal Semiconductor Nanocrystals, Selected Topics in Quantum Electronics, IEEE Journal of, 15 (2009) 1163-1170.
[12] S. Lu, A. Madhukar, Nonradiative Resonant Excitation Transfer from Nanocrystal Quantum Dots to Adjacent Quantum Channels, Nano Lett, 7 (2007) 3443-3451.
[13] S. Chanyawadee, P.G. Lagoudakis, R.T. Harley, M.D.B. Charlton, D.V. Talapin, H.W. Huang, C.-H. Lin, Increased Color-Conversion Efficiency in Hybrid Light-Emitting Diodes utilizing Non-Radiative Energy Transfer, Adv Mater, 22 (2010) 602-606.
[14] Y.-J. Lee, S.-Y. Lin, C.-H. Chiu, T.-C. Lu, H.-C. Kuo, S.-C. Wang, S. Chhajed, J.K. Kim, E.F. Schubert, High output power density from GaN-based two-dimensional nanorod light-emitting diode arrays, Applied Physics Letters, 94 (2009) 141111-141113.
[15] M.J. Park, J.S. Kwak, InGaN-Based Nano-Pillar Light Emitting Diodes Fabricated by Self-Assembled ITO Nano-Dots, J Nanosci Nanotechno, 12 (2012) 4265-4268.
[16] M. Hoheisel, A. Mitwalsky, C. Mrotzek, Microstructure and etching properties of sputtered indium—tin oxide (ITO), physica status solidi (a), 123 (1991) 461-472.
[17] S.J. Pearton, C.R. Abernathy, F. Ren, Gallium Nitride Processing for Electronics, Sensors and Spintronics, Springer, London, 2006.
[18] V.L. Colvin, M.C. Schlamp, A.P. Alivisatos, Light-emitting diodes made from cadmium selenide nanocrystals and a semiconducting polymer, Nature, 370 (1994) 354-357.
[19] S. Coe, W.-K. Woo, M. Bawendi, V. Bulovic, Electroluminescence from single monolayers of nanocrystals in molecular organic devices, Nature, 420 (2002) 800-803.
[20] Q. Sun, Y.A. Wang, L.S. Li, D.Y. Wang, T. Zhu, J. Xu, C.H. Yang, Y.F. Li, Bright, multicoloured light-emitting diodes based on quantum dots, Nat Photonics, 1 (2007) 717-722.

[21] S. Nizamoglu, G. Zengin, H.V. Demir, Color-converting combinations of nanocrystal emitters for warm-white light generation with high color rendering index, Applied Physics Letters, 92 (2008) 031102.
[22] E. Jang, S. Jun, H. Jang, J. Lim, B. Kim, Y. Kim, White-Light-Emitting Diodes with Quantum Dot Color Converters for Display Backlights, Adv Mater, 22 (2010) 3076-3080.
[23] S. Chanyawadee, P.G. Lagoudakis, R.T. Harley, M.D.B. Charlton, D.V. Talapin, H.W. Huang, C.H. Lin, Increased Color-Conversion Efficiency in Hybrid Light-Emitting Diodes utilizing Non-Radiative Energy Transfer, Adv Mater, 22 (2010) 602-606.
[24] F. Zhang, J. Liu, G. You, C. Zhang, S.E. Mohney, M.J. Park, J.S. Kwak, Y. Wang, D.D. Koleske, J. Xu, Nonradiative energy transfer between colloidal quantum dot-phosphors and nanopillar nitride LEDs, Opt. Express, 20 (2012) A333-A339.
[25] M. Ikeda, H. Matsunami, T. Tanaka, Defect Luminescence in SiC Light-Emitting Diodes, Jpn J Appl Phys, 19 (1980) 1201-1202.
[26] C.-K. Sun, S. Keller, G. Wang, M.S. Minsky, J.E. Bowers, S.P. DenBaars, Radiative recombination lifetime measurements of InGaN single quantum well, Applied Physics Letters, 69 (1996) 1936-1938.

Chapter 4

Alternating current gallium nitride light emitting diodes

4.1 Introduction

Advances in gallium nitride (GaN) based semiconductor have offered great prospects for developing efficient and bright light emitting diodes (LEDs) [1-7]. The emission wavelength can be tuned from visible to ultraviolet (UV) depending on the composition of the GaN based material [8, 9]. Also, due to the strong chemical bond of the material, it is very stable under high power and high temperature conditions [10-13]. In addition, the power efficiency of the GaN LEDs is much higher than other light sources like light bulb and fluorescent lamp [14]. Consequently, these advantages of the GaN LEDs make it a promising candidate for next-generation light sources.

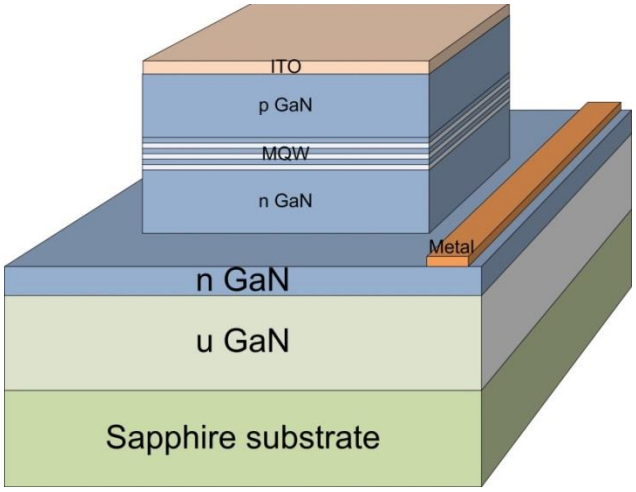

Figure 4-1. Schematic of the structure of a typical GaN LED.

Figure 4-1 shows the schematic structure of a typical GaN LED. The LED wafers employed in this study were purchased from Xinguanglian Technology Co., Ltd. It is configured with an InGaN/GaN MQW-embedded p-i-n heterojunction, comprising a patterned sapphire substrate, an undoped GaN buffer layer (~2.5 μm), an n-type ($N_d \approx 1\times10^{18}$cm^{-3}) GaN layer (~2 μm), eight pairs of 2.5nm-thick $In_{0.1}Ga_{0.9}N$ quantum wells sandwiched between 12nm-thick GaN barriers, a p-type ($N_a \approx 5\times10^{17}$cm^{-3}) GaN layer (~0.1 μm), as well as a p-type ($N_a > 1\times10^{18}$cm^{-3}) GaN capping layer (~0.1 μm). Silicon and magnesium are the n- and p-type dopants in the LED heterojunction, respectively. The anode material is indium tin oxide (ITO) and cathode material is Ti/Al/Ti/Au.

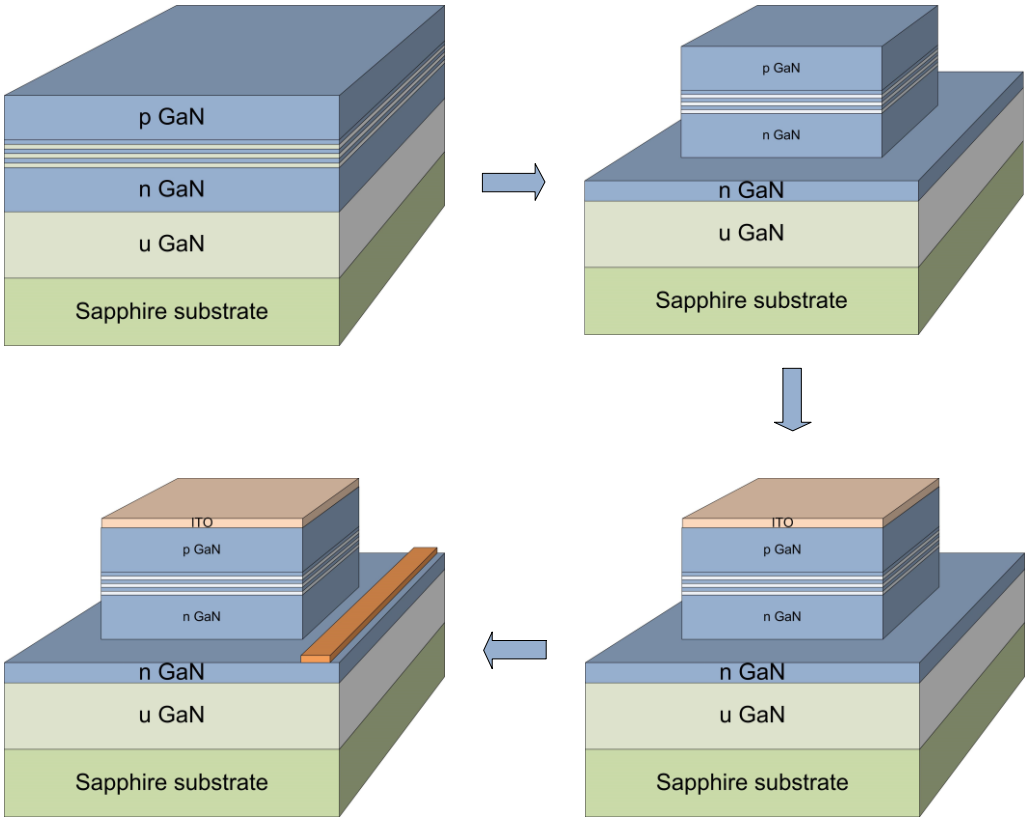

Figure 4-2. fabrication procedures of a single LED.

The fabrication procedures of a single LED are shown in figure 4-2. The first step is etching to n-type GaN by inductively-coupled-plasma (ICP) etching, and the mesa structure was obtained. Then ITO (300nm) was deposited, patterned and annealed on the p-type GaN as anode. For the formation of the cathode, Ti/Al/Ti/Au (10nm/40nm/40nm/100nm) was deposited, patterned and annealed on the n-type GaN.

For a single GaN LED, it is usually operated at a voltage around 3~5V [10]. However, the voltage of power supplies is usually larger than 3~5V in the applications of GaN LEDs. The power supply in our daily lives is alternating current (AC) power supply with voltage from 110V to 240V. To address this problem, the method widely used today is including a driving circuit into the LED light source, converting the 110V~240V AC voltage to an appropriate lower DC voltage [15]. Nevertheless, there are several disadvantages for this method. Firstly, during the voltage conversion, the power conversion efficiency cannot reach 100%, thus power loss will be introduced. Secondly, the cost will be increased due to the electrical components of the driving circuit. During the rapid development of the LED technology recently, the price of the LED chip is decreasing fast these years, but the price of electrical components does not change that much compared to the LED chip. As a result, the cost of the electrical components will become more and more significant in the future with the decreasing price of the LED chip. In addition, the lifetime of these electrical components is much shorter than the LED chip. Therefore, the lifetime of the LED light source will be limited by these electrical components, cannot reach the extreme long lifetime of GaN LED chip.

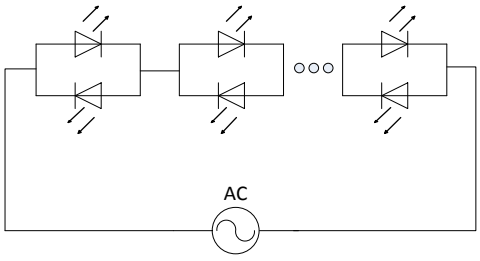

(a)

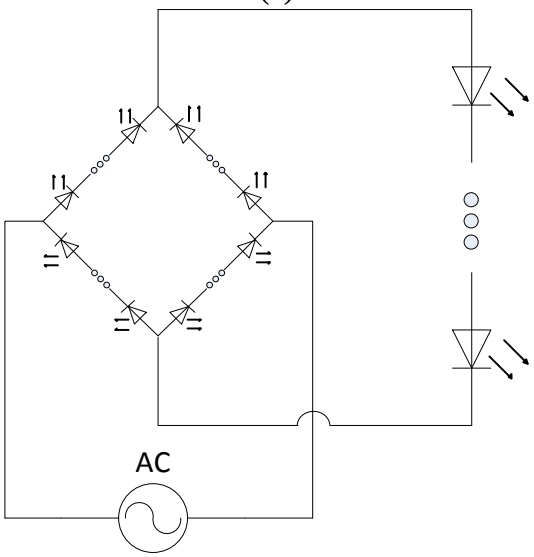

(b)

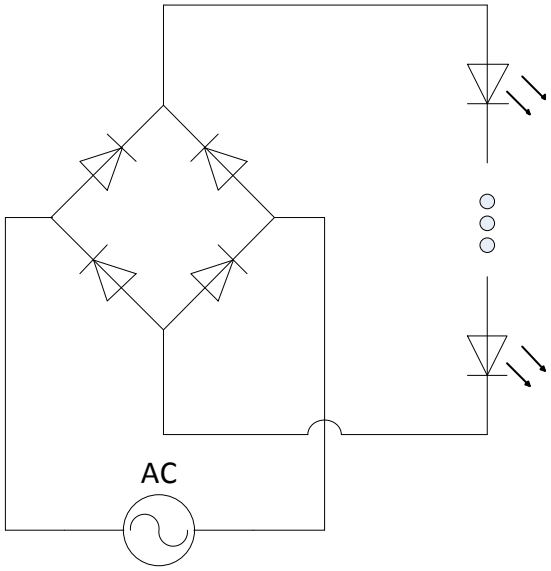

(c)

Figure 4-3. Schematic diagram of the circuit of (a) an anti-parallel AC LED and (b) a Wheatstone bridge AC LED (c) an AC LED integrated with Schottky diodes.

Toward this end, intense investigations are being conducted to develop AC LEDs without electrical driving circuit to address this driving problem [16-19]. There are several ways to realize a chip level AC LED. A simple way is called anti-parallel AC LEDs as shown in Fig. 4-3(a) [16, 17]. In this type of AC LEDs, several pairs of LEDs are connected together as a series circuit. In each pair, two single LEDs are connected together as a parallel circuit in opposite direction. Half of the LEDs emit light during the first half period of the AC voltage, while the other half of the LEDs emit light during the second half period of the AC voltage. However, there is one significant disadvantage for this type of AC LEDs. Only half of the single LEDs in the circuit would emit light, which means compared to the normal LEDs driven by DC voltage, if the same amount of light output is required, the area of anti-parallel AC LEDs should be twice as large as the area of DC driven LEDs. This disadvantage would decrease the area usage and increase the cost.

Another way to realize a chip level AC LED is called Wheatstone bridge (WB) AC LEDs [18, 19]. Several single LEDs are connected together to form a WB bridge circuit as shown in Fig. 4-3(b). The LEDs in each rectifying branch are forward biased and reverse biased alternatively during each half period of the AC power supply, while the LEDs in the output branch are forward biased during the entire AC period. As a result, more than half of the single LEDs would emit light during each half AC period. By tuning the number and are of the LEDs in the rectifying branches and the output branch, the area usage, defined as the ratio of the area of the LEDs emit light during each

half period to the total LED area on the chip, can be increased from 50% for anti-parallel AC LEDs to 60% to 80%. Nevertheless, there is a serious problem for this type of AC LEDs. During operation, the LEDs in the rectifying branches would undergo a high reverse biased voltage. According to a research reported by Hsi-Hsuan Yen, *et al*. [20], this high reverse biased voltage would damage those single LEDs by forming Ga_2O_3 on the surface of n-type GaN, leading to an accelerated failure of the AC LEDs. According to the study [20], a Wheatstone bridge AC LED with was reported to fail after 650 hours of operation, which is not acceptable for a usable device.

More recently, Hsi-Hsuan Yen *et al*. proposed to integrate Schottky diodes with LEDs to build on-chip WB circuitry for AC LED operation [21], as shown in Fig. 4-3(c). Two integration approaches are proposed, one method involves growing a rectifying layer of intrinsic semiconductor AlGaN on the LED wafer by epitaxy or deposition [22]. The other method is to form the rectifying region by ion implanting donor species into the top p-type GaN layer of the LED wafer [23]. These fabrication methods, however, request sophisticated post-growth modification of the LED epi-layer by deposition, ion implantation or diffusion, which would lead to the dramatic increase of the LED fabrication cost, and hence have never been employed to date.

In this study, we successfully demonstrated Schottky diodes with both high breakdown voltage and low forward biased voltage at working current (20 mA) on an LED wafer. This is the first time that Schottky diodes with good performance on a commercial available LED wafer can be realized, and is the first that a monolithic integration of LED arrays with on-chip Schottky diode Wheatstone bridge was demonstrated.

In order to make an AC LED by any of the three ways mentioned previously, a chip level series of single LEDs, which can operated at a DC high voltage (HV), should be realized first. As a result, the fabrication, and characterization of an HV LED is first introduced and discussed in the next section.

4.2 High voltage gallium nitride light emitting diodes

4.2.1 Device structure and fabrication

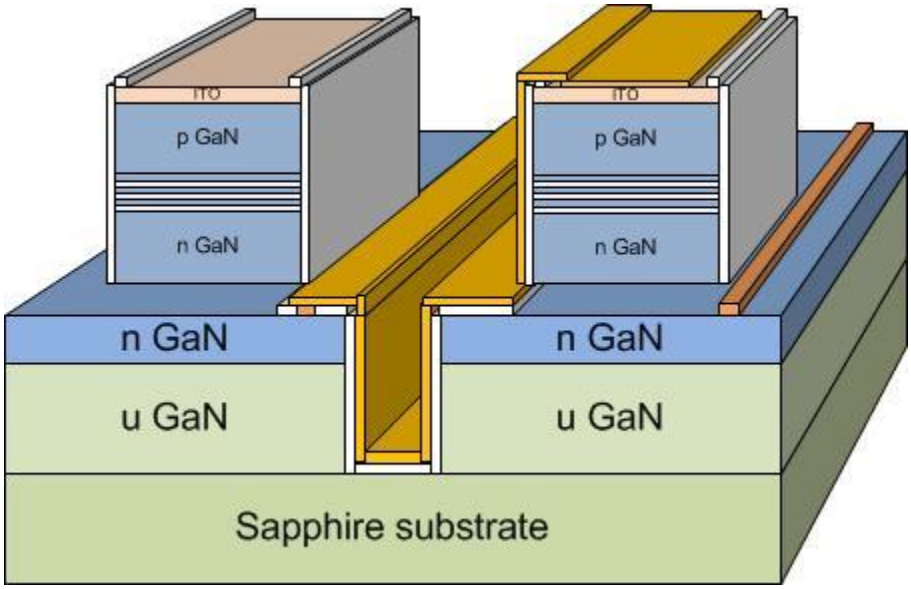

Figure 4-4. Schematic of the structure of two GaN LEDs connected together.

Figure 4-4 shows the schematic structure of two GaN LEDs connected together. In real device, there can be more than two single LEDs according to the requirement of the operation voltage.

The fabrication procedures are similar to single LED fabrication; the only difference is that two additional steps are required. Each single LED needs to be separated with each other by etching the gap to sapphire substrate. In the end, the interconnection metal Ti/Al/Ti/Au (50nm/1000nm/100nm/100nm) was deposited and patterned. The picture of a fabricated HV GaN LED is shown in Fig. 4-5 (a). There are 23 single LEDs in the device. Figure 4-5(b) shows the picture of a lighted HV LED.

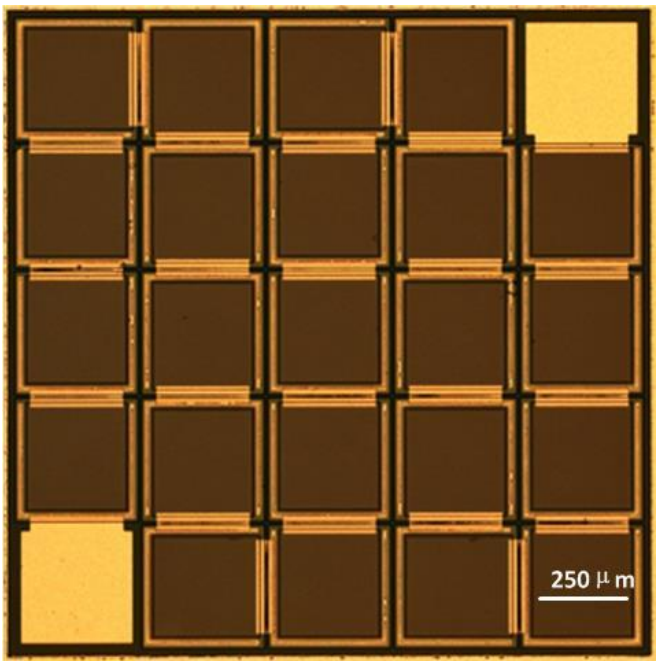

(a)

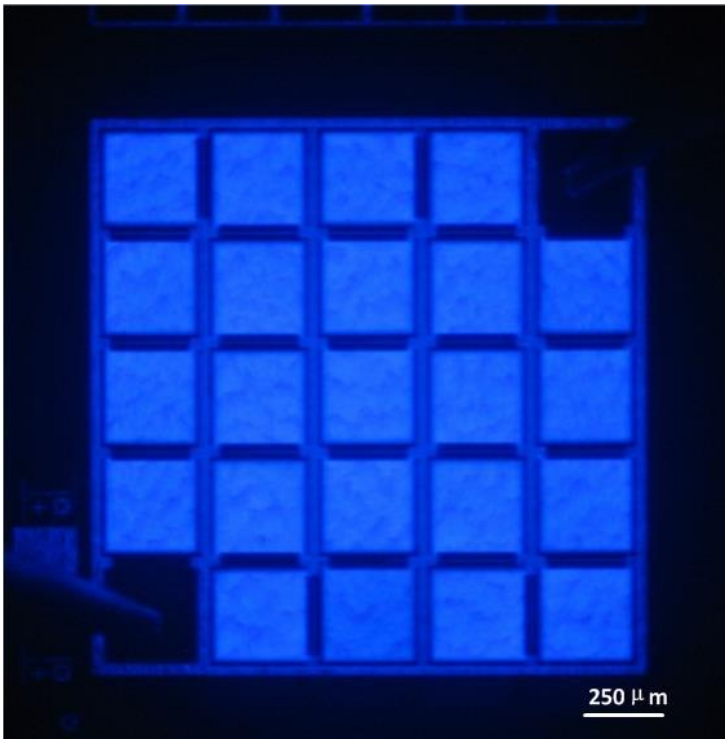

(b)

Figure 4-5. Microscope pictures of (a) a fabricated and (b) a lighted HV LED.

4.2.2 Results and discussion

A single LED and an HV LED were measured and the results are shown in Fig. 4-6.

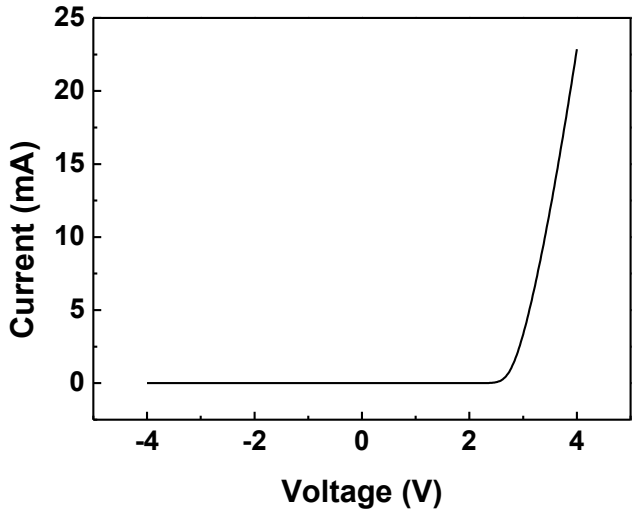

(a)

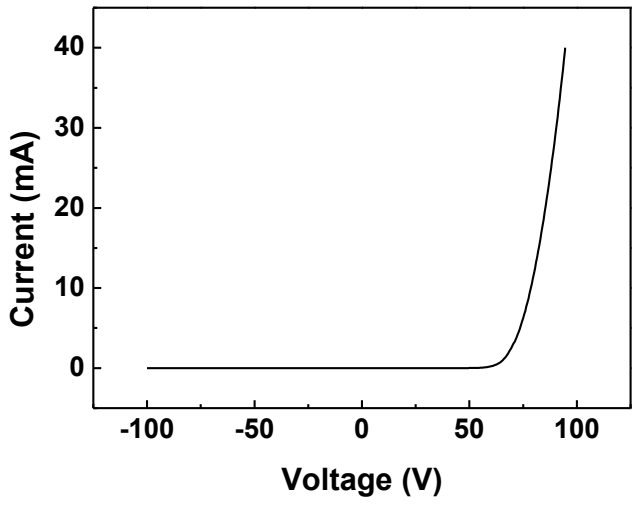

(b)

Figure 4-6. Current -voltage (I-V) of (a) a single LED and (b) an HV LED.

For a single LED, the result in Fig. 4-6(a) shows the turn on voltage is 2.52V, and the working voltage is 3.88V when the current is 20mA. According to the structure of the HV LED, it consists of 23 single LEDs connected together. As a result, the turn on voltage should be 2.52V×23=58V, and the working voltage should be 3.88V×23=89V. From the I-V curve in Fig. 4-6(b), the turn on and working voltage is measured to be 58V and 85.5V, respectively, agree well with the calculated value.

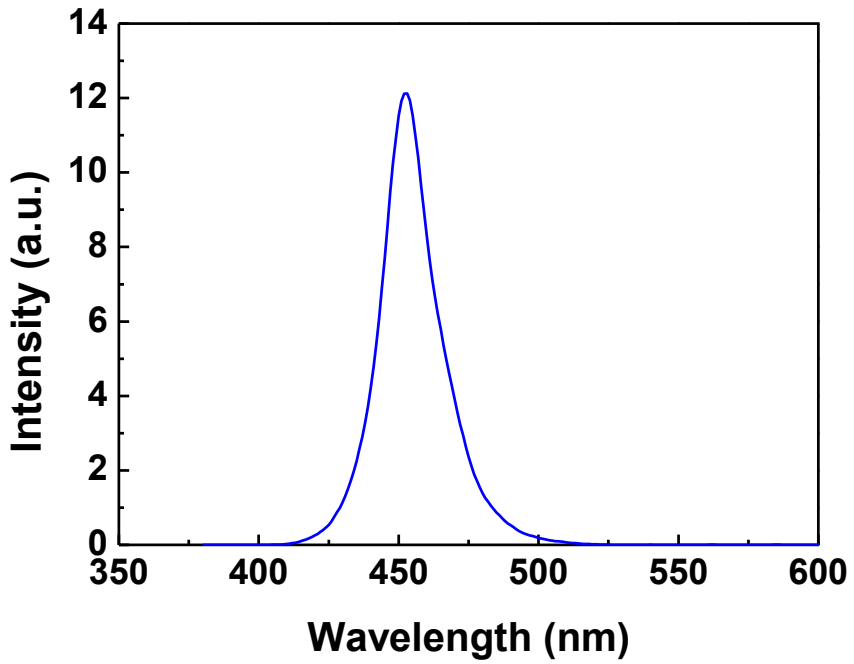

Figure 4-7. Electroluminescence spectrum of the HV LED.

Figure 4-7 shows the Electroluminescence (EL) spectrum of the HV LED. The peak wavelength locates at 451.5 nm, and the full width at half maximum (FWHM) bandwidth is 20.7 nm. This result shows the HV LED emits pure blue light. The output power was measured to be 352mW while the input electrical power was fixed at 1W, thus

the external quantum efficiency of the device is 35.2%, which is a typical value for a blue GaN LED [24, 25].

4.2.3 Conclusion

In summary, a chip level HV LED, consisting of several single LEDs connected together as a series circuit on the same wafer, was demonstrated. The device has a turn on voltage of 58V, and a working voltage of 85.5V when the current is 20mA. With an integrating sphere and a measuring system, a pure blue emission from the device with peak wavelength 451.5 nm and the FWHM bandwidth is 20.7 nm was characterized. The external quantum efficiency is measured to be 35.2%.

4.3 Chip level alternating current light emitting diodes integrated with Schottky diode

In this study, we demonstrated a chip level AC LED integrated with good performance Schottky diode. All single LEDs in the device can emit light during both positive and negative half period of the AC voltage.

4.3.1 Device structure and fabrication

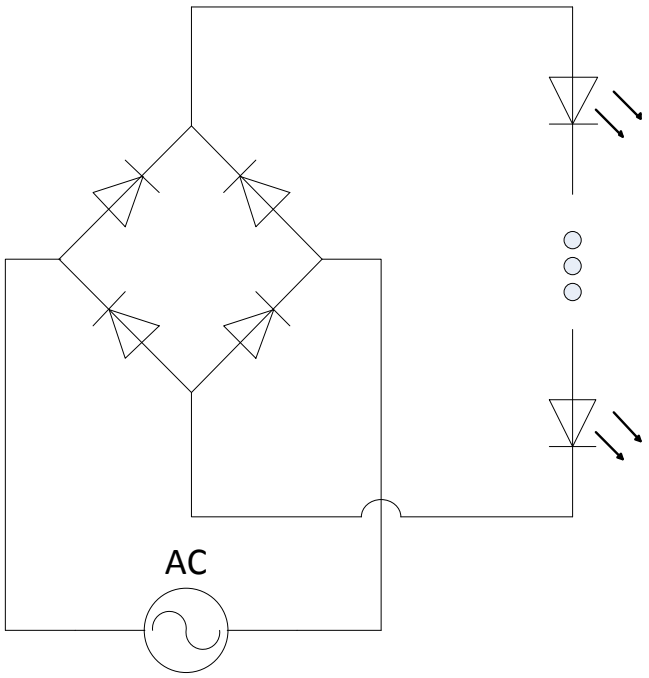

(a)

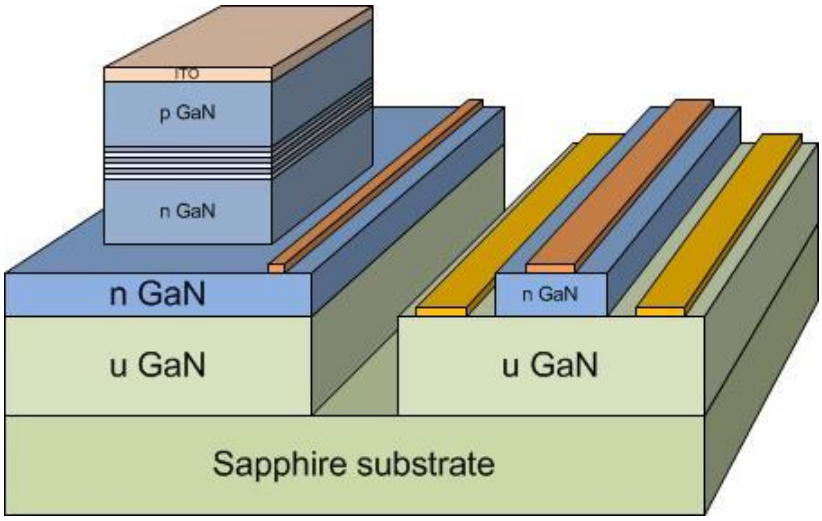

(b)

Figure 4-8. Schematic diagram of (a) the circuit and (b) the structure of the AC LEDs with Schottky diode.

Figure 4-8(a) shows the circuit of the AC LEDs with Schottky diode. Using at least four Schottky diodes, a WB circuit can be obtained. If the breakdown voltage of the Schottky diodes is high enough, no matter which direction of the voltage applied on the circuit, the current would flow through the Schottky diodes on two branches and the series of LEDs, while the Schottky diodes on the other two branches would undergo a reverse biased voltage. As a result, in order to obtain an AC LED with high power efficiency, the forward biased voltage of the Schottky diodes while the current flows through them should be as low as possible, and the breakdown voltage of the Schottky diodes while they are reverse biased should be as high as possible. Here we define V_f as the forward working voltage of the Schottky diode while the forward current reaches 20 mA, and V_r as the reverse working voltage of the Schottky diode while the reverse

leakage current reaches 0.1 mA. As a result, a low V_f value and a high V_r value are preferred.

Figure 4-8(b) shows the schematic structure of the chip level AC LEDs integrated with Schottky diode. The LEDs and the Schottky diodes are fabricated on the same LED wafer. The LED wafers employed in this study were purchased from Xinguanglian Technology Co., Ltd.

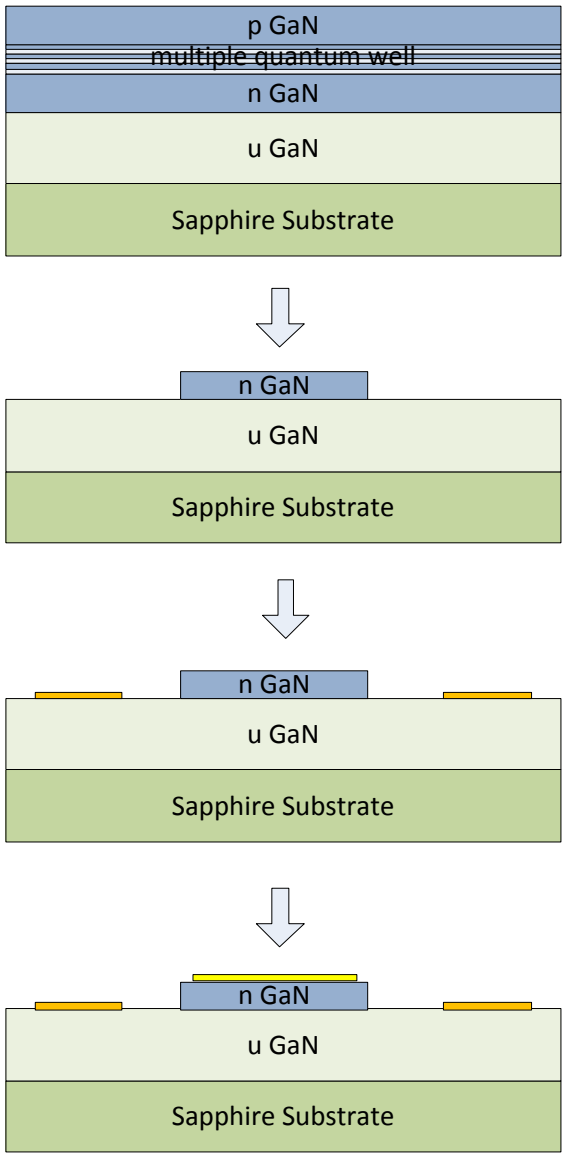

Figure 4-9. Fabrication procedures of the integrated Schotty diode in the AC LEDs.

The fabrication procedures of the LED series are the same as the procedures of the HV LED described previously. Fig. 4-9 shows the fabrication procedures of the Schottky diodes in the AC LEDs. The first step is etching to n-type GaN by inductively-coupled-plasma (ICP) etching, and the mesa structure was obtained. The second step is etching to un-doped GaN with ICP etching, thus the Schottky contact area is exposed. For the formation of the cathode, Ti/Al/Ti/Au (10nm/40nm/40nm/100nm) was deposited, patterned and annealed on the n-type GaN. Later the Schottky contact metal was also deposited and patterned on the un-doped GaN.

4.3.2 Schottky diode design

In order to increase the power efficiency of the AC LEDs, the forward biased working voltage V_f of the Schottky diode need to be decreased, and the reverse biased working voltage V_r need to be increased. To meet this requirement, the design of the Schottky contact was investigated.

First of all, Schottky diodes with different Schottky contact areas were studied. The design of the Schottky diodes was shown in Fig. 4-10, the areas of the Schottky contact varies from 6400 μm^2 to 100 μm^2, while the Ohmic contact remains the same.

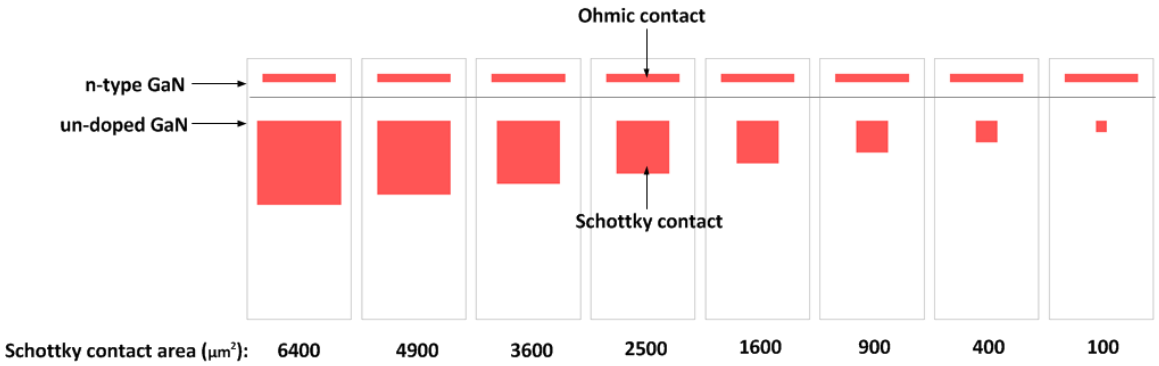

Figure 4-10. Schematic design diagram of the Schottky diodes with different Schottky contact areas.

The IV curves of the fabricated Schottky diodes were shown in Fig. 4-11, the measured V_f and V_r were listed in table 5-1. While the area of the Schottky contact decreases, both the forward working voltage V_f and the reverse working voltage V_r increases. As a result, in order to keep V_f low and V_r high, the Schottky contact area should not be too large or too small. A medium value 2500 μm^2 was chosen to balance those two requirements.

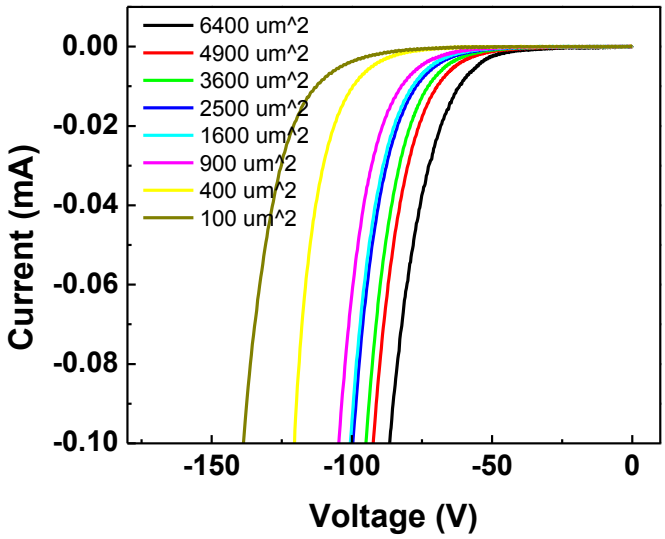

(a)

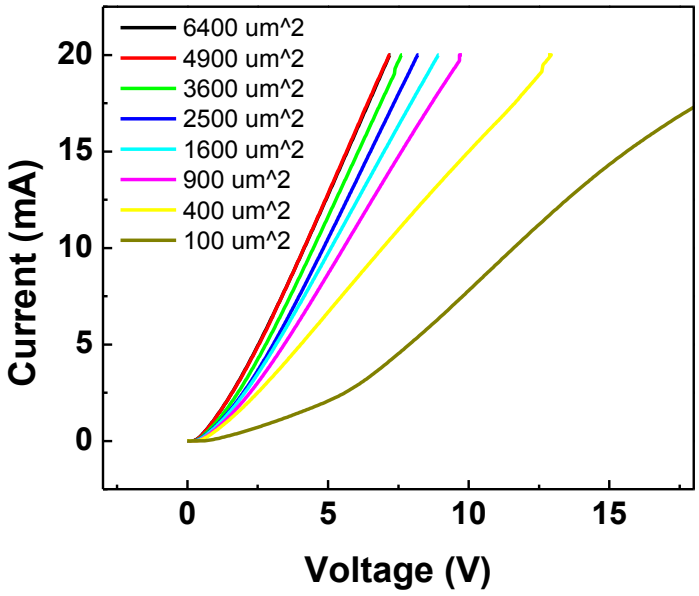

(b)

Figure 4-11. (a) Reverse biased and (b) forward biased IV curves of the Schottky diodes with different Schottky contact areas.

Table 4-1. Forward working voltage V_f and reverse working voltage V_r of the Schottky diodes with different Schottky contact areas.

Schottky contact area(μm^2)	6400	4900	3600	2500	1600	900	400	100
V_f **(V)** (I_f=20mA)	7.19	7.18	7.61	8.18	8.93	9.68	12.93	21.73
V_r **(V)** (I_r=0.1mA)	94.76	99.75	102.2	106.5	107.2	111.5	125	146.5

The Schottky diode in this study has a mesa structure, d is defined as the distance between the Schottky contact and the n-type GaN mesa, and this distance d would also affect the performance of the diode. Accordingly, Schottky diodes with different distance d were investigate as shown in Fig. 4-12, the distance d varies from 120 μm to 15 μm.

All Schottky diodes were fabricated with same techniques as the Schottky diodes with different contact areas.

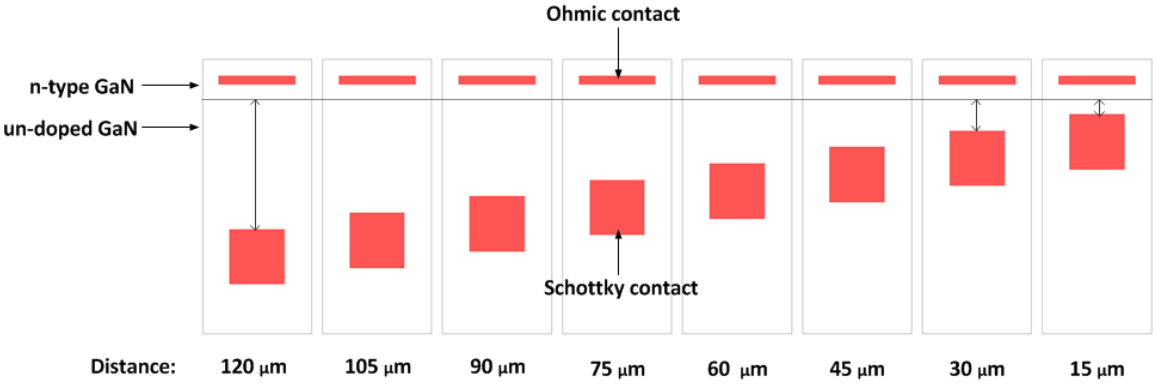

Figure 4-12. Schematic design diagram of the Schottky diodes with different distances between Schottky contact and n-type GaN mesa.

The IV curves of the fabricated Schottky diodes were shown in Fig. 4-13, the measured V_f and V_r were listed in table 4-2. While the distance d decreases from 120 μm to 15 μm, the forward working voltage V_f decreases from 11.85 V to 6.19 V, and the reverse working voltage V_r almost does not change. As a result, small distance between Schottky contact and n-type GaN mesa would be helpful to increase the diode performance. The distance 15 μm was chosen for the device fabrication.

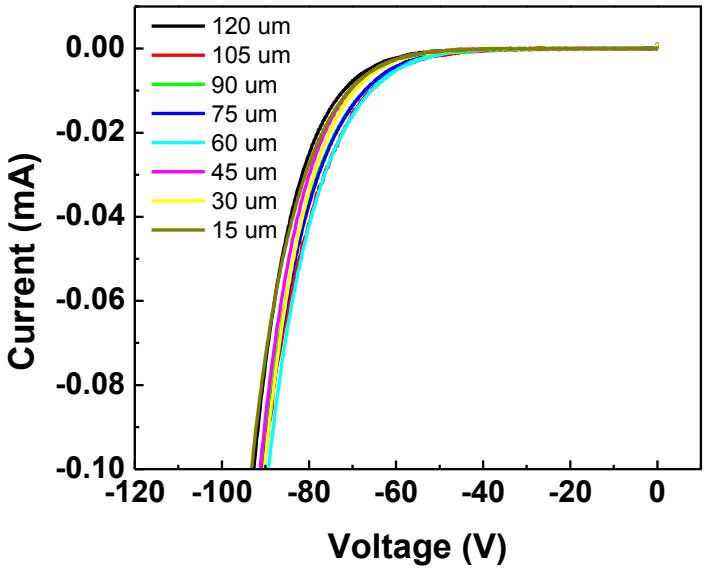

(a)

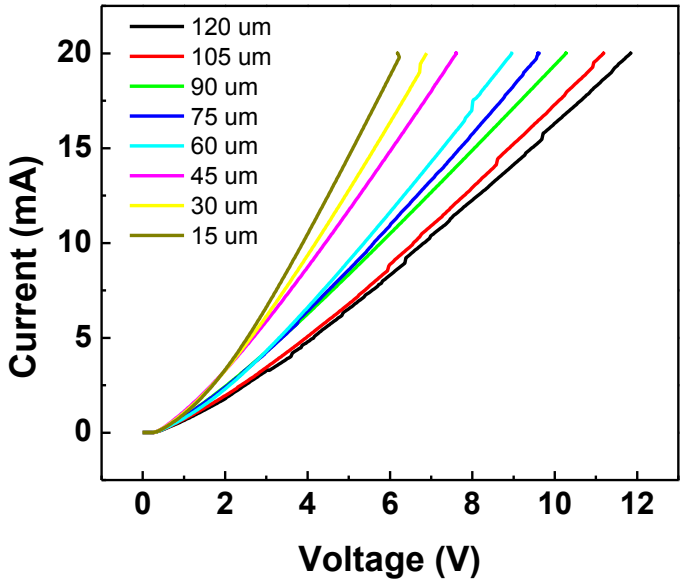

(b)

Figure 4-13. (a) Reverse biased and (b) forward biased IV curves of the Schottky diodes with different distances between Schottky contact and n-type GaN mesa.

Table 4-2. Forward working voltage V_f and reverse working voltage V_r of the Schottky diodes with different distances between Schottky contact and n-type GaN mesa.

Distance (μm)	120	105	90	75	60	45	30	15
V_f (V) (I_f=20mA)	11.85	11.19	10.27	9.62	8.96	7.61	6.89	6.19
V_r (V) (I_r=0.1mA)	92.75	90.83	91.01	90.51	89.50	91.25	90.25	93.26

In addition, Schottky diodes with different Schottky contact lengths were also studied. As shown in Fig. 4-14, the Schottky contact length changes with the n-type GaN mesa length from 30 μm to 150 μm. All Schottky diodes were fabricated with same techniques as the Schottky diodes with different contact areas.

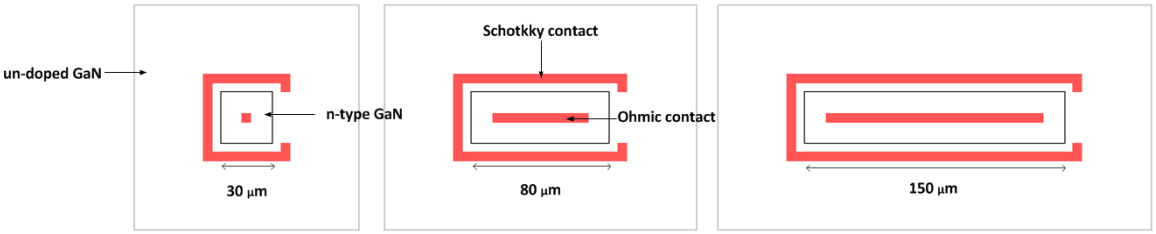

Figure 4-14. Schematic design diagram of the Schottky diodes with different Schottky contact lengths.

The IV curves of the fabricated Schottky diodes were shown in Fig. 4-15, the measured V_f and V_r were listed in table 4-3. While the n-type GaN mesa length increases from 30 μm to 150 μm, the forward working voltage V_f decreases from 6.51 V to 3.73 V, and the reverse working voltage V_r decreases from 90.41 V to 84.60 V. The result that V_f decreases a lot while V_r decreases a little suggests that longer Schottky contact length would be helpful to obtain a Schottky diode with better performance. The Schottky contact length 150 μm was chosen for the device fabrication.

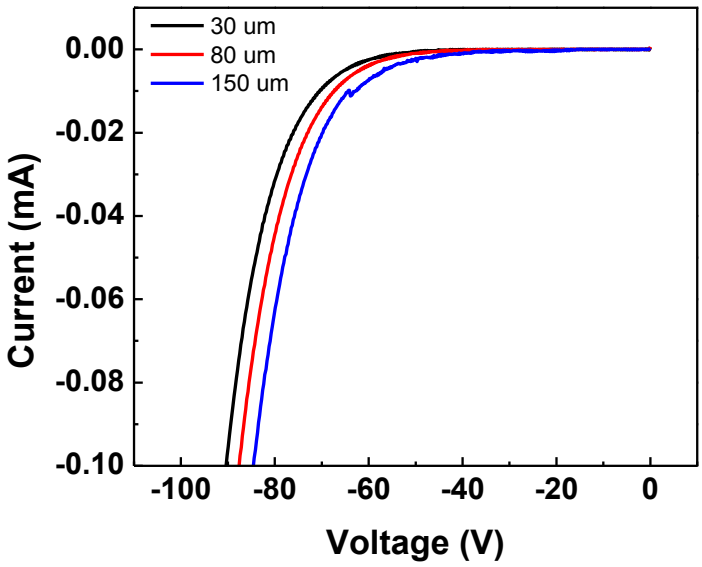

(a)

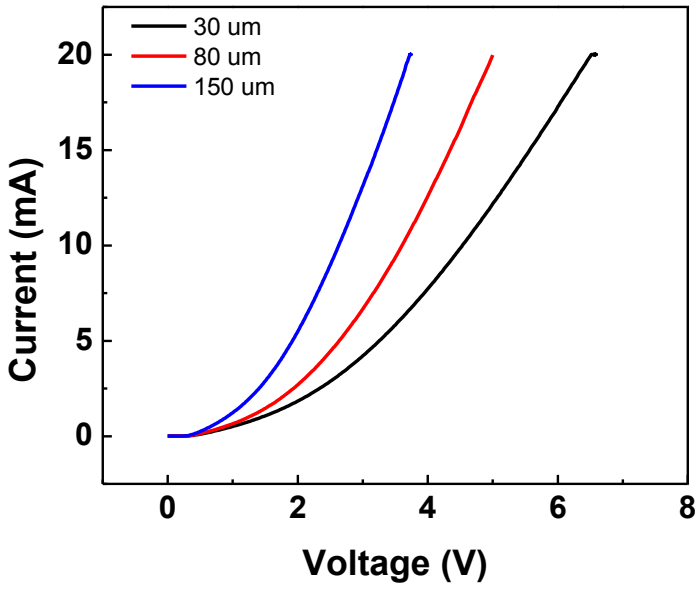

(b)

Figure 4-15. (a) Reverse biased and (b) forward biased IV curves of the Schottky diodes with different Schottky contact lengths.

Table 4-3. Forward working voltage V_f and reverse working voltage V_r of the Schottky diodes with different Schottky contact lengths.

Length (μm)	30	80	150
V_f (V) (I_f=20mA)	6.51	5.00	3.73
V_r (V) (I_r=0.1mA)	90.41	87.64	84.60

As a result, employing these three design rules: proper Schottky contact area, short distance between Schottky contact and the n-type GaN mesa, and long Schottky contact length, the forward working voltage V_f of the Schottky diode can be decreased.

4.3.3 Results and discussion

Finally, a Schottky diode using these design rules was fabricated. The IV curve was measured and the result is shown in Fig. 4-16. The reverse working voltage V_r was measured to be larger than 120 V, and the forward working voltage V_f was measured to be 3.16 V. Integrating this Schottky diode into an AC LED, the number of diodes on each rectifying branch of the WB circuit is 2, the voltage drop on the forward biased Schottky diodes is $2 \times 2 \times 3.16V = 12.64V$, thus the power lost on the Schottky diodes can be decreased to 12.64V/110V=11.5%.

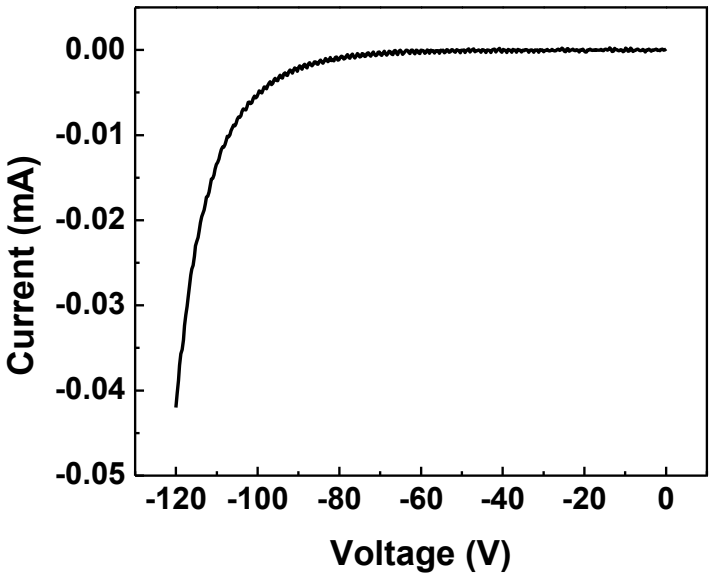

(a)

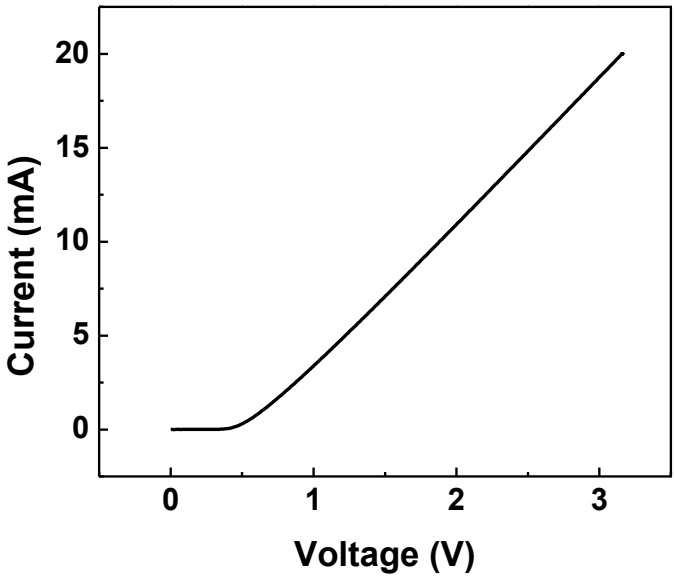

(b)

Figure 4-16. (a) Reverse biased and (b) forward biased IV curves of the Schottky diodes using Schottky contact design rules.

Consequently, integrating Schottky diodes with a series of single LEDs on the same LED wafer, a chip level AC LED integrated with Schottky diode was fabricated as shown in Fig. 4-17(a). There are 22 single LEDs in the device, and 2 Schottky diodes on each rectifying branch of the WB circuit. Fig. 4-17(b) shows a picture of a lighted AC LED.

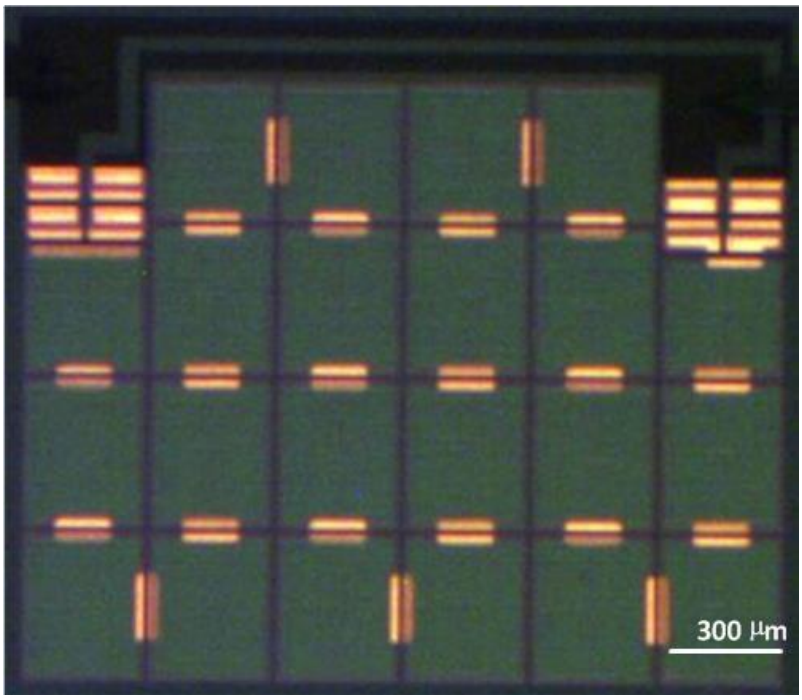

(a)

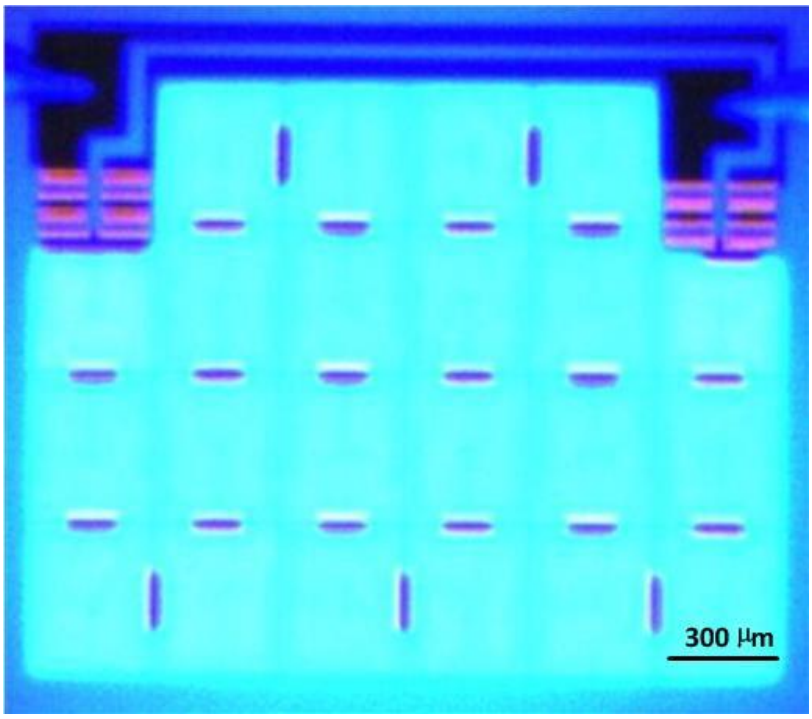

(b)

Figure 4-17. Microscope pictures of (a) a fabricated and (b) a lighted chip level AC LED integrated with Schottky diode.

The IV curve of the AC LED is shown in Fig. 4-18(a). The LED turned on when the voltage was applied to the device in both directions. The turn on voltage (current reaches 0.1 mA) and working voltage (when the current reaches 20mA) was measured to be 54V and 105V respectively for both directions.

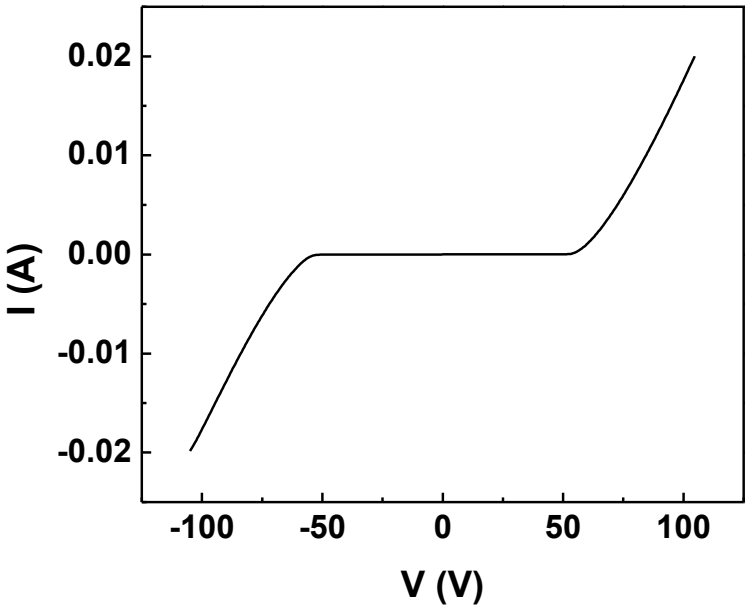

(a)

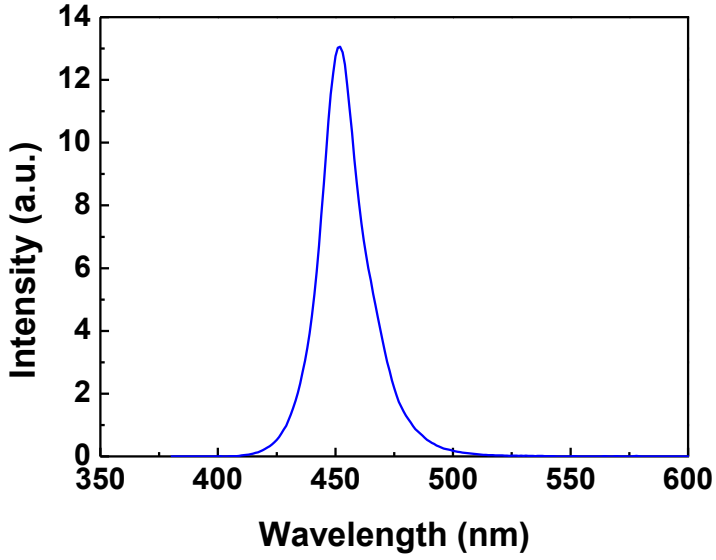

(b)

Figure 4-18. (a) IV curve and (b) Electroluminescence spectrum of the AC LED with Schottky diode.

Fig. 4-18(b) shows the EL spectrum of the chip level AC LED integrated with Schottky diode. The peak wavelength locates at 451.5 nm. The full width at half maximum (FWHM) bandwidth is 20 nm. The output power was measured to be 324.1mW while the input electrical power was fixed at 1W, thus the external quantum efficiency of the device is 32.4%. For comparison, the external quantum efficiency of the HV LED in the previous section was measured to be 35.2%. As a result, the external quantum efficiency of AC LED is 2.8% less than HV LED, implies the less than 10% of power loss is introduced by the integrated Schottky diodes in the WB circuit.

4.3.4 Conclusion

In summary, a chip level AC LED integrated with good performance Schottky diode was demonstrated. By integrating some Schottky diodes in the LED circuit on chip level, a WB circuit can be obtained. All the single LEDs emit light during the device operation. The measurement results show that the device has a turn on voltage of 54V, and a working voltage of 105V when the current is 20mA. With an integrating sphere and a measuring system, a pure blue emission from the device with peak wavelength 451.5 nm and the FWHM bandwidth is 20 nm was characterized. The external quantum efficiency is measured to be 32.4%.

Reference

[1] S. Nakamura, M. Senoh, N. Iwasa, S.-i. Nagahama, T. Yamada, T. Mukai, Superbright Green InGaN Single-Quantum-Well-Structure Light-Emitting Diodes, Jpn J Appl Phys, 34 (1995) L1332.

[2] T. Mukai, H. Narimatsu, S. Nakamura, Amber InGaN-Based Light-Emitting Diodes Operable at High Ambient Temperatures, Jpn J Appl Phys, 37 (1998) L479.

[3] S.N. Mohammad, A.A. Salvador, H. Morkoc, Emerging gallium nitride based devices, P Ieee, 83 (1995) 1306-1355.

[4] S.P. DenBaars, Gallium-nitride-based materials for blue to ultraviolet optoelectronics devices, P Ieee, 85 (1997) 1740-1749.

[5] T. Mukai, S. Nagahama, N. Iwasa, M. Senoh, T. Yamada, Nitride light-emitting diodes, Journal of Physics: Condensed Matter, 13 (2001) 7089.

[6] T. Mukai, Recent progress in group-III nitride light-emitting diodes, Selected Topics in Quantum Electronics, IEEE Journal of, 8 (2002) 264-270.

[7] T. Mukai, S. Nagahama, M. Sano, T. Yanamoto, D. Morita, T. Mitani, Y. Narukawa, S. Yamamoto, I. Niki, M. Yamada, S. Sonobe, S. Shioji, K. Deguchi, T. Naitou, H. Tamaki, Y. Murazaki, M. Kameshima, Recent progress of nitride-based light emitting devices, physica status solidi (a), 200 (2003) 52-57.

[8] J. Han, A.V. Nurmikko, Advances in AlGaInN blue and ultraviolet light emitters, Selected Topics in Quantum Electronics, IEEE Journal of, 8 (2002) 289-297.

[9] F.A. Ponce, D.P. Bour, Nitride-based semiconductors for blue and green light-emitting devices, Nature, 386 (1997) 351-359.

[10] M.R. Krames, O.B. Shchekin, R. Mueller-Mach, G.O. Mueller, Z. Ling, G. Harbers, M.G. Craford, Status and Future of High-Power Light-Emitting Diodes for Solid-State Lighting, Display Technology, Journal of, 3 (2007) 160-175.

[11] G. Chen, M. Craven, A. Kim, A. Munkholm, S. Watanabe, M. Camras, W. Götz, F. Steranka, Performance of high-power III-nitride light emitting diodes, physica status solidi (a), 205 (2008) 1086-1092.

[12] M.-H. Chang, D. Das, P.V. Varde, M. Pecht, Light emitting diodes reliability review, Microelectron Reliab, 52 (2012) 762-782.

[13] S. Nakamura, M. Senoh, N. Iwasa, S.-i. Nagahama, High-power InGaN single-quantum-well-structure blue and violet light-emitting diodes, Applied Physics Letters, 67 (1995) 1868-1870.

[14] D.A. Steigerwald, J.C. Bhat, D. Collins, R.M. Fletcher, M.O. Holcomb, M.J. Ludowise, P.S. Martin, S.L. Rudaz, Illumination with solid state lighting technology, Selected Topics in Quantum Electronics, IEEE Journal of, 8 (2002) 310-320.

[15] P. Kochcha, S. Sujitjorn, Converter Topologies of LED Lamp Drivers: A Review, Recent Patents on Electrical Engineering, 3 (2010) 152-156.

[16] H. Jiang, J. Lin, S. Jin, Light emitting diodes for high AC voltage operation and general lighting, U.S. Patent No. 6,957,899, (2005).

[17] M.-T. Lin, F.-C. Hwang, C.-T. Kuo, Structure of AC light-emitting diode dies, U.S. Patent No. 7,531,843, (2009).

[18] H.-H. Yen, H.-C. Kuo, W.-Y. Yeh, Characteristics of Single-Chip GaN-Based Alternating Current Light-Emitting Diode, Jpn J Appl Phys, 47 (2008) 8808.

[19] J. Cho, J. Jung, J.H. Chae, H. Kim, H. Kim, J.W. Lee, S. Yoon, C. Sone, T. Jang, Y. Park, E. Yoon, Alternating-current Light Emitting Diodes with a Diode Bridge Circuitry, Jpn J Appl Phys, 46 (2007) L1194.

[20] Y. Hsi-Hsuan, K. Hao-Chung, W.-Y. Yeh, Particular Failure Mechanism of GaN-Based Alternating Current Light-Emitting Diode Induced by GaOx Oxidation, Photonics Technology Letters, IEEE, 22 (2010) 1168-1170.

[21] W.-Y. Yeh, H.-H. Yen, Y.-J. Chan, The development of monolithic alternating current light-emitting diode, in, 2011, pp. 793910-793910-793912.

[22] J.-i. Chyi, G.-y. Lee, W.-s. Lin, Method for fabricating integrated alternating-current light-emitting-diode module, US Patent 20,130,034,919, (2013).

[23] H.-H. Yen, W.-Y. Yeh, Alternating current light-emitting device and fabrication method thereof, U.S. Patent No. 7,855,388, (2010).

[24] S. Nakamura, Current Status of GaN-Based Solid-State Lighting, Mrs Bull, 34 (2009) 101-107.

[25] M.C. Schmidt, K.-C. Kim, H. Sato, N. Fellows, H. Masui, S. Nakamura, S.P. DenBaars, J.S. Speck, High Power and High External Efficiency m-Plane InGaN Light Emitting Diodes, Jpn J Appl Phys, 46 (2007) L126.

Chapter 5

Future work

This dissertation discusses some studies in improving the light emitting diode (LED) technology from colloidal quantum dot (QD) LEDs to gallium nitride (GaN) based LEDs. For the future work, there are some suggestions can be noted in the following aspects.

5.1 Quantum dot light emitting diodes

According to the study in this dissertation, high temperature of the colloidal QD LEDs during operation could be one important factor limits the stability of QD LEDs. As a result, if a novel type of colloidal QDs with high quantum efficiency at high temperature can be obtained, QD LEDs with longer lifetime can therefore be demonstrated. Several techniques could be employed to achieve this purpose, such as synthesis of QDs with shorter ligands; passivation of QD surfaces with a thermally stable material to prevent damage.

Besides the QD material, the material of other layers of QD LEDs can also be studied in the future to improve the device performance. In this dissertation, IGZO was studied as the electron transport material, some other novel semiconductor material can also be studied in the future to act as the electron or hole transport material.

5.2 Nonradiative energy transfer between colloidal quantum dot-phosphors and inorganic diodes

In this dissertation, the nonradiative energy transfer between colloidal quantum dot-phosphors and inorganic diodes was studied. In order to further increase the color conversion efficiency, a resonant cavity GaN LED can be employed and studied in the future work, as shown in Fig. 5-1.

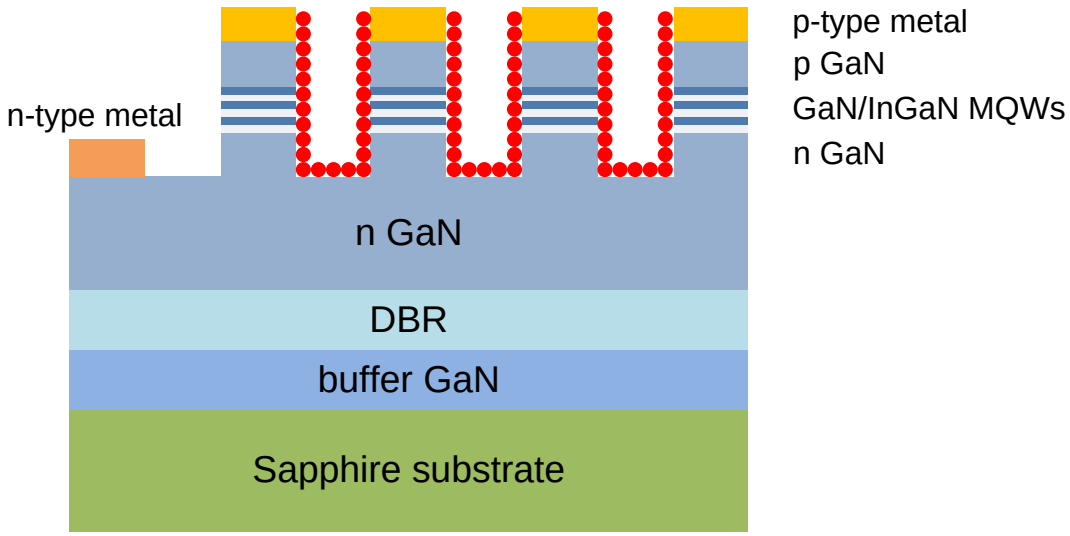

Figure 5-1. Structure of the resonant cavity GaN LEDs with micro holes.

In this resonant cavity GaN LEDs, the distributed Bragg reflector (DBR) is designed to reflect the emission of multiple quantum well (MQW). Unlike in the ordinary resonant cavity LEDs, the cavity length is not designed to the wavelength of GaN emission, but to the wavelength of QDs emission. Consequently, the blue emission of GaN will be reflected by the upper metal reflector and lower DBR, but there will not be a resonance. As a result, the blue light will be trapped in the cavity. In this case, the QDs can be illuminated by the blue light for several times, and the portion of blue light

absorbed by the QDs would be enhanced. Assuming the effective quantum efficiency of the QDs does not change, the emission from the QDs would be enhanced.

Moreover, it is also possible to increase the effective quantum efficiency of the QDs.

$$\eta_{eqi} = \eta_i \left(1 + \frac{r_{transfer}^{QW \to QD}}{r_r^{QW}(1-T)} \right)$$

According to the above equation, if we can increase $r_{transfer}^{QW \to QD}$ the energy transfer rate from InGaN QWs to QDs, or decrease r_r^{QW} the energy transfer rate of radiative relaxation in the InGaN QWs, the effective quantum efficiency can be increased. In the resonant cavity LEDs, r_r^{QW} does not change because there is no resonance for emission from InGaN QWs. Meanwhile, the emission from QDs can resonant in the cavity because the cavity length is designed to this wavelength. In this case, $r_{transfer}^{QW \to QD}$ could be enhanced, and more energy can be transferred from GaN LEDs to QDs.

5.3 Alternating current gallium nitride light emitting diodes

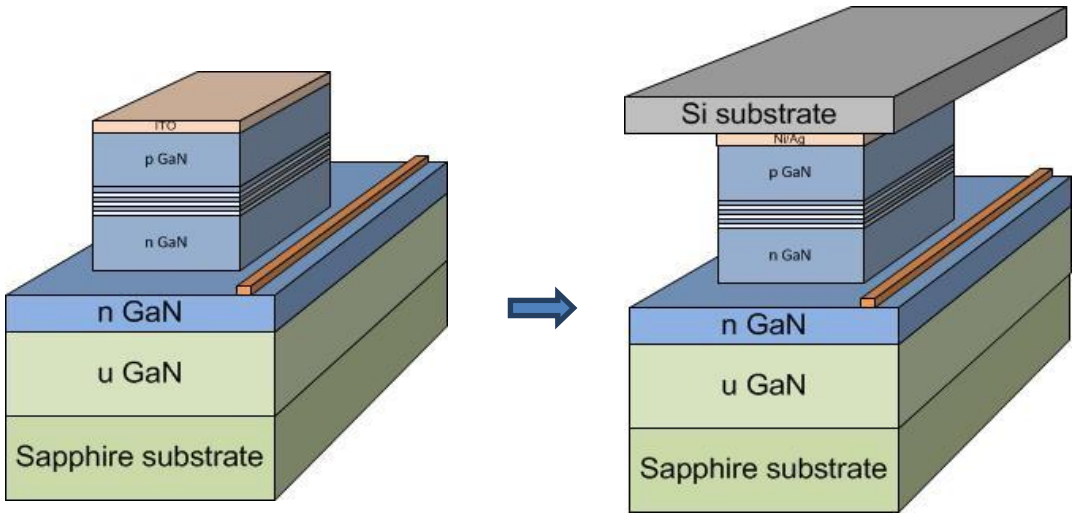

Figure 5-2. Schematic picture of the structure of top emission and flip-chip GaN LEDs.

This dissertation demonstrated chip level high voltage (HV) and alternating current (AC) LEDs. In order to further improve the device performance, flip-chip design can be employed for the future study, as shown in Fig. 5-2. There are two advantages for flip-chip design. The anode is changed from ITO for top emission design to metal for flip-chip design, and the metal anode would lead to lower turn on and working voltage, thus increasing the external quantum efficiency of the device. The other advantage is that silicon substrate has much larger thermal conductivity than sapphire substrate, which is good for heat dissipation.

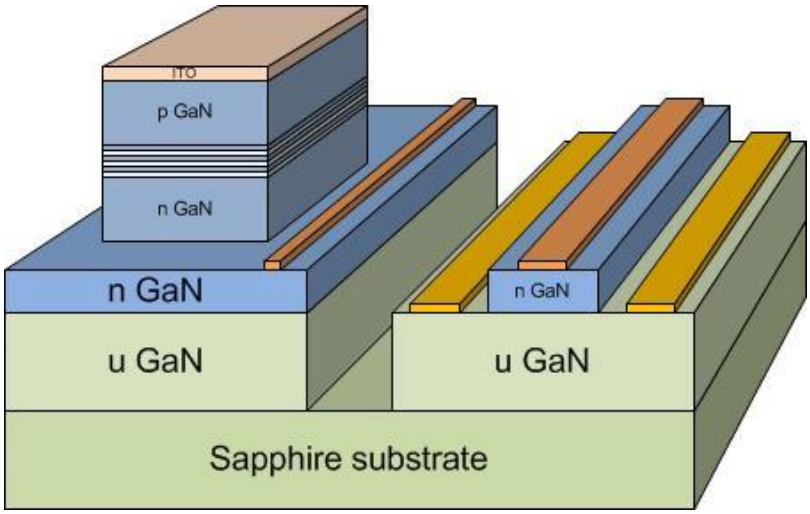

Figure 5-3. Schematic picture of the structure of the device integrated with LED and UV detector.

In addition, based on this study, a novel device integrating LED and UV detector can be obtained, as shown in Fig. 5-3. The LED and UV detector can be fabricated on the same chip. This device would possess the lighting and detecting functions simultaneously, and could have potential application in the future visible light communication.

Appendix

CIE -1931 color space

CIE-1931 color space is a mathematic definition of color space created by the International Commission on Illumination (CIE) in 1931. The color of the output light from the LEDs can be characterized by the CIE-1931 chromaticity coordinates. By integrating the products of the measured LED spectrum with three color matching functions, the three fundamental tristimulus values of X, Y, and Z can be calculated as follows:

$$X = \int_{380}^{780} I(\lambda)\bar{x}(\lambda)d\lambda \qquad (1)$$

$$Y = \int_{380}^{780} I(\lambda)\bar{y}(\lambda)d\lambda \qquad (2)$$

$$Z = \int_{380}^{780} I(\lambda)\bar{z}(\lambda)d\lambda \qquad (3)$$

Where λ is the wavelength measured in nanometer; $I(\lambda)$ is the intensity of the output light at different wavelength, as known as spectrum; $\bar{x}(\lambda), \bar{y}(\lambda)$ and $\bar{z}(\lambda)$ are three color matching functions. By projecting these tristimulus values on to the unit plane, the color of the light spectrum can be expressed in a two-dimensional plane. The color can be specified by the chromaticity coordinates (x, y), defined by:

$$x = \frac{X}{X+Y+Z} \qquad (4)$$

$$y = \frac{Y}{X+Y+Z} \qquad (5)$$

Take the white light with a flat spectrum ($I(\lambda)$ is a constant) for example, its CIE-1931 coordinate (x, y) is calculated to be (1/3, 1/3).

Color rendering index

The present industry standard for color rendering properties of light relies on color rendering index (CRI), which is a numerical measurement of how true colors look when illuminated with the light source. It is measured in 0–100 scales, with 100 representing true color reproduction.

When determining the CRI value of a light source, several reflective samples are employed to be illuminated by the test light source and a reference source. A special CRI for a reflective sample is specified through the color shift in the CIE 1964 uniform color space

$$R_i = 100 - 4.6 \times \Delta E_i \qquad (6)$$

Where ΔE_i is the color difference of the reflective sample illuminated by the test light source and the reference source. The general CRI of the test light source is the average of the special CRIs obtained from those reflective samples:

$$R_a = \frac{1}{n}\sum_{i=1}^{n} R_i \qquad (7)$$

Where n is the number of the reflective test samples.

VITA

Jie Liu

EDUCATION

Ph.D. *Department of Engineering Science and Mechanics* **01/2010~12/2013**
The Pennsylvania State University, University Park, PA, USA

Graduate student *Department of Electrical and Computer Engineering* **08/2009~12/2009**
Purdue University, West Lafayette, IN, USA

M.E. *Department of Precision Instruments and Mechanology* **09/2005~07/2008**
Tsinghua University, Beijing, P.R. China

B.E. *Department of Electronic Engineering* **09/2001~07/2005**
Tsinghua University, Beijing, P.R. China

SELECTED PUBLICATIONS AND PRESENTATIONS

[1] **J. Liu**, F. Zhang, G. You, Y. Zhang, L. Wei, F. Zhao, Y. Wang, R. Henderson, J. Xu, Nonradiative Energy Transfer Between Colloidal Quantum-Dot Phosphors and Silicon Carbide Diodes, J Electron Mater, (2013) 1-4.

[2] **J. Liu**, Y. Wang, P. Wellenius, G. You, A.Y. Wang, J.F. Muth, J. Xu, Colloidal Quantum Dot Light Emitting Diodes Using Indium Gallium Zinc Oxide as Electron Transport Medium, MRS Fall Meeting, (2012) (presentation).

[3] **J. Liu**, F. Zhang, G. You, Y. Zhang, L. Wei, F. Zhao, Y. Wang, J. Xu, Nonradiative Energy Transfer between Quantum Dot-phosphor and Indirect Band-gap Material Diodes, The Electronic Materials Conference (EMC), (2012) (presentation).

[4] **J. Liu**, C. Xie, Y. Zhang, W. Hu, S. Pickering, G. You, A.Y. Wang, J. Xu, Degradation studies of colloidal quantum dot light-emitting diodes, in: 2010 MRS Fall Meeting, November 29, 2010 - December 3, 2010, Materials Research Society, Boston, MA, United states, 2011, pp. 152-157.

[5] **J. Liu**, C. Yang, G. Claire, G. Jin, A novel photonic crystal fiber with high nonlinearity and flattened dispersion, Acta Optica Sinica, 26 (2006) 1569-1574.